Titre: Title:	Effect of Sealant Structure and Sealing Condition on Heat Sealing Performance of Polyethylene Films
Auteur: Author:	Zahra Kanani Aghkand
Date:	2021
Type:	Mémoire ou thèse / Dissertation or Thesis
Référence: Citation:	Kanani Aghkand, Z. (2021). Effect of Sealant Structure and Sealing Condition on Heat Sealing Performance of Polyethylene Films [Thèse de doctorat, Polytechnique Montréal]. PolyPublie. https://publications.polymtl.ca/5620/

URL de PolyPublie: PolyPublie URL:	https://publications.polymtl.ca/5620/
Directeurs de recherche: Advisors:	Abdellah Ajji, & Charles Dubois
Programme: Program:	Génie chimique

POLYTECHNIQUE MONTRÉAL

affiliée à l'Université de Montréal

EFFECT OF SEALANT STRUCTURE AND SEALING CONDITION ON HEAT SEALING PERFORMANCE OF POLYETHYLENE FILMS

ZAHRA KANANI AGHKAND

Département de génie chimique

Thèse présentée en vue de l'obtention du diplôme de *Philosophiae Doctor*

Génie chimique

Mars 2021

POLYTECHNIQUE MONTRÉAL

affiliée à l'Université de Montréal

Cette thèse intitulée :

EFFECT OF SEALANT STRUCTURE AND SEALING CONDITION ON HEAT SEALING PERFORMANCE OF POLYETHYLENE FILMS

présentée par **Zahra KANANI AGHKAND**

en vue de l'obtention du diplôme de *Philosophiae Doctor*

a été dûment acceptée par le jury d'examen constitué de :

Pierre LAFLEUR, président

Abdellah AJJI, membre et directeur de recherche

Charles DUBOIS, membre et codirecteur de recherche

Jason Robert TAVARES, membre

Phil BATES, membre externe

DEDICATION

To my lovely husband and my family

for their unconditional love and support

ACKNOWLEDGEMENTS

Foremostly, praise and thank Almighty God for his guidance, blessing and kindliness.

I would like to express my deepest gratitude to my supervisor, Professor Abdellah Ajji, for his support, patience and for providing me with a friendly atmosphere for doing research and writing my thesis, especially during this pandemic time. His vision, broad-minded and tolerant have deeply inspired me and it was a great privilege to work and study under his guidance.

I also would like to thank my co-supervisor Professor Charles Dubois for his insightful comments and suggestions on the first part of the project.

A special word of thanks is owed to Dr. Amir Saffar, for his help during this study and to Reza Fasihanifard for his valuable comments on the second part of the project.

I would like to thank my friends and members of our research group in the Department of Chemical Engineering, especially Richard Silverwood and Claire Cercle that help me a lot for doing laboratory tests. I greatly value our friendship and I will keep in my mind our sweet memories in the group.

I also would like to thank the technical and administrative staff of the Chemical Engineering Department of École Polytechnique de Montréal.

Last but not least, I would like to thank my parents and sister, who have always supported me throughout my life.

A special thanks to my dear Husband, Dr. Ebrahim Jalali Dil, who has always stood by me and supported me through the good times and bad. This journey would not have been possible without his valuable supports, unconditional love, presence, patience.

RÉSUMÉ

En dépit de l'importance significative du scellage à chaud dans l'industrie de l'emballage flexible, certains aspects de ce processus ont reçu une attention très limitée dans la littérature et n'ont pas encore été examinés en détail. Dans cette thèse, une étude approfondie a été menée sur les effets du procédé de scellage et des conditions de ce scellage sur sa performance pour des films à base de polyéthylène.

Le procédé de scellage est basé sur le chauffage de films de matière plastique en les superposant et en les poussant ensemble entre des mâchoires chauffées. Cependant, il n'y a pas encore eu une étude approfondie sur le transfert de chaleur au cours du processus de scellage à chaud dans la littérature. Dans la première partie de ce travail, le transfert de chaleur se produisant lors du thermoscellage de films multicouches avec une couche de scellant en polyéthylène a été étudié en détail. Des films multicouches composés d'une couche externe en polyamide (PA), d'une couche intermédiaire de polyéthylène greffé avec de l'anhydride maléique (PE-g-MA) et d'une couche de scellant en polyéthylène ont été produits par co-extrusion en filière plate. La température à l'interface des deux côtés du scellage a été mesurée à l'aide d'un thermocouple très fin connecté à un système d'acquisition de données. Les effets de la température de la mâchoire chauffée, de l'épaisseur de la couche de polyéthylène, du type de polyéthylène et de la pression de scellage sur l'évolution de la température à l'interface entre les côtés du joint ont été examinés. Les résultats obtenus ont montré que la température de la mâchoire, l'épaisseur du scellant et la cristallinité du polyéthylène sont les paramètres les plus importants affectant le temps nécessaire à l'interface pour atteindre la température de scellage désirée.

Afin de modéliser le transfert de chaleur lors du thermoscellage, toutes les propriétés des matériaux nécessaires à la modélisation du transfert de chaleur, y compris les variations de densité avec la température, de conductivité thermique et de chaleur spécifique, ont été mesurées expérimentalement. De plus, la conductivité thermique a été mesurée à différentes pressions et il a été montré que, dans la plage étudiée, la pression n'avait pas d'effet significatif sur la conductivité thermique du polyéthylène. La rugosité de surface des échantillons de film a également été déterminée par microscopie à force atomique (AFM). Le transfert de chaleur pendant le thermoscellage des films multicouches a été simulé à l'aide du logiciel COMSOL Multiphysics. La résistance de contact thermique (TCR) a été considérée comme étant la

condition limite entre les mâchoires et la couche de PA extérieure car le scellage à chaud a été effectué à des températures bien inférieures à la température de fusion du PA. En comparant les prédictions de différents modèles avec les résultats expérimentaux, il a été montré que le modèle de Cooper - Mikic - Yovanovich (CMY) est celui qui prédit le mieux la condition limite dans ce système par rapport aux autres. Les résultats de la simulation étaient en accord avec les données expérimentales à la fois en dessous et au-dessus de la température de fusion du matériau de scellage. De plus, la simulation peut prédire de façon précise les effets des conditions de scellage sur la température d'interface. À notre connaissance, il s'agit de la première simulation de transfert de chaleur en thermoscellage qui ne nécessite aucun paramètre d'ajustement.

La possibilité d'effectuer un joint étanche même en présence d'une contamination est une caractéristique essentielle qu'une couche de scellant doit présenter pour l'emballage de produits en poudre et granuleux tels que le café ou le lait en poudre. Cette propriété est connue sous le nom de 'caulkability' dans l'industrie et est directement liée à l'écoulement en compression du matériau de scellage, ce qui est important pour encapsuler les résidus de produits emballés dans la zone de scellage. En dépit de son rôle essentiel dans l'obtention d'une bonne performance de scellage dans les applications mentionnés ci-dessus, les flux de compression dans le thermoscellage n'ont été étudiés que par très peu d'auteurs. Dans la deuxième partie de ce travail, les effets des caractéristiques du matériau de scellage utilisé et des conditions de scellage sur l'écoulement de compression lors du thermoscellage ont été examinés. Des échantillons de films multicouches avec une structure PA / PE-g-MA / polyéthylène ont été produits par co-extrusion. Les effets de l'épaisseur de la couche de polyéthylène, de la viscosité de ce polyéthylène, de la température de scellage et de la pression de scellage sur le flux en compression pendant le thermoscellage ont été étudiés. Une méthode basée sur l'analyse d'images de la zone scellée a été proposée pour mesurer le flux de compression. Les résultats obtenus ont montré que l'épaisseur du scellage et les propriétés rhéologiques du matériau de scellage sont les facteurs les plus importants dans le déclenchement de l'écoulement de compression. De plus, l'effet de la pression de scellage et de la température de scellage sur l'écoulement de compression s'est avéré être très important dans les films avec une couche de scellage épaisse. L'écoulement de compression a également été moulé à l'aide de trois approches: un modèle analytique unidimensionnel basé sur l'hypothèse d'un fluide de la loi de puissance, un modèle numérique unidimensionnel du fluide de Carreau-Yasuda utilisant la méthode des différences finies (FDM) et un modèle bidimensionnel d'un Carreau -

Fluide Yasuda utilisant l'analyse par éléments finis (FEA). Parmi ces modèles, les deux premiers modèles peuvent être considérés comme des modèles prédictifs tandis que le troisième modèle est plus approprié pour l'analyse des résultats expérimentaux car il nécessite un taux de compression comme entrée. De plus, le transfert de chaleur a également été modélisé en utilisant une approche par éléments finis. Les résultats de la modélisation ont montré qu'en considérant le retard dans l'écoulement de compression dû au transfert de chaleur, le modèle FDM présenté pouvait prédire l'écoulement de compression avec une bonne précision. De plus, il a été constaté que l'écoulement de compression lors du thermoscellage se produisait à des taux de cisaillement entre les régions d'écoulement Newtonien et de loi de puissance. Cela peut expliquer pourquoi les études précédentes n'ont pas pu trouver de relation entre l'écoulement de compression des scéllant polymères et leur viscosité à cisaillement nul.

Les films de scellage multicouches doivent offrir une bonne flexibilité mais aussi un bon équilibre entre performance et coût. Les films de scellage multicouches ont été largement utilisés dans l'industrie de l'emballage, mais une étude détaillée de l'effet de leur structure sur les performances de scellage fait défaut dans la littérature. Dans la dernière partie de cette étude, les effets de la structure des films de scellage multicouches sur leur performance ont été étudiés. Des films à deux couches, composés d'une couche de mPE (Polyéthylène Métallocène) et d'une autre couche à l'arrière de polyéthylène ('back layer', couche arrière), ont été produits par co-extrusion. Les effets de l'épaisseur de la couche de mPE, du type de polyéthylène dans la couche arrière et des conditions du procédé de scellage sur les performances de scellage de ces échantillons ont été étudiés. L'augmentation de l'épaisseur de la couche de mPE permet d'augmenter la force d'adhérence à chaud. Chose intéressante, il a été constaté que lorsque le polyéthylène de haute densité (HDPE) est utilisé comme couche arrière, la force d'adhérence à chaud est beaucoup plus faible que lorsque c'est un polyéthylène linéaire à basse densité (LLDPE) ou un polyéthylène à basse densité (LDPE) qui est utilisé. L'augmentation du temps de refroidissement après le scellage et avant de tester les performances du scellage augmentait la résistance de collage à chaud dans tous les films. Cependant, pour les couches arrière de LDPE et LLDPE, cela ne conduisait qu'à un changement de type de rupture du scellage de pelable à joint integre. En utilisant la simulation de transfert de chaleur, il a été montré que le comportement pelable observé dans les films avec une couche arrière en HDPE ne peut pas être attribué à un mauvais transfert de chaleur. Il a été discuté que la

résistance du scellage provient de deux mécanismes: l'arrachement des chaînes à l'extrémité de la région de pelage et la dissipation viscoélastique dans le volume (bulk). Les effets observés de l'épaisseur de la couche arrière et du mPE sur les performances du scellage sont expliqués par la théorie de la dissipation viscoélastique dans le volume. Il a été montré que la taille de la zone plastique dans laquelle la plus grande dissipation viscoélastique se produit est assez grande pour inclure non seulement la couche de mPE, mais aussi la couche arrière. Par conséquent, l'utilisation d'une couche arrière rigide, telle que le HDPE, entraîne une moindre dissipation d'énergie pendant le processus de pelage et conduit à une concentration élevée de contraintes sur le bord de la zone de pelage. Les forces pour tirer les chaines de polymère à l'extrémité de la région de pelage sont donc réduites et cela diminue la résistance du scellage.

Les résultats obtenus dans ce travail fournissent de nouvelles connaissances pour une meilleure compréhension du processus de scellage à chaud et permettent un meilleur contrôle sur la performance du scellage final dans les applications industrielles.

ABSTRACT

Despite the significant importance of heat sealing in flexible packaging industry, some aspects of this process have been poorly studied in the literature and few aspects have not been examined in detail yet. In this dissertation, attempts have been made to provide a comprehensive study on the effects of sealant structure and sealing condition on seal performance of polyethylene-based sealant films.

Heat sealing process is based on heating of plastic films by sandwiching and pushing them together between heated jaws, but a comprehensive study on heat transfer in heat sealing process is lacking in the literature. In the first part of this work, heat transfer in heat sealing of multilayer films with polyethylene sealant layer was studied in detail. Multilayer films composed of a polyamide (PA) outer layer, a polyethylene grafted maleic anhydride (PE-g-MA) middle layer and a polyethylene sealant layer were produced by cast co-extrusion. The interface temperature between two seal sides was measured using a fine thermocouple connected to a data acquisition system. Effects of heated jaw temperature, polyethylene layer thickness, type of polyethylene, and sealing pressure on the temperature evolution at the interface between seal sides were examined. The obtained results showed that jaw temperature, sealant thickness and crystallinity of polyethylene are the most important parameters that can affect the time required for the interface to reach the set sealing temperature. In order to model heat transfer in heat sealing, all material properties needed for modeling of heat transfer including temperature variations of density, thermal conductivity, and specific heat capacity were measured experimentally. In addition, thermal conductivity was measured at different pressures and it was shown that, in the studied range, pressure did not have a considerable effect on thermal conductivity of polyethylene. In addition, the surface roughness of film samples was also determined by atomic force microscopy (AFM). Heat transfer during heat sealing of multilayer films was simulated using COMSOL Multiphysics software. Thermal contact resistance (TCR) was considered as the boundary condition between jaws and the outer PA layers because heat sealing was done at temperatures far below melting temperature of PA. By comparing model predictions with experimental results, it was shown that the Cooper−Mikic−Yovanovich (CMY) model predicts much better the boundary condition in this system. The simulation results were in very good agreement with experimental data both below and above melting temperature of sealant material. Moreover, the simulation could predict well observed effects of sealing

conditions on the interface temperature. To our knowledge, this was the first simulation of heat transfer in heat sealing that did not require any fitting parameter.

Seal through contamination is an essential characteristic that a sealant layer should exhibit for packaging of powder and grainy products such as coffee or powdered milk. This property is known as caulkability in the industry and is directly related to the squeeze flow of the sealant to encapsulate the packaged product residues in the seal area. Despite its essential role in achieving a good seal performance in the above-mentioned applications, squeeze flow in heat sealing has been studied only by few authors. In the second part of this work, effects of sealant material characteristics and sealing conditions on squeeze flow in heat sealing were examined. Multilayer film samples with the structure of PA/PE-g-MA/Polyethylene were produced by cast co-extrusion. Effects of polyethylene layer thickness, polyethylene viscosity, sealing temperature, and sealing pressure on squeeze out flow during heat sealing was investigated. A method based on image analysis of sealed area images was proposed to measure the squeeze out flow. The obtained results showed that sealant thickness and rheological properties of sealant material are the most important factors in triggering squeeze flow. In addition, effects of sealing pressure and sealing temperature on squeeze out flow were found to be much pronounced in films with thick sealant layer. Squeeze flow was also molded using three approaches: an analytical one-dimensional model based on Power-law fluid assumption, a numerical one-dimensional model of Carreau-Yasuda fluid using finite difference method (FDM), and two- dimensional model of a Carreau-Yasuda fluid using finite element analysis (FEA). Among these models, the first two models can be considered as predictive models while the third model is more appropriate for analysis of experimental results as it requires squeezing rate as an input. In addition, heat transfer was also modeled using a finite element approach. Modeling results showed that by considering the delay in squeeze flow due to heat transfer, the presented FDM model could predict squeeze flow with good precision. In addition, it was found that the squeeze flow in heat sealing occurred at shear rates between Neptunian and Power-law regions. This can explain why previous studies could not find a relation between squeeze flow of polymeric sealants and their zero-shear viscosity.

Multilayer sealant films can offer design flexibility and much better balance between performance and cost. Multilayer sealant films have been widely used in packaging industry, but a detailed study on the effect of their structure on seal performance is lacking in the literature. In the last part

of this thesis, effects of structure of multilayer sealant films on their seal performance were studied. Two-layer films composed of an mPE layer and another polyethylene back-layer were produced by cast film co-extrusion. Effects of the thickness of mPE layer, polyethylene type in the back-layer and processing conditions on seal performance of these samples were studied. Increasing mPE layer thickness was found to increase hot tack strength (seal strength when the temperature of the films is still above room temperature, is called hot tack strength). Interestingly, it was found that when high density polyethylene (HDPE) was used as the back-layer, the hot tack strength was much lower than when linear low density polyethylene (LLDPE) or low density polyethylene (LDPE) were used. Increasing cooling time after sealing and before testing the seal performance, increased hot tack strength in all films but only led to shifting peeling behavior from peelable to lock-seal in the films with LDPE or LLDPE back-layers. Using heat transfer simulation, it was shown that the observed peelable behavior in films with HDPE back-layer cannot be attributed to poor heat transfer. It was discussed that the seal strength originates from two mechanisms: chain pullout at the tip of the peeling region, and the bulk viscoelastic dissipation. The observed effects of back- layer and mPE layer thickness on seal performance were explained by considering the bulk viscoelastic dissipation theory. It was shown that the size of the plastic zone in which the bulk viscoelastic dissipation occurs is large enough to include not only mPE layer but also the back-layer as well. Therefore, using a stiff back-layer, such as HDPE, results in less dissipation of energy during peeling process and leads to much concentration of stress on the peeling edge. This will finally result in chain pull out at the tip of the peeling front at lower forces and a reduced seal strength.

The obtained results in this work, provide new knowledge for a better understanding of heat sealing process and allows much control on final seal performance in the final applications.

TABLE OF CONTENT

LIST OF TABLES

LIST OF FIGURES

LIST OF SYMBOLS AND ABBREVIATIONS

Greek Letters

ΔH_m	Enthalpy of fusion
ΔG_m	Gibbs free energy of mixing
χ_{AB}	Florry-Huggins interaction parameter
ρ	Density
φ	Volume fraction
μ	Viscosity
ν	kinematic viscosity

List of Abbreviations:

CPP	Cast polypropylene
DSC	Dynamic scanning calorimetry
EMA	Ethylene methacrylate copolymer
EAA	Ethylene acrylic acid copolymer
EVA	Ethylene vinyl acetate
HDPE	High density polyethylene
LCB	Long chain branching
LDPE	Low density polyethylene
LLDPE	Linear low density polyethylene
MW	Molecular Weight

Me	Molecular weight of entanglement
m-VLDPE	metallocene very low density polyethylene
m-LLDPE	Metallocene polymerized linear low density polyethylene
MWD	Molecular weight distribution
OPP	Oriented polypropylene
PB	Polybutene
Rg	Radius of gyration
SSp	Plateau Seal Strength
SCB	Short chain branching
SOF	Squeeze out flow
T_{si}	Seal initiation temperature
T_{pi}	Seal plateau initiation temperature
T_{pf}	Final Plateau Temperature
Tg	Glass transition temperature
Tm	Melting temperature
TCR	Thermal contact resistance
VFFS	Vertical form fill seal
V-LDPE	Vey low density polyethylene
WAXS	Wide-angle x-ray scattering
Zn-LLDPE	Ziegler-Natta polymerized linear low density polyethylene

CHAPTER 1 INTRODUCTION

Flexible plastic packaging has been used in a wide range of applications due to its low cost, ease of processing and tunable design [1]. Packaging properties are mainly designed to satisfy requirements for targeted applications. For instance, a plastic film for cheese packaging needs to comply with food safety regulations and have high barrier against moisture and oxygen. On the other hand, a film for packaging vegetables still needs to comply with food contact regulations but requires such a low barrier property that, in most cases, perforated films are used for this application. Despite differences in design criteria based on the application, providing a good sealing performance is the common requirement in almost all plastic packaging. Sealing is one of the most delicate parts in any packaging that requires much attention as if the sealing fails, the whole package will fail. Sealing is mainly provided through the fusion of the interior surfaces of the plastic films using different sealing methods.

Among the various sealing technologies, heated bar sealing, which is also known as heat sealing, is the most common method in flexible plastic packaging industry due to its low required capital cost, ease of operation and low maintenance cost. Polyethylene (PE) has been the most widely used material for sealing in flexible plastic packaging due to its wide range of properties including: complying with food contact safety regulations, low price, variety of optical and mechanical properties, high moisture barrier, low melting temperature and high chemical resistance. Despite the importance of heat sealing in plastic packaging, few studies have been dedicated to this subject and the literature is lacking in some important aspect of heat sealing. For example, heat sealing process is based on the heat transfer from the heated bars toward the interior surfaces of the film. As will be discussed later, it has been shown that changing the sealing temperature significantly affects seal performance. However, studies on heat transfer in heat sealing have been limited in the literature. As a result, trial and error is a common approach to find the optimum sealing condition. For example, by changing the film thickness, the sealing time and temperature need to be optimized to ensure good sealing while maintaining the production speed as high as possible. The trial and error, especially in industrial scale, is costly and leads to increasing operation cost and material waste. This clearly indicates the importance of a detailed study on heat transfer in heat sealing process. Another aspect of heat sealing that has been poorly examined in the literature

is caulkability which is defined as the ability of the sealant material to encapsulate contaminations in the seal area. This is a critical property when packaging liquid or grainy products in vertical form fill sealing (VFFS) machines. A schematic of the VFFS process is shown below.

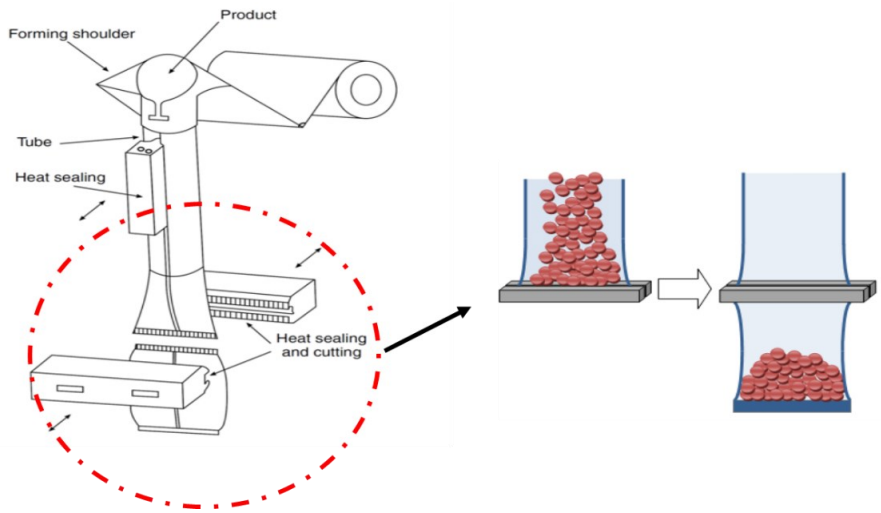

Figure 1.1 left) a schematic of the vertical form fill seal (VFFS) process; right) product filling steps. (modified from [2])

Some examples of these applications are milk packaging, vinegar, detergents, cereals, coffee bags, pasta, pretzel, nuts, spices, etc. If the sealant material cannot encapsulate the product residue in the seal area, channeling in the seal area can cause leaking (specially in liquid products) resulting in a reduction of the product shelf life. In extreme cases, high level of product residue in the seal area can even cause seal failure. Few studies examined caulkability of polymeric sealants in heat sealing applications and attempted to find a correlation with material properties. However, no correlation could have been established so far, a comprehensive study on the effects of seal processing condition and material characteristics is still lacking in the literature. Metallocene linear low-density polyethylene (m-LLDPE) is a relatively new polyethylene family that can provide superior clarity, and high caulkability and seal performance. This family of PE has replaced conventional PE in almost all applications that require superior seal performance. However, despite its superior properties, the higher cost of m-LLDPE compared to the conventional PE has limited its application in packaging industry. Two main approaches have been used in flexible packaging industry to reduce the material cost: (i) using multilayer sealant films with a layer of m-LLDPE in the seal side and conventional PE layers as back-layer(s) and (ii) blending m-LLDPE with

conventional PE. Although these two approaches are used commonly in the industry, few studies examined the effect of these strategies on seal performance. Especially, examining the effect of replacing a single layer m-LLDPE sealant with a multilayer sealant film on seal performance has not been the subject of any previous study in the literature. It is worth mentioning that according to the society of plastic industry (SPI), m-LLDPE films can be considered as recyclable if used alone or in multicomponent films with LDPE or conventional LLDPE. All above-mentioned, have motivated us to perform a comprehensive study on the effects of sealing condition and film structure on seal performance of multilayer plastic films.

CHAPTER 2 LITERATURE REVIEW

2.1 Plastic Joining Methods

The different techniques that have been used to join plastic components can be categorized in three main groups: mechanical joining, adhesive bonding, and welding [3]. In mechanical joining, external grips or fasteners are used to join the plastic parts. In adhesive bonding, an adhesive is applied between two polymeric surfaces which bonds the surfaces together. Finally, in welding method, the polymeric surfaces are melted, and polymer molecules diffuse across the interface between two parts and bond the parts together. Figure 2.1 shows different joining techniques categories with some of the methods under each category.

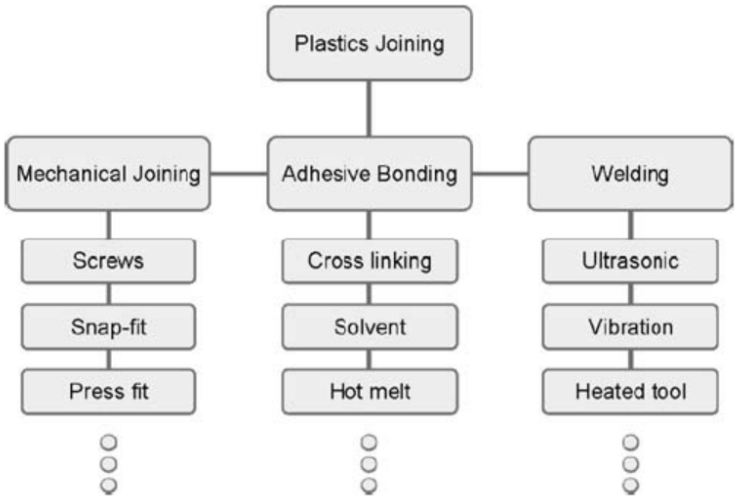

Figure 2.1 Different plastics joining methods [3].

The main differences between welding and the two other methods is the lack of the need for a third component (fixtures or adhesive) and heating that is applied (by different means) in the welding techniques. Considering the heating method, welding techniques can be categorized in two main groups: internal heating and external heating. These groups with some methods under each group are listed in Figure 2.2. In the internal heating methods, heat is generated inside the material by either electromagnetic waves or mechanical forces. However, in the external heating methods, heat needs to be transferred to the interface between two parts. This indicates that in the external heating methods, heat transfer is an important parameter that needs to be considered. Therefore, welding

of thick parts is done commonly by internal heating methods such as ultrasonic in order to reduce the welding time and avoid burning of external material surfaces.

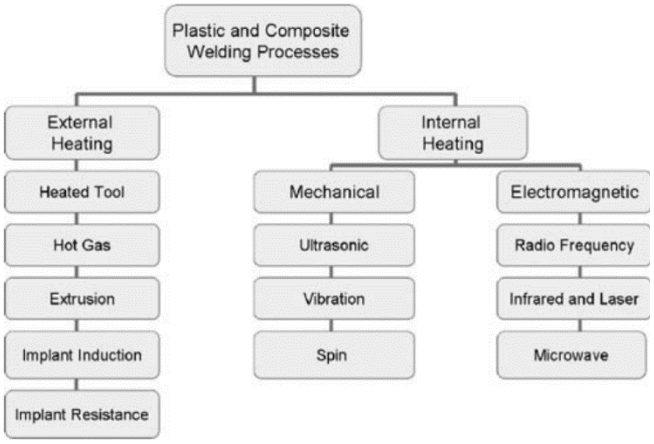

Figure 2.2 Different welding techniques based on the applied heat methods [3].

On the other hand, the low capital requirement, ease of processing, versatility of machines and suppliers and low maintenance cost in external heating methods and more specifically in heated tool process made this category more popular in plastic packaging industry. Different heated tools are used in packaging industry in which hot knives (or wires) [4, 5] and heated bars (or jaws) [6] are the most common ones. The heated bars sealing method are of different types depending on the applied heat cycle. In the most common industrial heat sealing processes, jaws or bars are always heated even when they are not in the sealing cycle. Another type of heated bar sealing is the impulse heat sealer in which the bars are cold, and they begin to heat up when they are pressured against the film surface. They remain heated at the set temperature for the required sealing time (dwell time) and then the heaters are switched off even if the bars remain in contact with the film. The bag sealers that are used to seal bags in kitchens and small shops are some examples of impulse heat sealers. Although impulse sealers have better energy efficiency, but as it takes time for the jaws to heat up and reach the desired sealing temperature before the timer in the machine begins to count the dwell time, they have very poor control on sealing temperature and dwell times. This can lead to sealing inconsistency, especially in high production speed lines. In addition, the jaw heating time is added to the sealing time which in industrial scale can reduce the production speed considerably. Due to these points, heated jaws are the most common sealing

machines in the packaging industry. Therefore, in the rest of this project, the heat sealing machines are always heated bar machine unless indicated otherwise.

2.2. Heat Sealing Process

In this method, two sides of the seal are placed between two jaws (bars) that are both electrically heated. It should be mentioned that in some applications such as sealing of flexible lidding to rigid cups or trays, only the lidding side is heated but as this type of heat sealing is not common, it will not be examined in this work. The jaws apply a constant pressure (known as the sealing pressure) for a certain period (known as the dwell time) to seal the films together. Finally, the jaws are opened after the dwell time and the seal is removed. The seal is tested after certain amount of time which is known as delay time or cooling time. This process is schematically shown below.

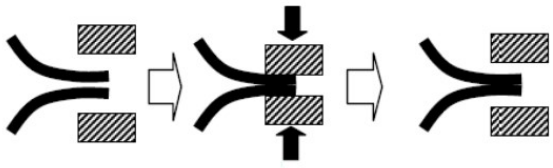

Figure 2.3 Schematic of heat sealing process, from left to right: approaching of the heated jaws, applying heat and pressure to the films for the duration of sealing, and jaw opening. [3].

Therefore, four main process parameters in heat sealing are: (i) jaw temperature, (ii) dwell time, (iii) sealing pressure, and (iv) delay time. The effect of these parameters on seal properties will be described in more detail later. It should be noted that, in addition to these parameters, the surface pattern of jaws can also affect seal properties. For example Selke et.al. [7] and Theller [8] showed that using serrated jaws (Figure 2.4) can improve seal performance by increasing the intimate contact between polymeric films especially when the thickness of the films is not uniform. Figure 2.4 shows some example of serrated jaw patterns.

Figure 2.4 Schematic showing the cross-section (left) and top-view (right) of some serrated sealing jaws [7]

2.3. Molecular Mechanism of Heat Sealing

Stehling and Meka [9] proposed a molecular mechanism to explain sealing process in semi-crystalline polymers. As can be seen in Figure 2.5, they considered the sealing process as a five steps process. In the first step, when the surfaces of polymeric films are brought together, surface roughness and crystalline regions prevent a complete contact between the surfaces and only Van der Waals forces exist between the surfaces. In the second step, by increasing temperature, crystalline regions melt which increases wetted areas (complete contact areas) between the surfaces. In the third step and by applying a slight pressure, the wetted area reaches its maximum and, in the fourth step, increasing contact time leads to polymer chain diffusion across the interface. Finally, in the fifth step, when heat and pressure are removed, the seal area is cooled down and recrystallization of the polymer chains can occur which results in achieving the ultimate seal strength.

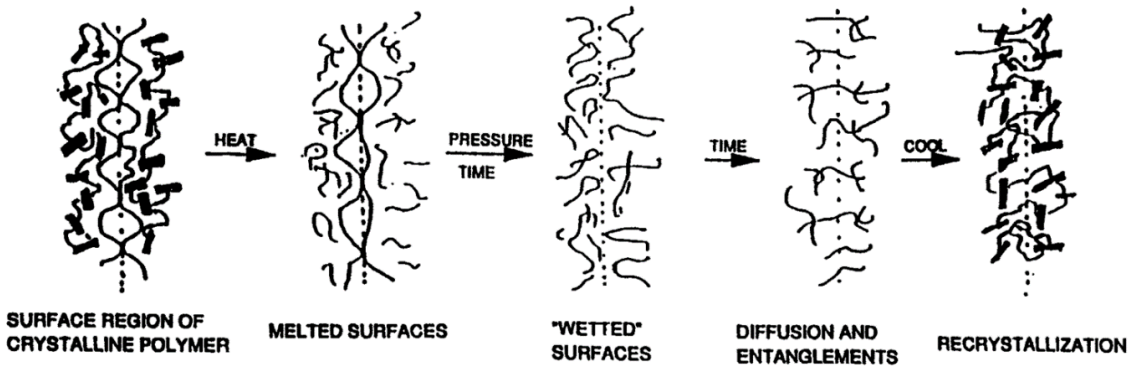

Figure 2.5 Schematic showing the five steps in molecular mechanism proposed for heat sealing process [9]

Different types of interfaces could be defined depending on different configurations of polymeric films that are brought together to make a seal (or joining area): symmetric polymer-polymer interfaces, asymmetric polymer-polymer interfaces, and multicomponent polymer interfaces [10]. As in the heat sealing method, the two polymer surfaces are usually the same, diffusion of polymer chains across a symmetric polymer-polymer interface will be reviewed in more detail here. Wool and O'Connor [10, 11] studied the adhesion of polymer-polymer at their interface by dividing the adhesion process into the following steps: 1) surface rearrangements, 2) surface approach, 3) wetting, 4) diffusion, 5) randomization. These steps are very similar to the steps presented by

Stehling and Meka [9] for heated bar sealing (see section 3.2). Each step will be discussed in more detail below.

2.3.1. Surface Rearrangement

It is important to consider the roughness or topography of the surface of each seal side and the changes in the surface topography with temperature, time and pressure. The most important parameters in the heat sealing process in this step are chain-end distributions [12] and crystalline regions [9] near the surfaces. The surface rearrangement can be due to the migration of low molecular weight chains to the surfaces [13] or rearrangement of crystalline regions close to the surface [12]. The dynamics of surface rearrangement is not much different from molecular movements in the bulk, however, due to the higher degree of freedom of chains in the surface layer, less energy is required for surface rearrangement compared to bulk processes [12].

2.3.2. Surface Approach

In this step, by applying pressure, the surfaces come in contact which allows polymer chains to begin diffusing across the interfaces. Therefore, eliminating the gap between the surfaces in this step is critical for molecular diffusion to occur in the next steps [9, 11, 12]. In heat sealing process, surface rearrangement and surface approach occur almost at the same time by applying heat and pressure by the jaws.

2.3.3. Wetting

When the surfaces are melted, they should wet each other through spreading mechanism. Spreading or wetting begins from the regions with the lowest surface roughness and then grows at the interface in a relatively two-dimensional space [11, 12, 14]. Finally, the coalescence of wetting regions leads to a complete interface wetting. The wetting phenomenon is shown schematically in Figure 2.6.

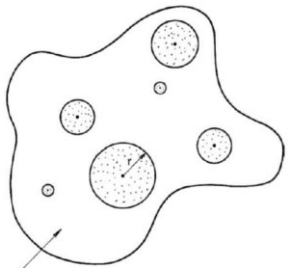

Figure 2.6 Schematic of wetting process, wetting starts from some points then these regions grow until they coalescence [10, 12, 14].

Wetting is a time-dependent process which depends on surface roughness, temperature, pressure, chain-end orientation and the presence of crystalline structure at the surfaces [10, 12, 14-17]. As the inter-diffusion across the interface can only occur at the wetted area, wetting stage affects inter-diffusion step and, consequently, strength development at the interface [12, 14].

2.3.4. Molecular Diffusion of Polymers

Molecular diffusion and creating entanglements across the interface are necessary to achieve high seal strength. Molecular diffusion of polymer chains in polymer melts and concentrated solutions have been the subjects of many studies in literature. Molecular diffusion of polymer chains can be explained using two models: Rouse model for low molecular weight polymer chains and the Reptation model for high molecular weight polymer chains.

2.3.4.1. Rouse model

The polymer chain in this model is considered as a series of beads that are connected by springs, (Figure 2.7). This structure is assumed to be embedded into a viscous surrounding medium.

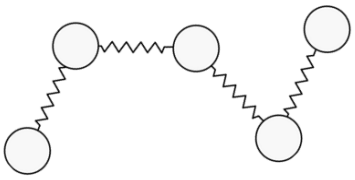

Figure 2.7 The Rouse model in which a polymer chain is represented by a series of beads and springs, N+1 beads and N springs.

As this model does not consider long-range effects such as entanglement, it is only valid for polymer melts with molecular weight (MW) smaller than the entanglement molecular weight (M_e). For melt polyethylene, M_e is around 1800g/mol [18].According to the Rouse model, the relaxation time of the chains (which is known as the Rouse relaxation time τ_R)is proportional to the number of repeat unites (N) or MW ($MW=M_0N$, M_0 is molecular weight per unit or spring)[19]:

$$\tau_R = \frac{6\eta_0 MW}{\pi^2 \rho RT} \qquad \text{Eq. 2.1}$$

η_0 is zero sheer viscosity, ρ is density and R is the ideal gas constant. This model also predicts the zero-shear viscosity of polymer melts to be proportional to N. This is in contrast with the empirical dependency of $N^{3.4}$ that has been confirmed experimentally for narrow molecular weight distribution (MWD) of linear homopolymers with MW greater than M_e [20].

2.3.4.2. Reptation Model

The breakthrough in understanding and analyzing the motion and diffusion of polymer chains was achieved by De Gennes model in 1971 [21]. In this model, a polymer chain is assumed as a chain in a network of topographical constraints similar to a polymer gel, Figure 2.8 (left). By assuming that the length of the chain is much larger than the length scale between constrains, the chain can be considered as if it is confined in a tube, Figure 2.8 (right).

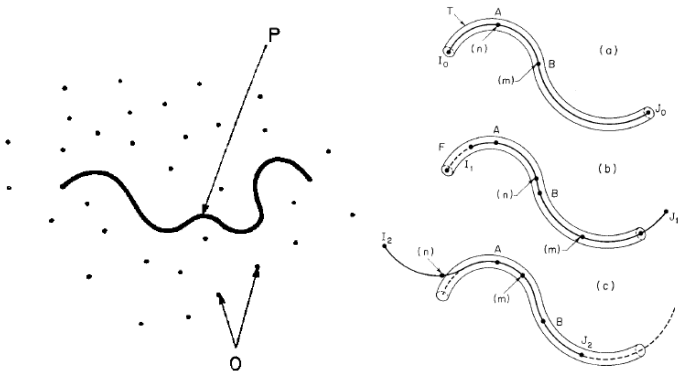

Figure 2.8 (left) De Gennes model basics: the chain P is free to move between fixed obstacles (o) but cannot cross them, (right) reptation of a polymer chain out of its initial tube [21].

The lateral displacement of polymer chain is prohibited by the neighboring obstacles and the only allowed motion is the motion along the surrounding tube length. Therefore, the chain can only do

a random back and forth Brownian motion which is called reptation motion. Due to this motion, a part of the chain exits the initial tube and enters a new tube, Figure 2.8 (right). Eventually, after a certain period, called the reputation time (τ_{rep}), the chain escapes completely from its initial tube. According to the De Gennes model [21], the reptation time is proportional to M^3 [22]:

$$\tau_{rep} = K\frac{M^3}{M_e} \qquad \text{Eq. 2.2}$$

K is the frictional factor; *M* is molecular weight and *Me* is the entanglement molecular weight.

Which indicates the much-pronounced effect of molecular weight compared to the Rouse model.

2.3.4.2. Diffusion Across the Interface

Both Rouse and Reptation models have been presented for self-diffusion within the bulk. However, in heat sealing process, the diffusion occurs across the interface of the two seal sides. The diffusion mechanism at the interface significantly depends on the configuration and situation of the chain ends relative to the interface. De Gennes [23] considered two different scenarios of the configuration and situation of the chain ends relative to the interface and found that:

(i) *If the chain ends are initially concentrated at the surface before contact:* In this regime, the macroscopic properties (such as welding strength or sealing strength) are proportional to $t^{1/4}$. Previous studies have confirmed that this model can explain the time dependency of strength in crack healing and fracture healing [11, 24]. This is expected as in those cases; the surfaces are mainly formed by chain scission which results in an accumulation of chain ends at the surface.

(ii) *If the chain ends are not initially situated at the interface*, then they will need to first diffuse in the bulk before reaching the interface. In this case macroscopic properties depend on diffusion time as $t^{1/2}$.

Wool [10] also studied diffusion of polymer chains across the interface and found that the number of monomers passing the interface (N_{int}) is proportional to $t^{1/2}$. In a previous study, Najarzadeh et al. [2] showed that the seal strength in heat sealing could be correlated with dwell time as $t^{1/2}$. These results indicate that the diffusion across the interface during sealing process should follow the second scenario of De Gennes. An interface can be considered as healed when a diffusion

length equal to the radius of gyration of polymer chain is reached [23]. The interdiffusion time to reach this diffusion length can be simply estimated using the Einstein theory of Brownian motion:

$$\tau_i = \frac{R_g^2}{2D} \qquad \text{Eq. 2.3}$$

Where Rg and D are the radius of gyration of polymer chain and the diffusion coefficient, respectively. The diffusion coefficients for polyethylene melt with different MWs have been reported by some previous researchers [25-27]. Qureshi et al. [28] estimated τ_i as 0.04 s at 140°C for a linear low density polyethylene (LLDPE) with M_w=120 kg/mol.

2.3.5. Randomization

In this step, by reducing the temperature of the films after opening of jaws, crystallization (in semi-crystalline polymers) and solidification increases interface strength [10]. Therefore, understanding the crystallization behaviour of polymers is important in studying their seal performance. However, first, it should be noted that there are several differences between bulk and interface crystallization. During film production, the highly ordered state of the chains near the interface increases the probability of formation of critical-sized nuclei for crystals at the film surface [29]. On the other hand, film surface experiences much higher cooling rates compared to the bulk which can suppress the crystal growth at the surface. In addition to crystallinity of the film, after heat sealing and depending on the extent of diffusion across the interface, the entanglement density and entropy at the sealed interface can also be different or similar to the bulk. Moreover, the small thickness of polymer films makes it challenging to examine the crystallinity and crystallography within the film. This indicates the complexity of studying the effect of crystallinity on seal performance. However, as this topic is not the focus of this research, it will not be reviewed in detail.

2.4. Seal Performance Evaluation Methods

Testing techniques used for evaluation of seal properties can be categorized based on the sealed area temperature during testing. If the seal area is examined when it is still hot, the obtained result is called hot tack strength. On the other hand, if the test is done when the seal area is cooled down to ambient temperature, the obtained result is known as the seal strength. Depending on the

packaging process and final required properties, either or both seal or hot tack properties can be important in designing a package. For example, hot tack is more important in VFFS packaging in which the package is filled when the bottom seal is still hot and should withstand the weight of the product. On the other hand, seal strength is much important in pouch applications in which pouch filling is done when the seal area is at room temperature. As will be discussed later, hot tack strength is lower than seal strength due to the higher mobility of polymer chains at higher temperatures [30]. A brief explanation of seal strength and hot tack measurement methods will be presented below.

2.4.1. Determining Hot Tack Strength

Hot tack is defined as capability of the seal to withstand stress or weight of the product when the sealing material is still hot. The unit of hot tack is force divided by the width of the test sample. Hot tack measurement tests should be done according to the ASTM F1921 [31] standard. In brief, two strip samples with a width of 25.4 or 15 mm should be cut. The strip samples are placed in an automated machine which has four main cycles: (i) sealing, (ii) delay, (iii) withdrawal, and (iv) force measurement. In the sealing step, the instrument loads the strip samples between the heated jaws, the jaws are pushed together at the sealing pressure for the duration of the dwell time. Then in the delay step, the jaws are opened, and the machine waits for a set delay time before pooling the seal sides apart in the withdrawal phase. The hot tack curve is obtained by repeating the test at different sealing temperatures. Figure 2.9 shows schematically a typical hot tack test configuration and test results.

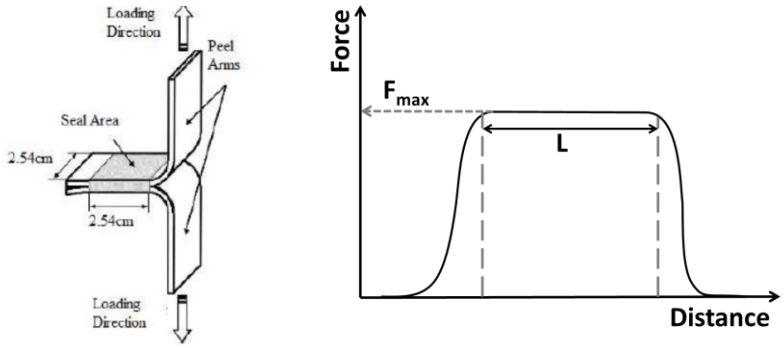

Figure 2.9 (*left*) schematic of sample configuration during hot tack test [32, 33], (*right*) typical obtained results for hot tack test of a sample with sealed area length of L.

Two methods can be used to report the hot tack strength, (i) reporting the maximum measured seal force divided by the sample width, (ii) reporting the average force required during peeling of the sealed area divided by the sample width. In addition to the hot tack strength, the mode of the failure should also be reported for each sample. Previous researchers proposed different classification of failure modes based on their observations [8, 32, 34, 35] but the most comprehensive classification was found in the ASTM standard and is shown in Figure 2.10.

In adhesive failures, the peeling occurs only at the interface between seal sides due to the weak inter-diffusion of polymer chains across the interface. In cohesive failure, the seal interface is strong enough to transfer the stress to the bulk and failure occurs within the bulk of the sealant. In delamination, poor inter-layer adhesion between layers of film results in delamination of the layers in either side of the sealant layer rather than in the sealant layer. In the material break mode, the break occurs at the edge of the seal area or in the bulk of the laminate structure (far from the seal area) due to the defects in the structure. Material elongation failures occur when the hot tack strength is higher than strength of other parts of the film which results in deformation and elongation of those parts.

2.4.2. Seal Strength Evaluation

Seal strength can be measured according to ASTM F88 [36] using a heat sealing machine and a tensile machine. Units of seal strength are the same as hot tack strength. Similar to hot tack test, strip samples with a width of 25 or 15 mm are used in seal strength measurements. The samples are sealed using a heat sealing machine at the desired sealing condition and then they need to be conditioned at 23^{o}C and 50% RH for 40 h before testing (in the absence of information showing that heat seal strength stability of the materials under test is reached in shorter times). The samples then are tested using a tensile machine. As shown in Figure 2.11, three different sample supporting options can be used: (i) technique A: unsupported sample, (ii) technique B: supported 90^{o} by hand and (iii) technique C: supported 180^{o}. The unsupported sample is the most common in flexible packaging and the supported 180^{o} configuration is used usually for testing seal strength of a flexible film sealed to a rigid sheet or substrate. The obtained result from tensile machine is very similar to hot tack results (Figure 2.9) and is shown as a plot of required peeling force per peeling distance. The seal strength is then reported as the maximum peeling force during peeling process

divided by the sample width. Repeating seal test at different sealing temperatures results in a seal curve. Similar to hot tack test, the failure mode needs also to be reported for each sample.

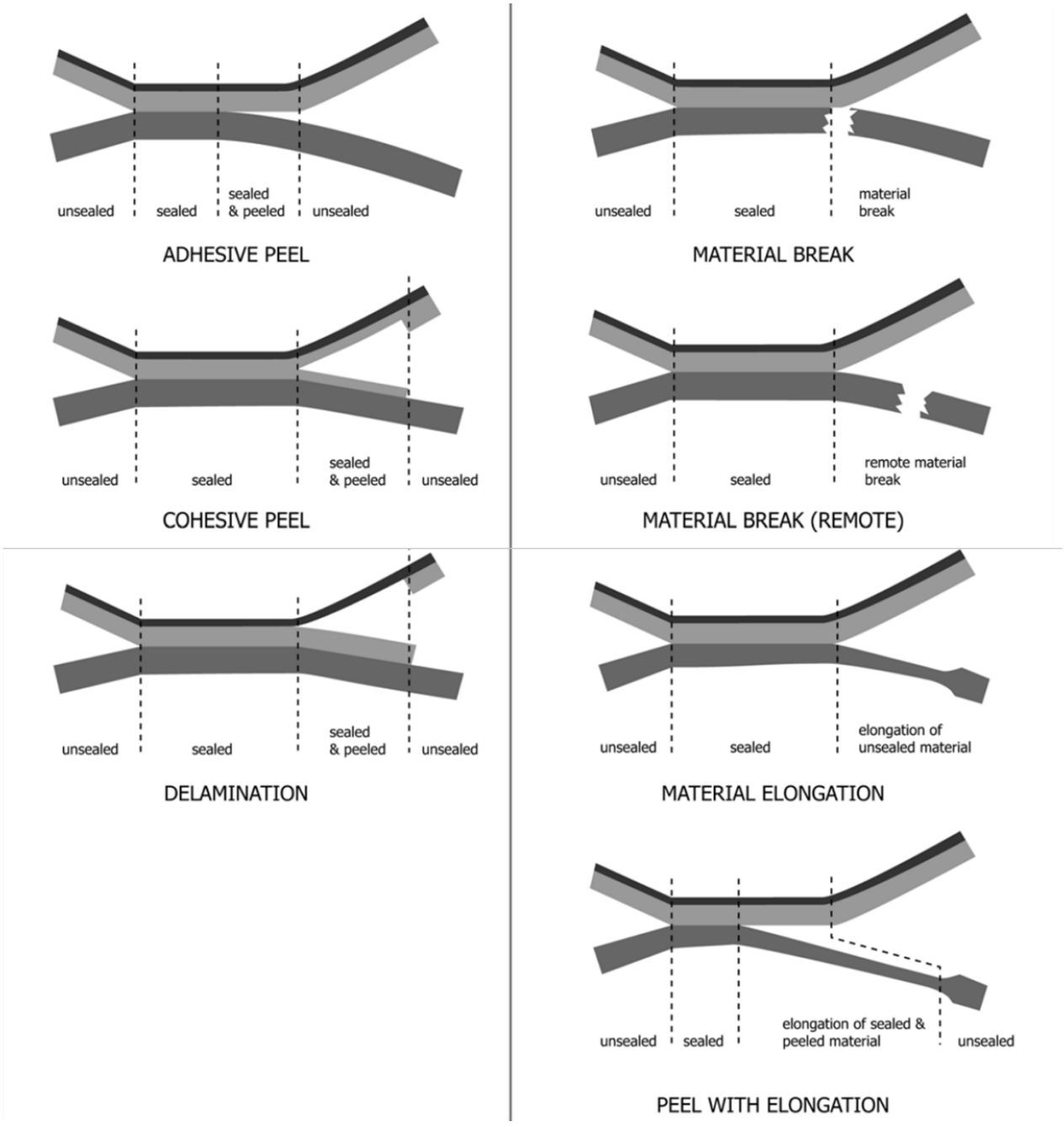

Figure 2.10 Schematic of failure modes in the seal area between two films [37].

.

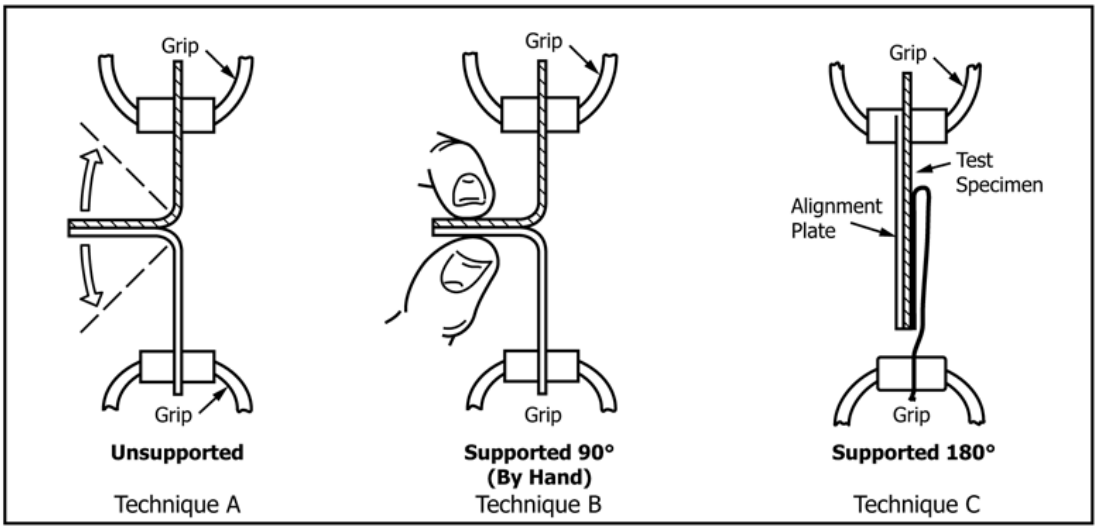

Figure 2.11 Different supporting options for peel test: (*left*) unsupported sample, (middle) supported 90°, (*right*) supported 180° [32, 33].

2.5. Effect of Processing Condition and Material Properties on Seal Performance

Achieving a good seal performance cannot be attained without understanding the effects of processing conditions and material characteristics on seal properties. Therefore, previous studies on the effects of these parameters will be reviewed in this section.

2.5.1. Effect of Processing Parameters

The main sealing process parameters that affect seal performance are sealing temperature, dwell time, sealing pressure and delay time. Effect of these parameters on seal properties will be discussed in detail below.

2.5.1.1. Effect of Sealing Temperature

Previous researchers showed that temperature is a critical parameter in heat sealing and needs to be carefully adjusted to achieve a good seal performance. All previous studies that investigated effect of temperature on seal strength observed similar trends in which seal strength increased by increasing sealing temperature and reached a plateau at higher temperatures [2, 38-46]. Considering these results, Stehling and Meka [9, 32] established some important points in the seal strength curve that are shown in Figure 2.12 .

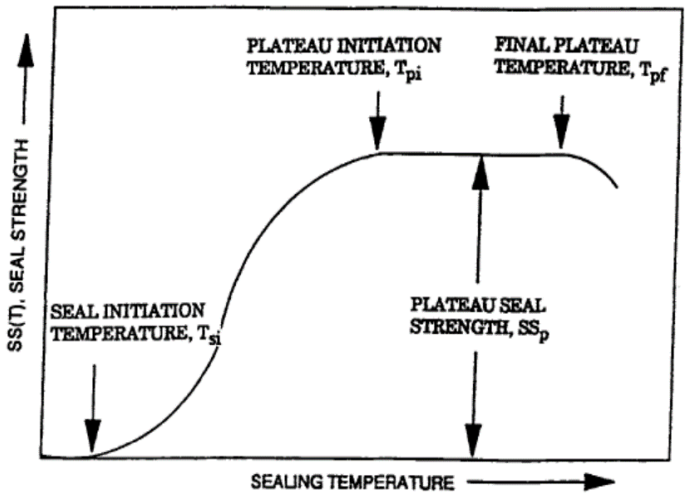

Figure 2.12 General curve of seal strength versus sealing temperature. The arrows show important points in the curve [9, 32].

The points shown in previous figure can be defined as:

(1) The seal initiation temperature (T_{si}): an onset temperature in which after that the seal strength begins to increase rapidly with temperature.

(2) The plateau initiation temperature (T_{pi}): the temperature where the seal strength reaches a plateau and does not change considerably by further increasing temperature.

(3) The final plateau temperature (T_{pf}): the temperature in which the seal strength begins to decay rapidly, and extensive seal distortion is observed.

These points have important practical implications. For example, from industrial viewpoint, a broad sealing range (which is defined as temperature range between T_{si} and T_{pf}) is an important parameter for a sealant material in industrial applications where peelable sealing is needed. This allows one to consider and compensate the variation of processing conditions such as temperature of jaws or humidity or food contaminations in industrial packaging plants[47].

The very high temperature ramp in heat sealing process and thin thickness of films cause difficulties in measuring temperature at the interface between seal sides. Therefore, in most previous studies, effect of jaw temperature on the seal performance was investigated instead of the effect of the interface temperature. Theller [8] examined LDPE cast co-extruded films and

HDPE/EVA-PB blown co-extruded films and showed that increasing jaw temperature increased the seal strength. He attributed these results to the increase in the energy level of chain ends and the free volume which enhanced the chain ends diffusion across the interface. When the temperature at the interface between seal sides reached the melting temperature of the sealant material, molecular diffusion across the interface was enhanced considerably which increased the number and strength of the links created between the interfaces. This finally created a fused interface which could not be peeled apart. He also found that the highest peelable seal strength could be obtained around the melting temperature of the sealant material which is in agreement with the results of Aithani et al. [39].

Based on the established points by Stehling and Meka [9, 32], Tetsuya et al. [38] showed that oriented polypropylene (OPP)/cast polypropylene (CPP) laminate films which were sealed below T_{si} (~ 110 ℃) showed a very low seal strength. The maximum seal strength in this system could be achieved by increasing temperature to 120℃ but further increase in temperature reduced the seal strength. Similar results were reported by Yuan et al.[35]. However, Morris [1] reported high seal strength at temperatures higher than melting point of sealants. Najarzadeh [46] also studied the effect of temperature on seal properties and concluded that a general optimum temperature cannot be defined as other process parameters and material characteristics also play a role in seal strength. Mazzola et al. [44] studied multilayer polyolefin films with different propylene-ethylene copolymers as the sealant layer and by using successive self-nucleation and annealing thermal analysis (SSA-DSC), they proposed a close relation between the temperature at which 40% of the polymer is molten and the seal strength. However, they did not present an explanation on why they selected temperature of 40% molten polymer as the main criterion in their correlation. Mueller et al. [48] studied effects of temperature on seal strength of LLDPE sealant films in the range of 100℃ to 130℃ and observed a rapid increase in the seal strength by increasing the sealing temperature from 115℃ to 125℃ (Figure 2.13).

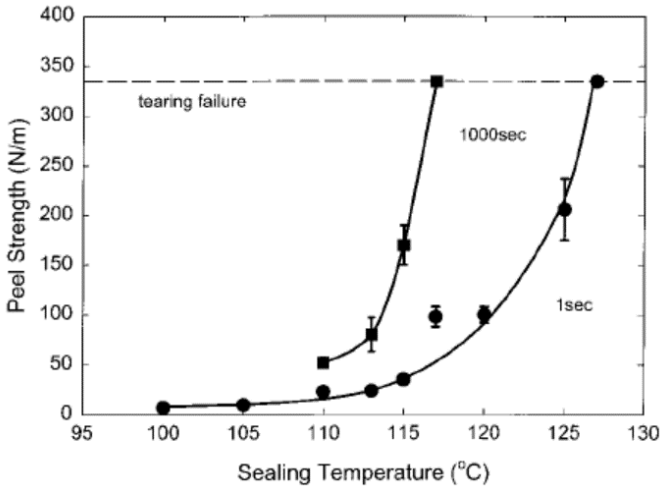

Figure 2.13 Seal strength versus sealing temperature for a LLDPE sealant for different dwell times [48].

In order to understand the observed sealing behavior, they studied the morphology of the peeled surfaces at different temperatures (Figure 2.14) and observed a shift in the surface morphology from small, isolated fractured fibrils for the samples sealed below 115℃ to a membrane-like connected pattern in the samples sealed at 120 ℃ and 125 ℃.

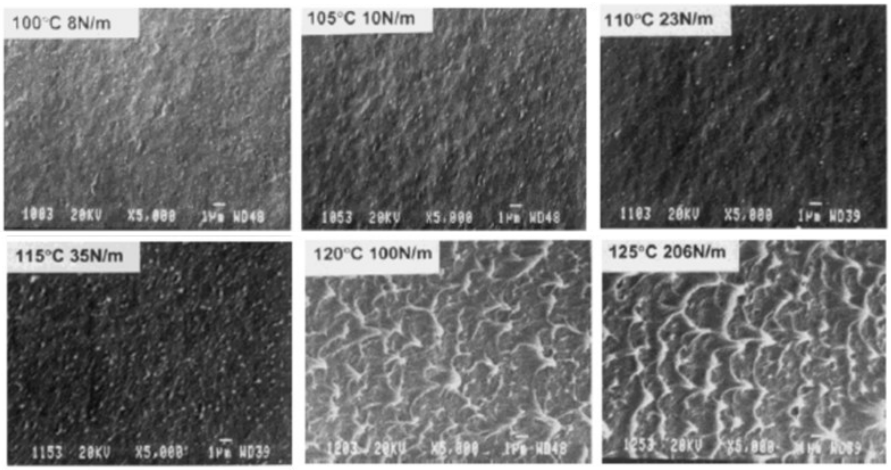

Figure 2.14 SEM images of peeled films at dwell time =1s. seal temperature and obtained seal strength are shown on each image [48].

They also found that increasing temperature below 115℃ increased the fibril density which was related to increasing chain diffusion across the interface. Increasing temperature above 115℃ led

to a significant improvement in the diffusion and increasing of highly deformed surface morphology. Najarzadeh and Ajji [46] also studied the topography of the peeled surfaces of LLDPE films sealed at different temperatures using AFM and SEM (Figure 2.15) and found that increasing sealing temperature, increased the number of micro-fibrils or bridges between the surfaces.

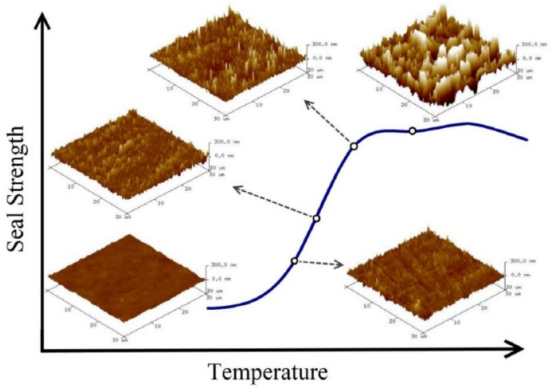

Figure 2.15 AFM images showing the effect of sealing temperature on the morphology of peeled surfaces that were sealed at dwell time= 0.5 s and pressure =0.5 N/mm^2 [46].

The effect of sealing temperature on hot tack of polymer sealants has also been studied in the literature. Figure 2.16 shows an example of hot tack curve of different sealants reported by Mesnil et al. [49].

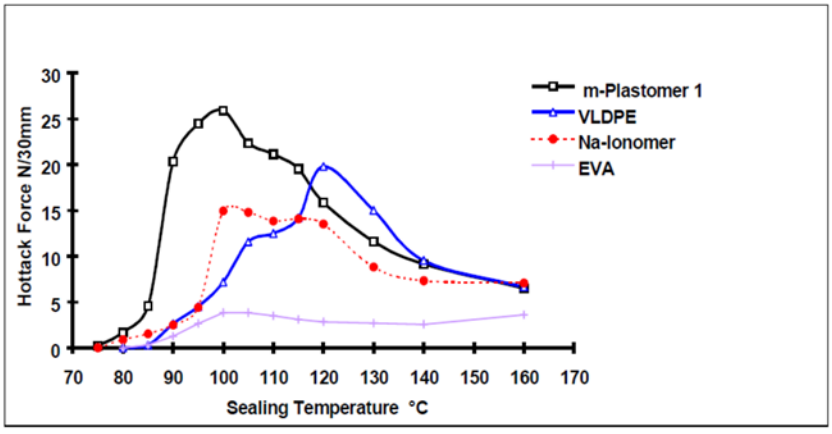

Figure 2.16 Hot tack at different sealing temperature for metallocene plastomer (m-plastomer), very low density polyethylene (VLDPE), Sodium ionomer (Na-ionomer) and ethylene vinyl acetate (EVA) [49].

It has been shown that by increasing sealing temperature, hot tack strength increased until reached a maximum and then decreased again [30, 49-56]. The observed decrease in hot tack at higher temperature has been attributed to the easy pull out of polymer chains at high temperatures which results in poor hot tack strength [2].

As discussed in section 2.3.4.2, the interdiffusion time to reach to the diffusion length at which the interface between two sides of the polymeric sample can be considered as healed, depends on Rg. Therefore it is worth mentioning that, in amorphous polymers, the effect of temperature on Rg is similar to the effect of temperature on polymer molar volume ($Rg/Rg_0 \sim v/v_0$) [19]. However, in semi-crystalline polymers such as Polyethylene, establishing a relation between Rg and temperature below melting temperature is challenging due to polymer crystallinity. Above the melting temperature of polymer crystals, the same behavior as of amorphous polymers can be expected, which indicates that Rg dependence on temperature should be similar to that of molar volume. Figure 4.7 shows the variation of density (~1/v) of polymers with temperature. As can be seen, the variation of density of polyethylene above their melting temperature is not significant. Jia-Ye et. al. [57] used molecular simulation to examine the effect of temperature on Rg of single short polyethylene chains in melt state and showed that Rg did not change considerably with temperature below polymer degradation temperature. Therefore, the variations of Rg above the melting temperature of polymers should not be considerable (which is in line with other studies [58-60] and the inter-diffusion length required to achieve seal strength should be independent of temperature. However, it should be noted that Rg still depends on MW and MW distribution of polymers [19], therefore, a single value cannot be used for polymers and each case needs to be examined individually.

2.5.1.2. Effect of Dwell Time

During the dwell time, two phenomena should occur to achieve good seal or hot tack strength [8]: (i) the interface between seal layers should reach the temperature that allows chain ends to diffuse across the interface, (ii) Brownian motion of the chain ends across the interface should occur with a length scale large enough to create entanglement. Increasing dwell time increases the seal or hot tack strength by increasing interface temperature and diffusion depth of the polymer chain ends [56]. On the other hand, increasing dwell time above certain period does not improve considerably the seal strength as the interface temperature approaches the jaw temperature and the diffusion

length becomes comparable to critical length scale required for entanglement [35]. Therefore, an optimum dwell time that ensures strong seal while allowing high production rate needs to be determined for any desired application. It has been well established in the literature that increasing the sealing temperature reduces the required dwell time to reach high seal strength [9, 32, 35, 38, 46, 61]. This indicates that a combination of sealing temperature and dwell time can provide a powerful designing tool to control and optimize seal properties. Yuan et al. [35] showed that in two layers laminated films of oriented polypropylene (OPP)/ cast polypropylene (CPP), increasing dwell time at temperatures below seal initiation temperature(T_{si}=122℃) did not have a considerable effect but above this temperature, the effect of dwell time was considerable, Figure 2.17. They also found that the effect of dwell time became negligible (even at temperatures above T_{si}) after reaching plateau seal strength.

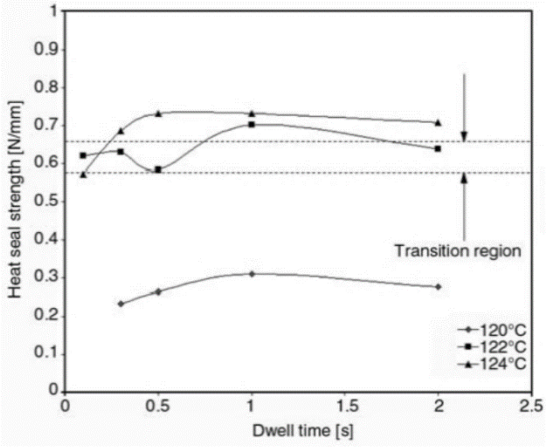

Figure 2.17 Seal strength of OPP/CPP film versus dwell time at different jaw temperatures. Seal initiation temperature for the sealant was 122^{o}C [35].

Also, as can be seen in Figure 2.13, Mueller et. al. [48] observed very low seal strength up to 115 ℃ when dwell time is 1second, but higher dwell time (1000s) shifted the increasing point of seal strength to lower temperatures, and based on the reptation model, they proposed a linear relation between seal strength and square root of dwell time (Figure 2.18). This relation was confirmed later by Qureshi et al. [28] and Najarzadeh and Ajji [46].

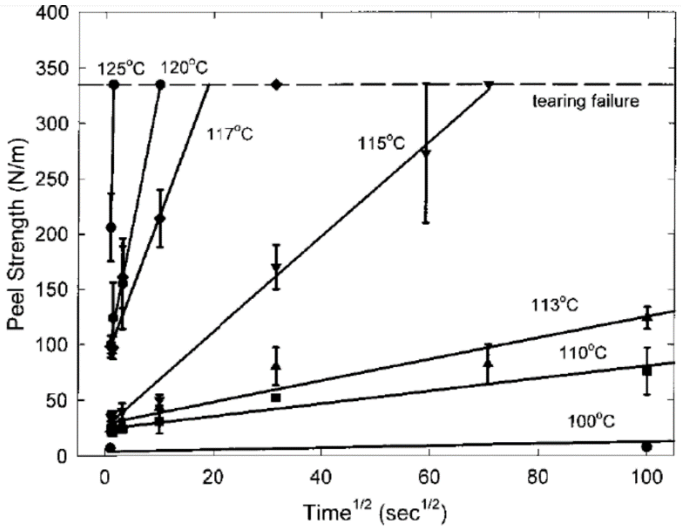

Figure 2.18 The linear relation of peel strength and $t^{1/2}$ proposed by Mueller, for different temperatures [48].

Najarzadeh and Ajji [46] plotted a 3D graph (Figure 2.19) to show the combination effect of dwell time and temperature on seal strength and found a strong dependency of seal strength on these two parameters. They found that there is an optimum region of dwell time and temperature which results in the highest seal strength (orange colour region in Figure 2.19).

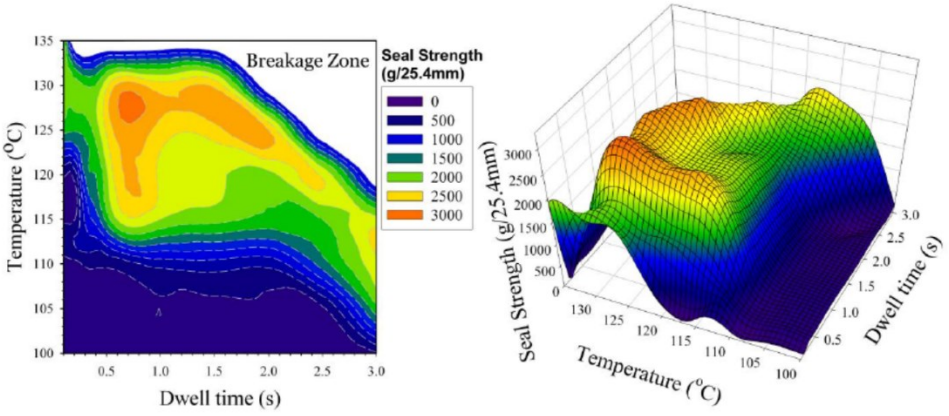

Figure 2.19 2d (left) and 3D (right) plot of seal strength versus different temperatures and dwell times [46].

Dwell time has been shown to have a similar effect on hot tack as dwell time effects on molecular diffusion of chains across the interface is similar to seal strength [2, 62, 63].

2.5.1.3. Effect of Sealing Pressure

Theller [8] showed that sealing pressure is needed to bring seal layers to close contact and overcome micro-roughness between surfaces. The applied pressure improves contact area and wetting and enhances chains diffusion across the interface. He also observed that increasing pressure from 0.27 MPa to 2.75 MPa changed slightly the seal strength of HDPE films but did not have a considerable effect on the seal strength of LDPE films. He finally concluded that the effects of dwell time and sealing temperature are much important than sealing pressure. This conclusion has also been reported by other researchers [7, 9, 32, 35, 41, 46]. It has been mentioned that excessive pressure may squeeze out the molten fraction of material from the seal area and distort the seal [46]. A minimum required pressure has also been reported which below that, no seal strength could be attained. It should be mentioned that this minimum pressure limit depends on the material, film thickness and surface roughness of the films and a general limit cannot be presented [7].

Najarzadeh and Ajji [46] presented a 3D graph which shows the relation between pressure, temperature and seal strength of metallocene PE films. The orange region in Figure 2.20 shows the optimum pressure and temperature that resulted in the highest seal strength. They found that a minimum pressure of 0.2 MPa at temperatures below 125℃ was needed to achieve good seal strength while at higher sealing temperatures, this limit disappeared. They also found that increasing pressure to a high value of 3 MPa allowed a reduction in the temperature range in which they could observe the high seal strength. The observed reduction in seal strength at high seal pressure was attributed to the squeeze out of the film at high pressures. Similar effect of sealing pressure has been reported for hot tack [62, 64-66] with a minimum pressure required to ensure the contact between the films during heat sealing

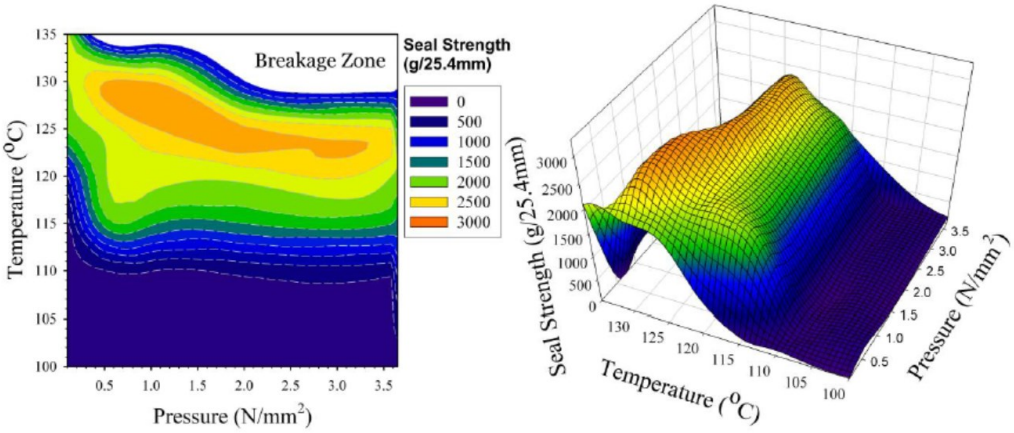

Figure 2.20 2D Countour (left) and 3D plot (right) of seal strength at different sealing pressure and temperature for metallocene PE films. Sealing was done at dwell time of 0.5 s [46].

2.5.2. Effect of Material Architecture and Crystallinity

Previous studies in the literature highlighted the important effects of molecular architecture and crystallinity on seal properties of sealant materials. Therefore, the effect of these parameters will be reviewed in detail in this section. It should be noted that crystallinity is not controlled only by material characteristics, also film preparation condition can affect it, but as film preparation parameters are out of the scope of this work, their effects will not be reviewed in this section.

2.5.2.1. Effect of Molecular Architecture on Seal Perforamnce

Previous studies showed that increasing the molecular weight (MW) of the sealant material increased the plateau seal strength, but also increased the seal initiation temperature (T_{si}) [2, 9, 48, 54, 67]. In a previous study, Najarzadeh [2] selected three metallocene linear low density polyethylenes (m-LLDPE) with different molecular weights, narrow molecular weight distribution (MWD) and almost identical branch densities. She found that increasing MW increased both hot tack strength and seal initiation temperature (Figure 2.21 (left)). She also reported a linear relation between the maximum hot tack strength and molecular weight (Figure 2.21, right). The observed effect of MW on seal properties can be attributed to the higher entangelments of polymer chains by increasing their MW [68].

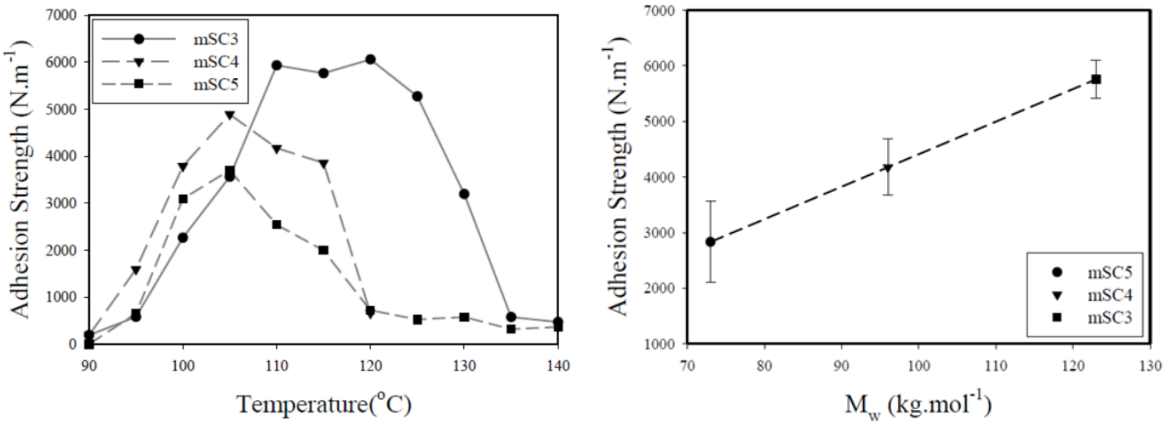

Figure 2.21 (Left) the effect of molecular weight on the hot tack or adhesion strength of metallocene short chain branched linear low density polyethylene. (Right) Liner relationship between maximum hot tack strength and MW. MW of mSC3, mSC4 and mSC5 are 123, 96 and 73 kg.mol^{-1}, respectively [2].

Before discussing the effect of chain branching on seal properties, it is worth mentioning the nomenclature that is commonly used to refer to branching in polyethylene. There are two types of chain branching in polyethylene: long chain branches (LCB) and short chain branches (SCB). If MW of branches is greater than critical entanglement molecular weight (M_e) (which is around 2800 g/mol or 100 c-c bond length [69]), the branch is considered as a long chain branch [46]. Branches with lower MW than this critical value, are considered as small chain branches. Branching can also affect the crystallinity of polymers which will be discussed in the next section. Najarzadeh and Ajji [2, 70] studied effect of branching on the hot tack of a conventional polyethylene with broad MWD and two metallocene long chain branched ethylene α-olefin copolymers with narrow MWD. Table 2.1 summarizes the molecular characteristics of the materials studied in their work. Their hot tack results are also shown in Figure 2.22.

Table 2.1 Molecular characteristics of branched PEs studied by Najarzadeh and Ajji [71].

Type	**Code**	**Mw (kg/mol)**	**MWD**	**LCB density (1/10^4 C atoms)**	**SCB density (1/10^4 C atoms)**
Conventional LDPE	LDPE	160	8.75	5.2	-
Metallocene LLDPE	mLC1	115	2.6	0.19	2.4
Metallocene LLDPE	mLC2	115	2.1	0.3	3.7

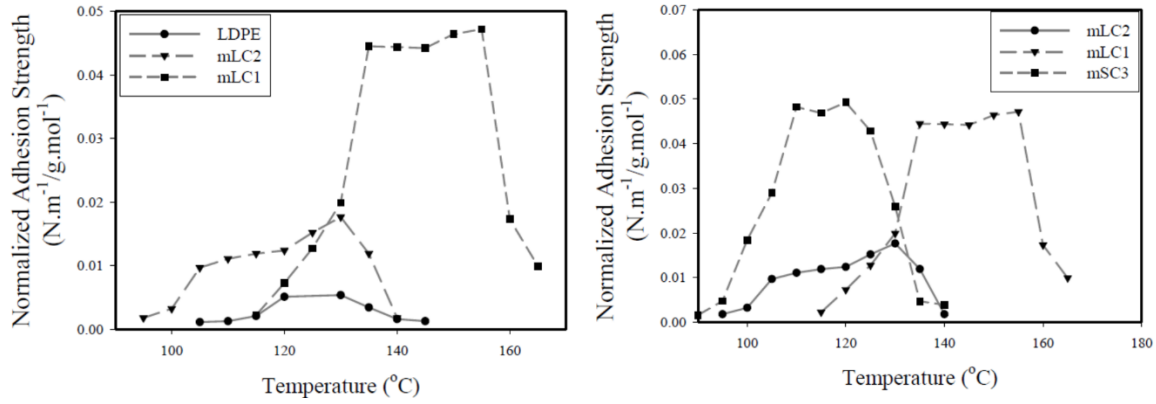

Figure 2.22 *left*, adhesion strength or hot tack normalized by Mw versus seal temperature for a conventional LDPE, and two metallocene LLDPE. *Right*: comparing normalized adhesion strength of LCB metallocene LLDPEs with SCB metallocene LLDPEs. (mSC3 had a Mw of 123 kg/mol and SCB density of 2.5 (1/10000 C atom)) [2].

As can be seen in Figure 2.22(left), increasing the density of long chain branches from 0.19 to 0.3 (per 10^4 C atoms) reduced significantly the hot tack strength. Further increase in the LCB density to 5.2 (in conventional LDPE) caused very poor hot tack properties. These results indicate that the presence of LCB increases seal initiation temperature and reduces significantly hot tack strength. Similar effects of LCB on hot tack was reported by Moreira et al. [56] for metallocene polyethylene. The effect of LCB on seal and hot tack strength can be attributed to much difficult chain diffusion in the presence of LCB due to the increased entanglement density with the surrounding chains [72]. As shown in Table 2.1, the SCB branching densities of mLC1 and mLC2 are different, therefore, Najarzadeh and Ajji also compared their hot tack results with the hot tack results of a short chain branched polyethylene and their results are presented in Figure 2.22 (right). As the SCB densities of mSC3 and mLC1 are almost identical, comparing the results of these two samples can clearly show that LCB retarded the diffusion due to an increased hindrance of LCB on molecular motion.

The observed differences between seal performance of metallocene PE and conventional PE have motivated some researchers to understand the origin of these differences. Previous researchers reported surface segregation in conventional polyethylene films in which an amorphous layer composed of highly branched and low molecular weight chains exist at the surface [25, 28, 73-75]. The observed segregation at the surface is attributed to the entropic gain due to presence of

low molecular weight chains at the surface. Moreover, the presence of highly branched copolymers increases significantly the chain end density at the surface which reduces the surface energy by increasing surface entropy [28]. During heat sealing of conventional PE films, the low molecular weight fraction in the segregated layer can diffuse rapidly but they cannot provide seal strength due to the lack of entanglement formation. The highly branched fraction of the segregated layer requires long dwell times to diffuse. Both phenomena believed to cause the poor seal properties of conventional PE films. These results clearly highlight the importance of high degree of control on molecular weight and branching density distribution in achieving high seal properties.

In addition to the effect of branching and MW on seal performance, few works studied effect of monomer sequences in ethylene α-olefin copolymers. Moreira [56] tried to find a relation between ethylene sequence in LLDPE and seal properties by defining a new parameter which they called the welding power. Thy ran hot tack tests at dwell times between 0.2-2 s and then plotted force/25 mm as a function of the dwell time. The welding power then was defined as the initial slope of this curve at dwell times between 0.2-0.5 s. They reported that increasing the ethylene dispersity (which means shorter ethylene sequences in LLDPE chains) decreased the seal initiation temperature by reducing the melting temperature.

2.5.2.3. Effect of Crystallinity on Seal Properties

During the heat sealing cycle and after opening the heated jaws at the end of dwell time, the sealed area begins to cool down due to the heat transfer to the surrounding environment. Cooling of the sealed area in semi-crystalline polymers can be considered as a non-isothermal crystallization process. In semi-crystalline polymers, crystallization can occur mainly between melt temperature (T_m) and glass transition temperature (T_g) [69]. Crystal nucleation and growth are the two main steps required for the formation of a new ordered solid crystalline phase within an existing disordered melt phase. These steps are mainly affected by material characteristics and external factors. For example, molecular order and cooling rate have been shown to considerably alter the crystallization [76]. At temperatures close to T_m, nucleation rate is slow due to the low thermodynamic drive which originates from high entropy of the chains at high temperatures. The nucleation rate increases by decreasing the temperature. On the other hand, crystal growth, which is controlled by molecular diffusion, is faster at higher temperatures. The opposing effects of temperature on nucleation and growth steps results in a maximum crystallization rate at a certain

temperature between T_m and T_g which is known as the crystallization temperature (T_c), Figure 2.23. This indicates the complexity of studying non-isothermal crystallization compared to isothermal crystallization (in which the temperature remains constant during crystallization).

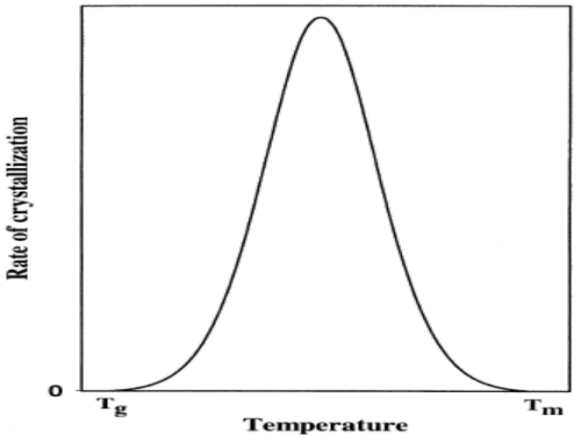

Figure 2.23 Schematic showing the crystallization rate versus temperature in non-isothermal crystallization of semi-crystalline polymers [77].

Crystallinity of sealant affects both seal and hot tack properties as increasing their crystallinity increases their melting temperature and retards chain diffusion. After sealing, re-crystallisation of diffused chains during delay time increases seal and hot tack strength. For example, Stehling and Meka [9] studied sealing behavior of 42 different types of sealants including m-LLDPE, LLDPE, HDPE, LDPE, very low density PE (VLDPE), PP and ethylene vinyl acetate (EVA). They estimated the amorphous fraction at any temperature, $f_a(T)$, using dynamic scanning calorimetry (DSC) and the following equation

$$f_a(T) = 1 - \left[\frac{\Delta H_S - \Delta H_T}{\Delta H_U}\right] \quad \text{Eq. 2.4}$$

where ΔH_T, ΔH_S and ΔH_U are the cumulative heat of fusion at temperature T, the total heat of fusion of the sample and the heat of fusion of 100% crystalline polymer, which is 293 J/g for polyethylene [78].

They found that for semi-crystalline polymers, amorphous fraction at sealing temperature has a significant effect on seal strength and concluded that seal initiation temperature occurs when amorphous fraction reaches 77%. By comparing the graphs shown in Figure 2.24 (left) and (right),

it can be seen that seal initiation temperature corresponds well with the temperature in which the amorphous fraction reaches around 80%. In addition, a broader distribution of f_a as a function of temperature results in broader transition region between seal initiation temperature and seal plateau. Similar results and conclusions were reported by Najarzadeh et al. [46].

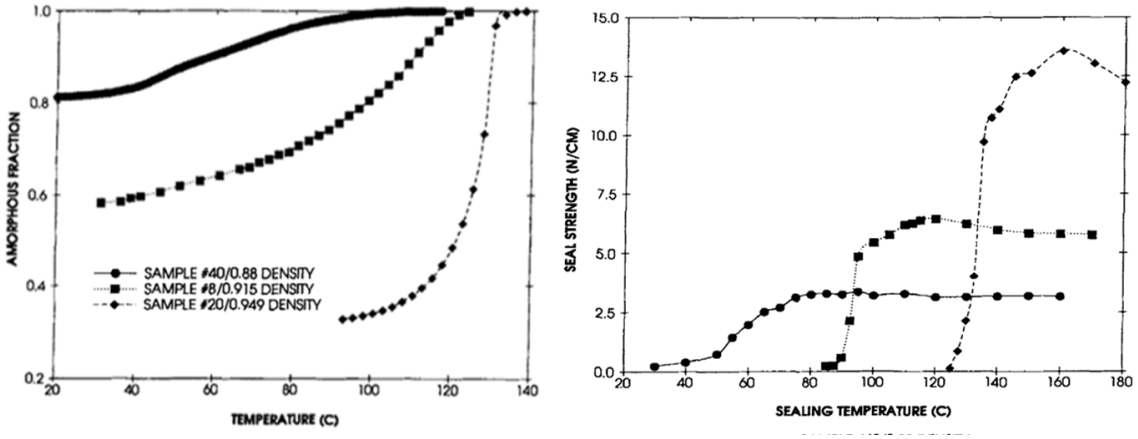

Figure 2.24 *Left*: Amorphous fraction versus temperature of, very low density PE (sample #40, ●), m-LLDPE (sample #8, ■), and HDPE (sample #20, ◆). *Right*: seal curve of the samples shown in left with the same symbols [9].

Based on the obtained results, Stehling and Meka presented a schematic to show the relation between amorphous fraction and the shape of the sealing curve in a semi-crystalline polymer which is shown in Figure 2.25.

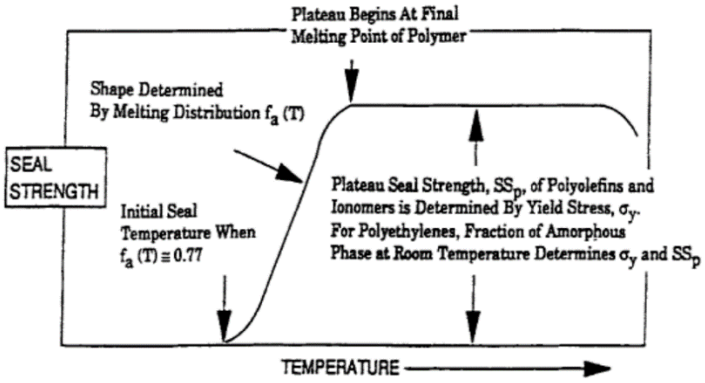

Figure 2.25 A schematic showing the proposed relation by Stehling and Meka between seal properties and the amorphous fraction(or amount of crystallinity) [9].

The addition of high molecular weight fractions to increase amorphous fraction of sealant materials has been examined by some researchers as a method in improving seal properties of highly crystalline polymers. For example, Miyata et al. [79] compared the wide angle x-ray scattering (WAXS) pattern and dynamic scanning calorimetry (DSC) scans of HDPE blends with different amounts of high molecular weight HDPE (HMW HDPE) before and after heat sealing. Their results showed that the addition of less than 10% of HMW HDPE reduced crystallinity and crystalline orientation and enhanced seal strength. Some researchers also showed that the addition of low crystalline ethylene-based copolymers such as EVA or plastomers reduced seal initiation temperature and increased seal strength by reducing the crystallinity of polyethylene matrices [67, 70, 80, 81]. Moreira et al. [56] attempted to establish a relation between Avrami crystallization rate and seal properties and concluded that good seal properties could be obtained when the Avrami crystallization rate at the sealing temperature was greater than 0.2. Nicastro et al. [82] studied crystallinity of PP during heat sealing and its effect on seal strength. By comparing crystallinity of films before and after heat sealing, they found that crystallinity of PP films increased from 38% for the film before sealing to 50-56% after cooling of the sealed area. By comparing seal strengths of film samples with different crystallinity, they found a linear relation between seal strength and crystallinity of the film, Figure 2.26.

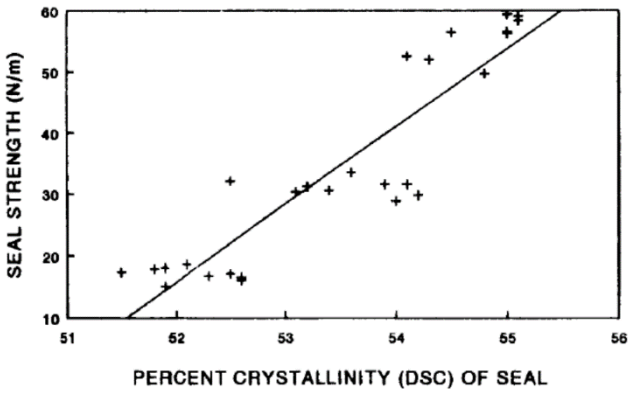

Figure 2.26 Seal strength as a function of crystallinity percentage in the film [82].

The observed different effect of crystallinity in the previous studies can be related to the complex effect of crystallinity on the seal properties of polymer films. Low crystallinity level enhances melting and diffusion during sealing while high crystallinity can provide higher seal strength after cooling of the seal.

2.6. Multicomponent sealant films

As mentioned before, multicomponent sealant films have been introduced as a solution to provide a balance between seal properties and cost when using expensive sealant materials such as metallocene PE. Considering the previous studies in the literature on this subject, multicomponent sealants can be categorized as (i) single layer films composed of a multicomponent polymer blends[70, 83-85], (ii) multilayer films with a single polymer in each layer [42, 86-88], and (iii) multilayer films with a mixture of different polymers in some or all layers [41, 64, 80, 89-91]. In this part, a summary of the previous works in the literature on sealing properties of multicomponent sealant films will be discussed.

2.6.1. Polyethylene-based Polymer Blends as Sealant Materials

Among different polyethylene-based blends, blends of different types of polyethylene and blends of polyethylene with EVA have received much attention. Therefore, previous works on these two blend systems will be reviewed in this section.

2.6.1.1. Thermodynamic of Polyethylene-based Polymer Blends

As any other blend system, when we talk about a polymer blend, the first aspect that needs to be examined is the miscibility of the components. Miscibility of polymer blends has been discussed in detail in the literature [69] and therefore, we will briefly review the concepts here. The thermodynamics of mixing in binary polymer mixtures can be examined using the Gibbs free energy of mixing:

$$\Delta G_m = RT\chi_{AB}.\varphi_A\varphi_B + RT\left[\frac{\rho_A\varphi_A \ln \varphi_A}{Mw_A} + \frac{\rho_B\varphi_B \ln \varphi_B}{Mw_B}\right] \qquad \text{Eq. 2.5}$$

Where, ΔG_m is the Gibbs mixing energy, χ_{AB} is the Flory-Huggins interaction parameter, φ_i is the volume fraction of the polymer components, ρ_i is the density of polymers, and Mw_i is the molecular weight of the polymer components. The first term on the right side of this equation shows the enthalpy of mixing, ΔH_m, according to Hilbrand-Scatchard-van Lard theory. The terms in the brackets represent the combinational entropy of mixing based on Flory-Huggins lattice theory. Considering the Gibbs free energy of mixing, binary polymer blends can be categorized into three main groups: (i) miscible polymer blends: where $\Delta G_m < 0$ and $\frac{\partial^2 \Delta G}{\partial \varphi^2} > 0$ over the full

composition range; (ii) partial miscible polymer blends in which $\Delta G_m < 0$ but $\frac{\partial^2 \Delta G}{\partial \varphi^2} < 0$ in some compositions; (iii) immiscible polymer blends where $\Delta G_m > 0$ over the full composition range. In miscible polymer blends, both components are miscible down to the molecular scale while in immiscible polymer blends, two separate phases of polymers are formed in which each phase consists of only one component. In partially miscible systems, two phases are formed but each phase is a miscible mixture consisting of both polymer components.

In the case of polyethylene/EVA mixtures, previous studies reported that when the VA content in EVA is between 9 to 18 wt.%, the blend is a partially miscible blend [81, 92-97]. In a detailed study, McEvoy and Krause [98] examined miscibility of EVA with different VA content from 9 to 45 wt.%. At VA ≤ 18 wt.%, they observed a trans-crystallization zone between HDPE or LDPE and EVA phase, Figure 2.27. They found that further increasing VA% to 27% disappeared the trans-crystallization region. They estimated the Flory-Huggins interaction parameter and showed that at VA ≤9 wt.%, both HDPE and LDPE should be miscible while greater VA contents can lead to phase separation. These results show that in the case of miscibility of PE and polyethylene copolymers, the comonomer content plays a critical role in miscibility of blends.

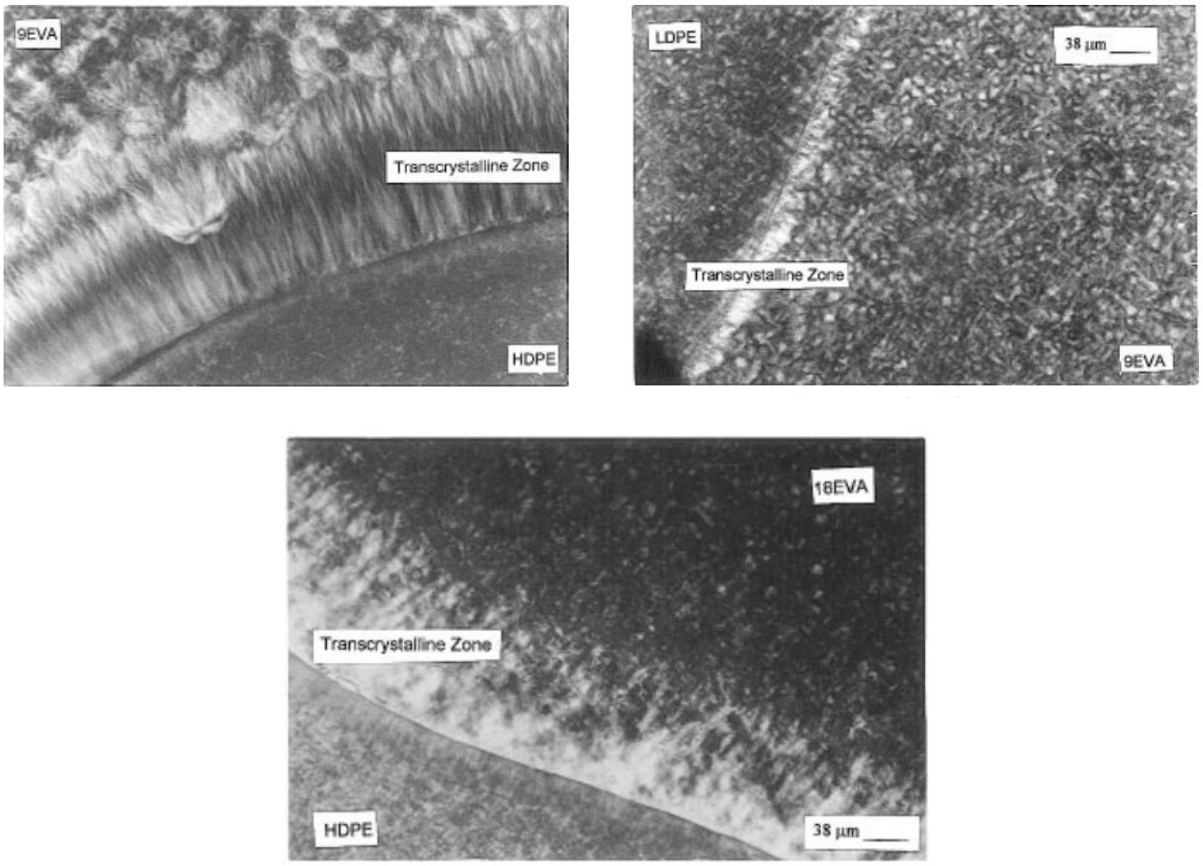

Figure 2.27 Optical microscopy images showing the trans-crystallization zone between HDPE or LDPE and EVA with VA ≤18% [98].

In the case of polyethylene/polyethylene blends, different techniques such as thermal analysis, spectroscopy analyses, rheological characterizations and microscopy techniques have been used to examine the miscibility of polyethylene mixtures, but the high level of similarity between phases in these mixtures makes the analysis of miscibility very dependant on the molecular characteristics and cooling condition from melt [99, 100]. For example, Hameed and Hussein [101] examined effect of MW and branching density on miscibility of m-LLDPE/HDPE blends and found that in the solid state, increasing MW and branching density of m-LLDPE did not alter the miscibility of the blend while in the melt state, increasing MW or branching density reduced miscibility of the mixture. Generally, it has been shown that reducing cooling rate from the melt state, increasing Mw, and increasing branching density reduce the miscibility of polyethylene pairs [101-108]. However, different threshold for observing the immiscibility for each of these parameters have been reported in the literature which avoid setting a general framework for polymer-based blend

miscibility. For example, Hussein [108] reported a threshold of branching density of 13 (CH3/1000 C) for miscibility of LLDPE and HDPE, while the same research group reported no branching density dependency in their later work on another LLDPE/HDPE blend [101].
Therefore, despite the high compatibility of polyethylene pairs, their miscibility state needs to be examined for any specific pair and condition.

2.6.1.2. Seal Performance of Polyethylene-based Blends

Poisson et al. [41, 80] showed that using blends of EVA and PE in the sealant layer of a three-layer film with the structure of Polyamide/tie/(PE/EVA blend) improved seal strength compared to the film with only PE as the sealant. They observed that increasing EVA content up to 50 wt.% reduced seal initiation by 15°C. Moreover, the addition of EVA increased the sealing window from 10°C for the neat PE sealant to 25°C in the sample with 50% EVA. Najarzadeh et al. [83] also examined seal properties of LDPE/EVA blends and found that the EVA content did not have a considerable effect on sealing properties up to 40% EVA but at higher EVA contents, the seal properties was improved considerably, Figure 2.28.

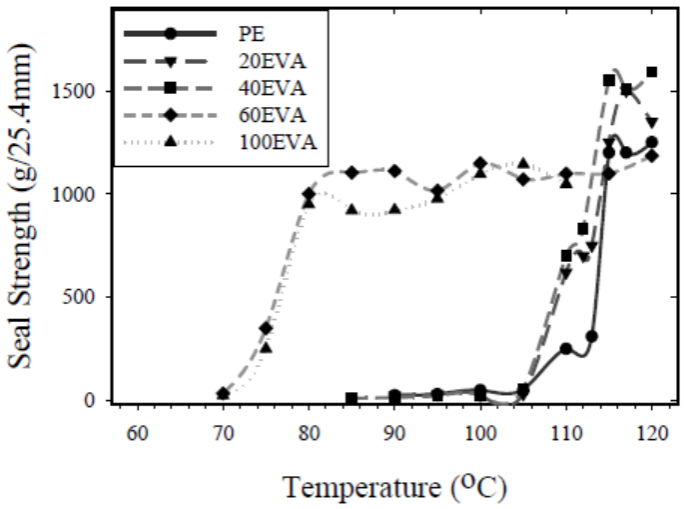

Figure 2.28 Seal strength as a function of sealing temperature for PE/EVA blends with different compositions [83].

They also found that the addition of EVA reduced the yield strength of the blend and at EVA contents above 60%, EVA became the continuous phase and a significant reduction in the yield strength of the blend was observed. Halle [54] examined the effect of blending plastomers with

metallocene very low density polyethylene (m-VLDPE) on seal strength and hot tack. As seen in Figure 2.29 (Top), he showed that blending m-VLDPE with plastomer reduced the seal initiation temperature but did not affect the seal plateau strength. The decrease in seal initiation temperature was attributed to the decrease in the crystallinity and density of the sealant layer. Moreover, as can be seen in Figure 2.29 (Bottom), blending m-VLDPE with plastomer could shift hot tack maximum temperature toward lower temperatures and, at the same time, increased the hot tack peak strength.

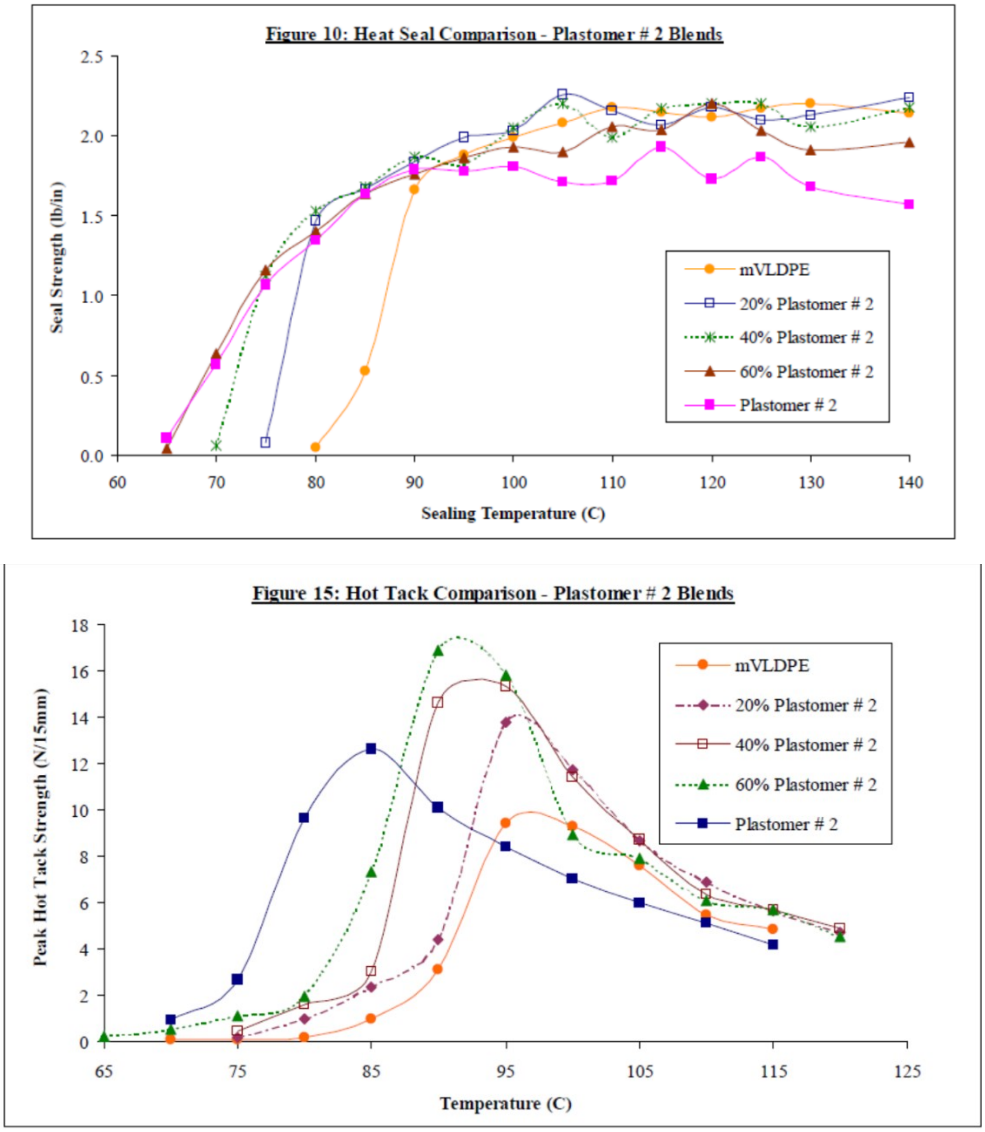

Figure 2.29 Top: effect of blending m-VLDPE with plastomer (Exact 8201, Exxon) at different compositions of plastomer on seal curve of m-VLDPE. Bottom: effect of blending m-VLDPE with different plastomer compositions on hot tack curve of the m-VLDPE [54].

Najarzadeh et al. [70] studied seal properties of blends of LDPE or Ziegler-Natta LLDPE (Zn-LLDPE) with metallocene LLDPE(m-LLDPE) or metallocene long chain branched PE (LCB-m). Their DSC results showed co-crystallization between different PE which they attributed to a high compatibility level between examined pairs. Their hot tack results are presented in Figure 2.30. The addition of m-LLDPE or long chain branched metallocene polyethylene (LCB-m) shifted hot tack curves toward lower temperatures except in the blend of LDPE/LCB-m. This can be explained by considering the melting temperature order of these materials: m-LLDPE<LDPE<LCB-m<Zn-LLDPE. Therefore, the addition of LCB-m to LDPE results in formation of crystals with higher melting temperature than the neat LDPE and shifted hot tack curves toward higher temperatures. In the studied pairs, the addition of m-LLDPE or LCB-m to either Zn-LLDPE or LDPE led to an increase in the maximum hot tack and broadening of the hot tack curves. These results indicate that the addition of metallocene polyethylene to conventional PE is a promising approach in improving hot tack and increasing the breadth of the hot tack window.

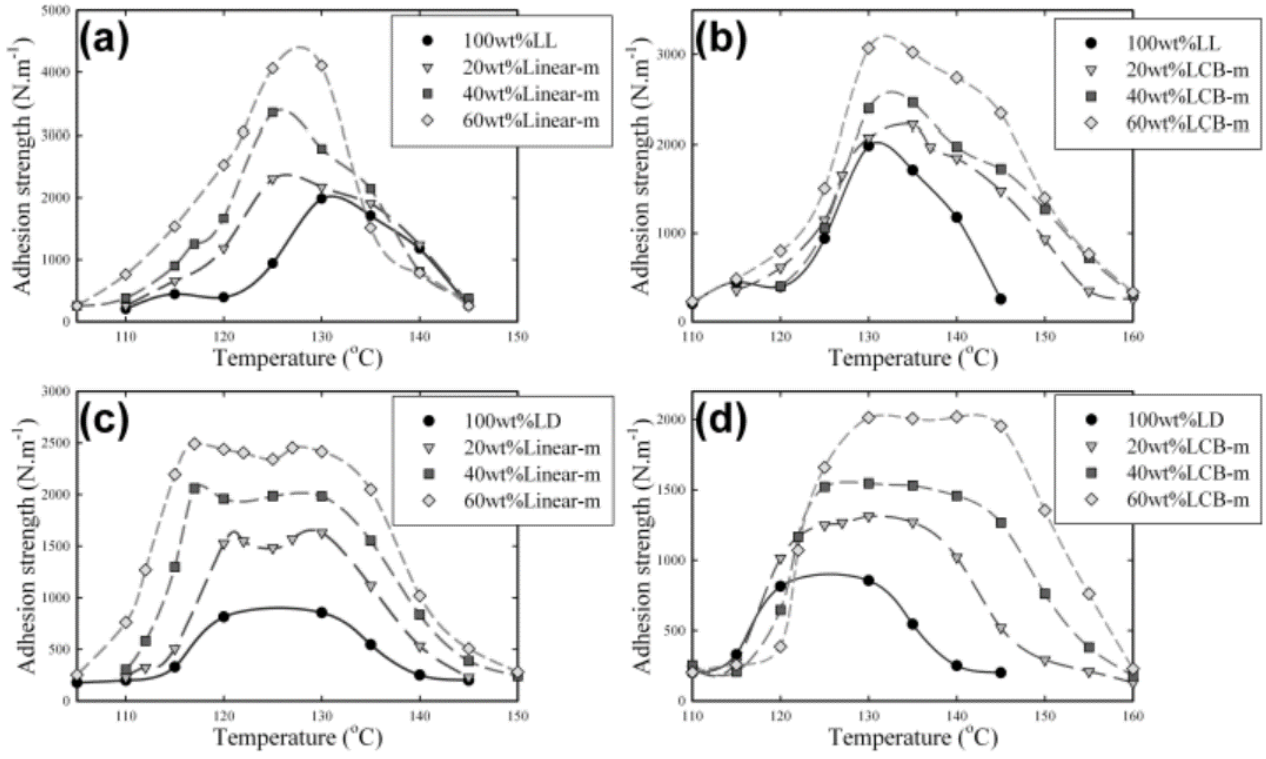

Figure 2.30 Hot tack curves of (a) LLDPE/ linear-m (b) LLDPE/LCB-m (c) LDPE/m-LLDPE(Linear-m) (d) LDPE/LCB-m blends with different metallocene copolymer composition [70].

Th maximum hot tack strength of the blends are shown in Figure 2.31. In both Zn-LLDPE and LDPE matrices, the best improvement in hot tack was observed when linear metallocene PE was added to the matrix. However, in all cases, blending of metallocene PE with conventional PE led to a significant reduction in their maximum hot tack strength.

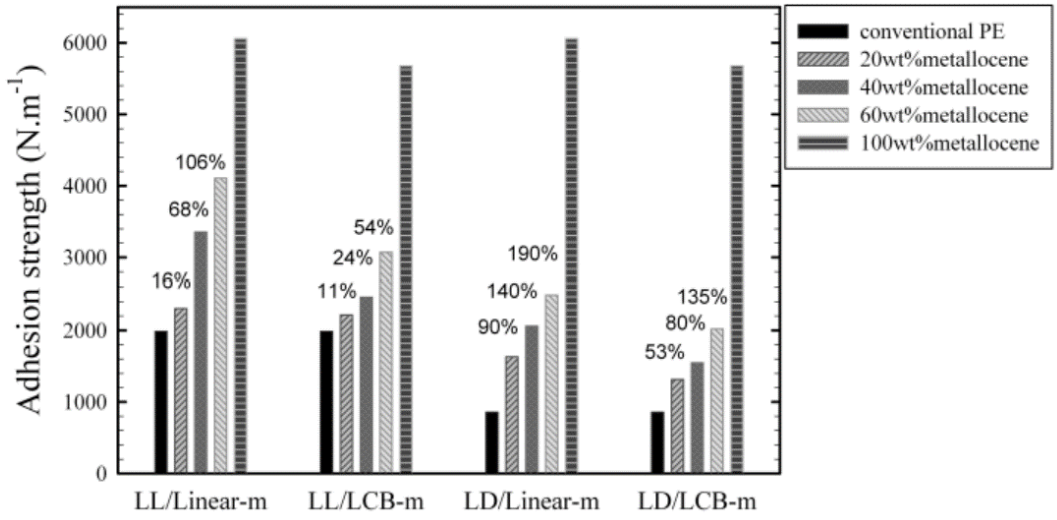

Figure 2.31 Maximum interfacial self-adhesion (or hot tack) of the blends, the numbers on top of the columns indicate the percentage of increase in respect to conventional PE [70].

Shih et al. [55] reported that the blends of m-LLDPE and LDPE (70/30 wt%) had higher hot tack than film of LDPE or m-LLDPE. They attempted to explain the reported higher hot tack than neat m-LLDPE using fracture mechanics, but their results can be explained by considering the fact that the authors only examined hot tack in temperature range of 100-115 ^{o}C which was below the melting peak temperature of m-LLDPE (120^{o}C). Sierra et al. [64] also examined the effect of addition of metallocene polyethylene (mPE) on heat sealing properties of LDPE and found that by increasing mPE content from 10 to 33%, the seal plateau initiation temperature (T_{pi}) reduced from 125^{o}C to 110^{o}C but the plateau seal strength did not change. They also examined the hot tack of the blends but as their hot tack evaluation method was not according to ASTM (they reported length of sealed area opened under 50 g force), comparing their results with other studies is not possible. They also ran DSC on the film samples, but their DSC results showed one melting peak at LDPE melting temperature which was not affected considerably by changing mPE content. On the other hand, their Tg measurements by DSC showed one Tg that changed by mPE composition and the measured Tg values were not in-line with Tg of a miscible blend of mPE and LDPE. The

authors concluded high compatibility of the polymers but did not explain the controversy in their DSC results. They also tried to find the optimum wt.% of mPE based on seal performance and cost and concluded that the addition of 15 wt.% mPE provided the best balance between performance and cost. Lamnawar et al. [84] studied sealing of LLDPE/cyclic olefin copolymer (COC) blend films to a neat LLDPE film. The blend samples were prepared in a very wide range of 10 μm film to 1 mm thick sheet. The authors used sealing temperature of 145ºC and dwell time of 0.8 s but did not report the thickness of the film or the sheet they used in sealing experiments. The concluded that the addition of only 5% COC led to peelable behavior. However, the authors used a seal width of only 1.5 mm and did not report seal force of neat LLDPE to LLDPE with this seal width. Therefore, there is a chance that the observed peelable behavior could be due to the sealing parameters and thickness rather than material characteristics.

2.6.2. Multilayer Sealant Films

Previous authors have shown that multilayer films offer better processability and mechanical properties compared to single layer films composed of blends with the same composition as of the layer ratio in multilayer films [109-111]. For example, Taylor and Baik [109] compared physical and mechanical properties of a composite three-layer film of LDPE/LLDPE/LDPE (10/80/10) and a single film of LLDPE/LDPE(80/20) blend (Figure 2.32). The multilayer structure can clearly offer better properties especially in dart impact and machine direction tear resistance. In addition, as shown in the previous section, although blending of metallocene polyethylene with conventional PE can enhance sealing performance, but the obtained seal performance especially in hot tack tests is much lower than the pure metallocene. Preparing a multilayer sealant film has been shown to offer a combination of good sealing and lower price while maintaining high seal performance close to mPE. The multilayer sealant structure is composed of a thin mPE layer in the sealant side to benefit from the superior seal performance of mPE and has one or more back-layers to provide mechanical properties and reduce the final cost of the film.

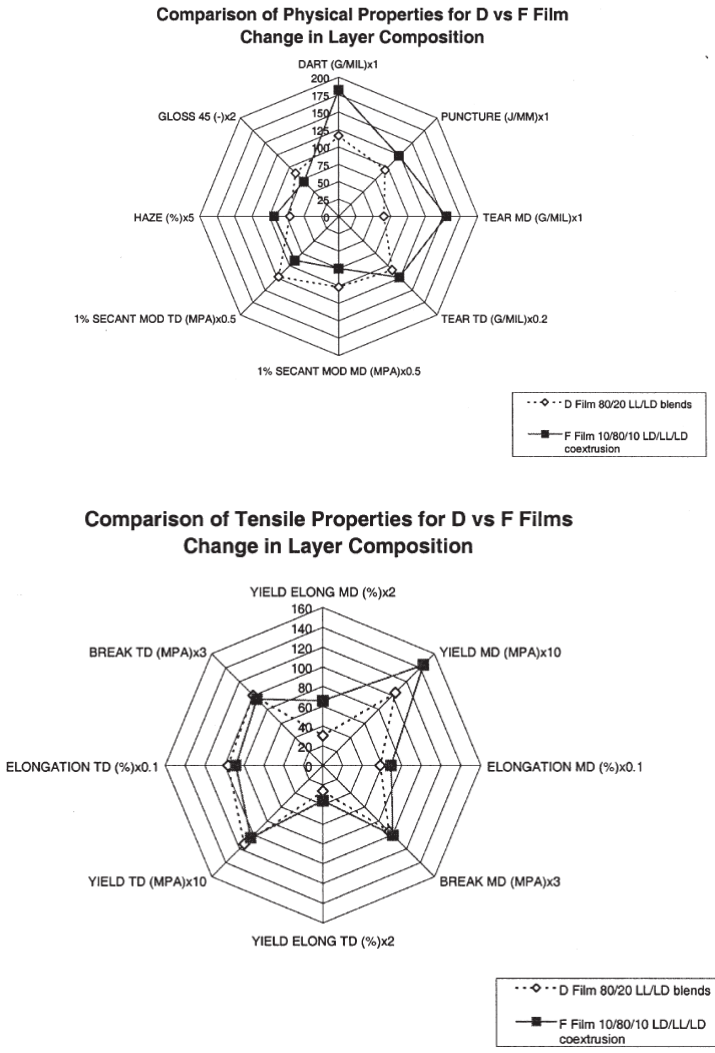

Figure 2.32 Comparing properties of symmetry composite film of LDPE/LLDPE/LDPE (10/80/10) with a single layer film of LLDPE/LDPE (80/20) blend. Both film had a thickness of 27.5 μm [109].

Viganò [112] studied ten different structures (listed in Table 2.2) to evaluate the effect of back-layer composition on hot tack strength. Different comonomers are shown as C4, C6 and C8 which correspond to butane, hexane and octane comonomers, respectively. He produced 3-layer co-extrusion polyethylene sealant films with different compositions at the thickness of 40μm. Finally, all PE films were laminated to an oriented polyamide substrate as the support layer using an adhesive layer. His hot tack results are shown in Figure 2.33.

Table 2.2 structures and compositions of 3-layer co-extrusion sealants with the layer thickness ratio of 1/2/1. Red texts show different material and composition which is used in each layer in comparison to sample 1 which was used as the reference structure [112].

	A - sealing side	B - middle	C - lamination side
1	90/10 C6-mLLDPE/LDPE	60/40 C6-mLLDPE/LDPE	90/10 C6-mLLDPE/LDPE
2	90/10 C6-mLLDPE/LDPE	60/40 C4-LLDPE/LDPE	90/10 C6-mLLDPE/LDPE
3	90/10 C6-mLLDPE/LDPE	60/40 C6-mLLDPE/LDPE	100 LDPE
4	90/10 C8-VLDPE/LDPE	60/40 C6-mLLDPE/LDPE	90/10 C6-mLLDPE/LDPE
5	90/10 C8-LLDPE/LDPE	60/40 C8-LLDPE/LDPE	90/10 C8-LLDPE/LDPE
6	90/10 C8-mLLDPE/LDPE	60/40 C8-mLLDPE/LDPE	90/10 C8-mLLDPE/LDPE
7	90/10 C6-mLLDPE/LDPE	70/30 C6-mLLDPE/HDPE	90/10 C6-mLLDPE/LDPE
8	90/10 C6-mLLDPE/LDPE	70/30 C4-LLDPE/HDPE	90/10 C6-mLLDPE/LDPE
9	90/10 C8-LLDPE/LDPE	70/30 C8-LLDPE/HDPE	90/10 C8-LLDPE/LDPE
10	90/10 C8-mLLDPE/LDPE	70/30 C8-mLLDPE/HDPE	90/10 C8-mLLDPE/LDPE

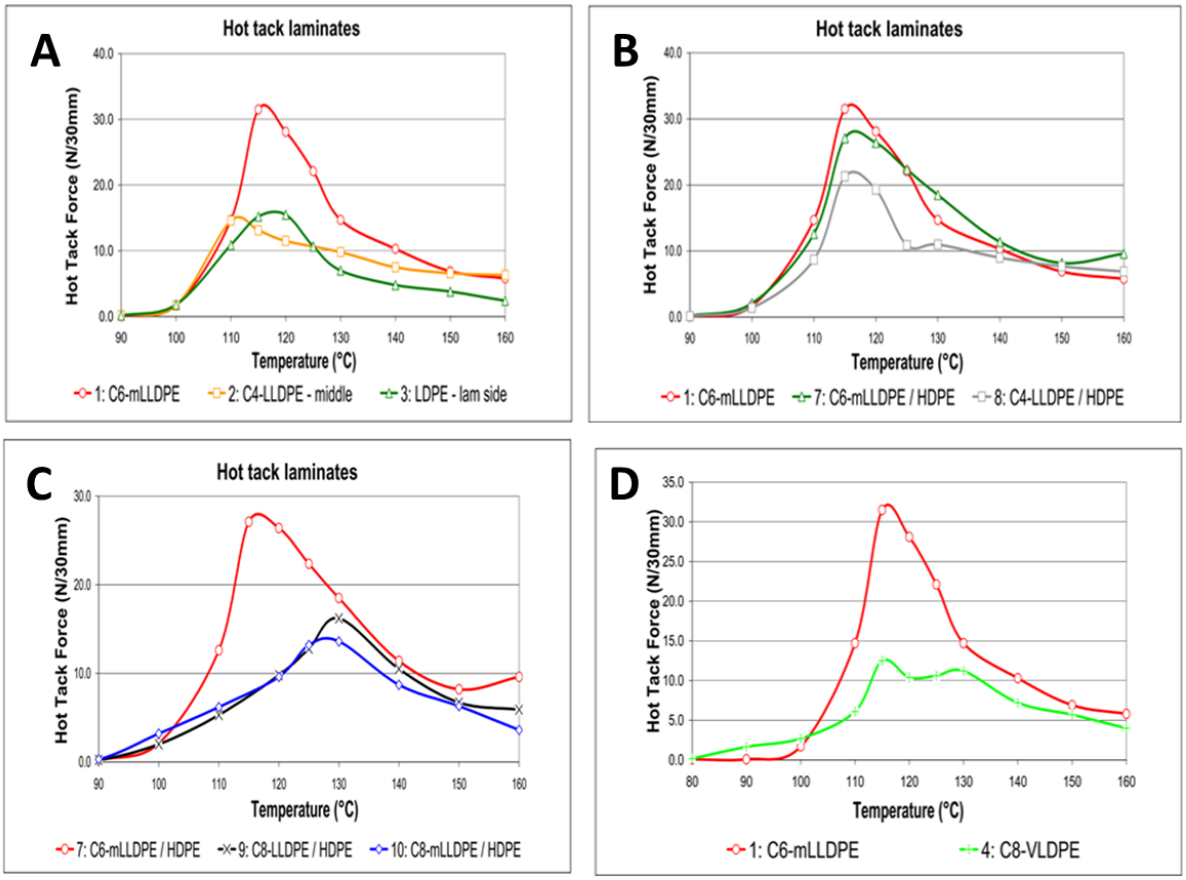

Figure 2.33 Comparing hot tack curves for different sealant film structures shown in Table 2.2 [112].

He showed in Figure 2.33(A) that by replacing C6-mLLDPE with C4-LLDPE in the middle layer, hot tack decreased significantly, and peak position shifted toward lower temperatures. By comparing sample 1 and 7 in Figure 2.33(B), he found that replacing LDPE by HDPE in the middle layer decreased hot tack values but as can be seen, film 7 has also less C6-LLDPE in the core which could also affect hot tack. In the same figure, replacing C6-LLDPE with C4-LLDPE in the middle layer reduced the hot tack strength. Based on the results in Figure 2.33(C), he observed that replacing C6-LLDPE with C8-LLDPE and C8-mLLDPE in all 3 layers reduced hot tack value and moved the maximum peak toward higher temperatures. This can be due to the higher melting temperature of C8-LLDPE compared to C6-LLDPE. Finally, replacing C6-mLLDPE with C8-VLDPE in the sealing side, (Figure 2.33(D), reduced dramatically hot tack strength. He concluded that sealant film design affects significantly sealing performance and replacing C6-mLLDPE with other polymers in any layer had a negative impact on hot tack. While this work has interesting information about the effect of structure of multilayer films on hot tack, due to some important weaknesses such as the lack of information regarding microstructure of polymers (for example branch density, MW, MWD), lack of information regarding miscibility of polymers (because they used blends of polymers in each layers), changing couple of parameters at the same time (for example changing both polymers and compositions or changing polymers in more than one layer), analysing the obtained results and finding the origin of the observed effects is complicated.

2.7. Modeling of Heat Sealing Process

As can be seen so far, many parameters can affect heat sealing and seal properties of sealant films. This indicates the need for finding the optimum processing conditions in heat sealing processes. In the large industrial scale, finding the optimum condition with trial and error causes extra cost and produces considerable amount of plastic waste. Predicting seal performance of sealant materials without doing time consuming and expensive trials is a very interesting approach that can reduce the optimization cost in heat sealing. In this part of the literature review, previous works on modeling and optimization of different aspects of heat sealing will be reviewed.

2.7.1 Modeling of Heat Transfer in Heat Sealing

In the first step of heat-sealing process, when films are pressed together by the heated jaws, it is essential for interface between seal sides to reach the melting temperature of the sealant material.

Determining the time in which the interface reaches this temperature is critical to optimize the sealing temperature and dwell time. Due to the difficulties in measuring the interface temperature between seal sides, in many studies jaw temperature is considered as the sealing temperature which can be very different from the real interface temperature. Some researchers tried to predict the interface temperature based on jaws' temperature using heat transfer models. For example, Meka and Stehling [32] attempted to model the heat transfer in heat sealing using finite element analysis (FEA). They considered a constant thermal conductivity of polymers and convective heat transfer between the heated jaw and surface of the film. They used the convective heat transfer coefficient as the fitting parameter to fit the model predictions with experimental data. To measure the interfacial temperature, they placed a fine copper/Constantin micro-thermocouple with a diameter of 25 μm between two 150 μm thick LDPE films and then sandwiched PE films between 25 μm Mylar polyester films and placed this assembly between heated jaws. By Changing the convective heat transfer coefficient in their model, they found that the model predictions for the interfacial temperature depends strongly on the heat transfer coefficient (h) between hot jaws and the Mylar layer (Figure 2.34, left). When the jaw temperature was below the melting temperature of LDPE sealant film, they found a good agreement between experimental data and modeling results (Figure 2.34, Right).

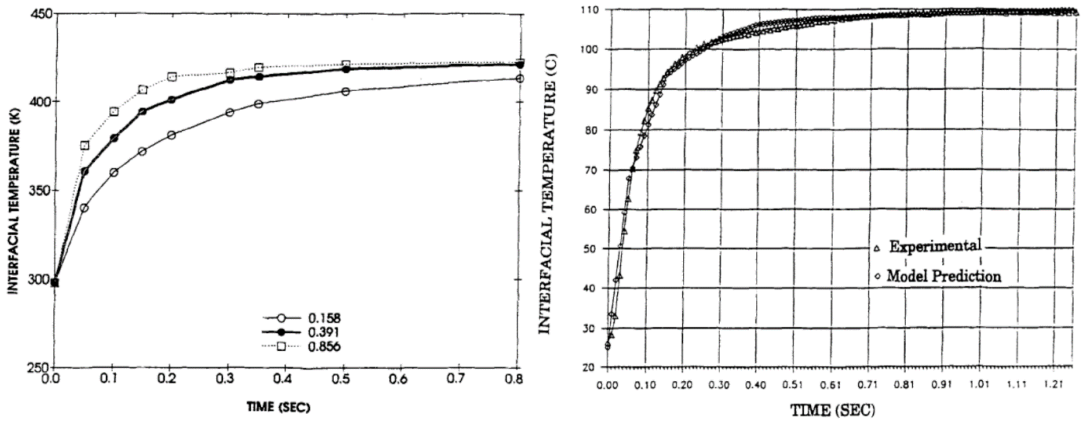

Figure 2.34 (Left) interfacial temperature versus dwell time predicted by FEA model at three different connective heat transfer coefficients at sealing temperature of 150℃. (right) comparison of model predicted and experimentally obtained interfacial temperature at sealing temperature of 110℃ using 0.391 W/cm^2 K as the heat transfer coefficient (melting point of the polymer is 118℃) [32].

However, at temperatures above the melting temperature of the sealant, they observed deviations between experimental data and their model predictions, Figure 2.35, which they attributed to neglecting the endothermic heat of fusion of polymers in their model and thinning of the polymer films during heat-sealing process due to squeezing out of polymers from the seal section.

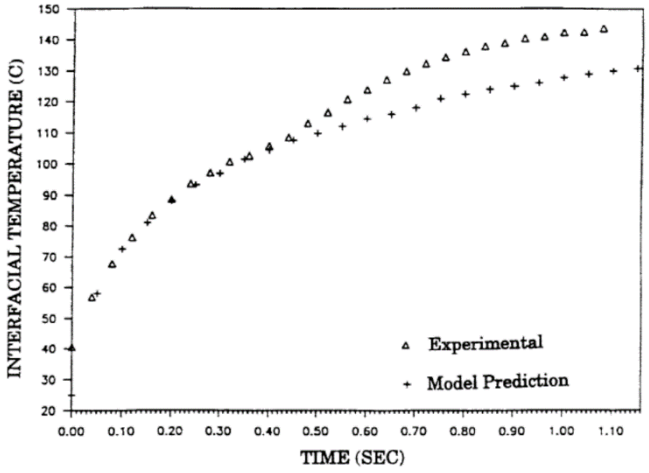

Figure 2.35 Comparing the interfacial temperature calculated by Meka and Stehling model and their experimental results at sealing temperature of 150℃ [32].

They concluded that proper selection of heat transfer coefficient (h) and thermal conductivity (k) as well as considering the heat of fusion of polymers can result in a better prediction. Although the authors did not glue the Mylar film to PE film, they consider the interface between these two films as a perfect interface which could introduce error in their model predictions. In addition, the authors did not report any properties related to Mylar film and it seems that the presented FEA model only considered the PE films in heat transfer. These parameters could considerably affect their model predictions. For example, the observed discrepancy between predicted and measured interface temperature above melting temperature of LDPE film can be due to a change in the heat transfer mechanism between Mylar and LDPE film from convective to conductive heat transfer. This enhances the heat transfer and results in higher experimental temperature compared to the model prediction which is the case in above sealant melting temperature.

Mihindukulasuriya and Lim [88] also predicted interfacial temperature in sealing of LDPE film using COMSOL Multiphysics software. They determined specific heat capacity (Cp) of polymer at different temperatures using DSC analysis of LDPE films. They also assumed incompressible

material, fix boundaries and one-dimensional heat conduction among all layers to model interfacial temperature between sealant surfaces. They assumed heat convection between solid layers and used thermal contact resistant (TCR) (which is defined as 1/h) as the fitting parameter, Figure 2.36.

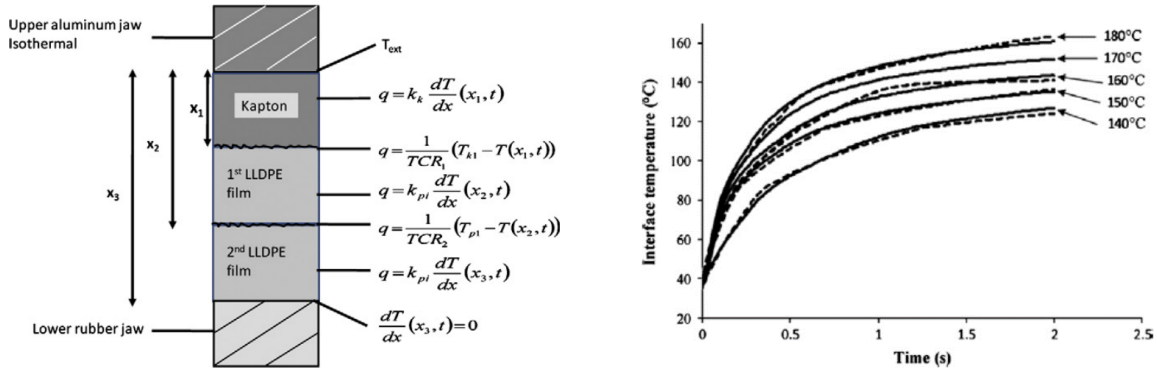

Figure 2.36 (left) Schematic of the layers and related boundary conditions and their equations. (right) Predicted interfacial temperature (dash line) and experimental data (solid line) versus time at different jaw temperatures [88].

They also reported that TCR between sealant layers are significantly affected by jaw temperature and this dependency is reduced at temperatures above sealant melting temperature (117°C -140°C). At these temperature range, phase change of polymer from solid to liquid allows chains to fill the micro-gaps between the layers and results in a shift in heat transfer mechanisms. The main drawback of their model is that they considered heat of fusion of LDPE as a step transition function and broke down the melting of LDPE into five regimes occurring at below 40, 40–87, 87–117, 117–140, and above 140°C rather than a smooth transition function. In addition, thermal conductivity, density and specific heat, suddenly changed from solid to liquid at the melting temperature of LDPE. These assumptions can explain the abrupt change in the slope of their predicted interfacial temperature compared to the measured interfacial temperature at the above-mentioned temperatures. In addition, the authors assumed the interface of the film with lower silicon jaw as an insulated boundary condition which is not necessarily a correct assumption and needs to be confirmed experimentally. Moreover, the authors mentioned they considered TCR between LDPE films but did not explain how they considered the transition from convective heat transfer to conductive heat transfer upon melting of LDPE layer.

The above-mentioned clearly indicate that the few previous heat transfer models of heat sealing are in fact fitting models which need experimental measurements of the interface temperature. This indicates the importance of a comprehensive model which can predict interface temperature based on the material properties.

2.7.2 Modeling of Squeeze Out Flow in Heat Sealing

When sealing temperature is close or above the sealant melting temperature, it is likely to expect squeezing out of the material from the seal area under the applied pressure. This can result in thinning of the seal section and can affect the heat transfer during sealing. Squeeze flow of liquids from the gap between solid surfaces has many applications in different fields. In the engineering field, motors, bearings and lubrication involve squeeze flow. The compression moulding of polymers is essentially a squeeze flow process. Valves and diarthrodial joints are examples for squeeze flows in biology and bioengineering. one of the applications of squeeze flow is in the field of rheology where a viscoelastic liquid is placed between two disks and then the top disk squeezes the liquid at a constant rate to squeeze out the liquid from between the disks. Squeeze out flow analyses can be done in two modes: (i) constant volume of the sample, or (ii) constant contact area between the sample and the solid surface. These two modes are schematically shown in Figure 2.37.

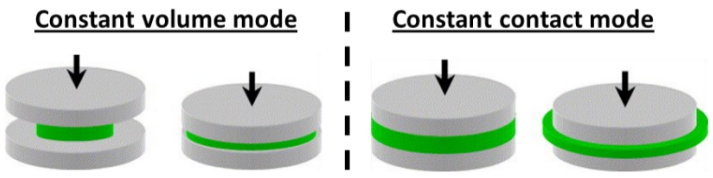

Figure 2.37 Two different modes of squeeze flow experiments: left) constant volume mode, right) constant contact area mode [113].

For a constant force (F) in the constant volume mode, Figure 2.37 (left), a Newtonian fluid with the volume of V and viscosity of μ, squeezes with a rate of [114] :

$$\frac{1}{H^4} = \frac{1}{H_0^4} + \frac{8\pi F}{3\mu V^2} t \qquad \text{Eq. 2.6}$$

For a constant force (F) in the constant contact area mode, Figure 2.37 (right), and a Newtonian liquid between two disks with the radius of R_0, the variation in liquid height can be explained by [115]:

$$\frac{1}{H^2} = \frac{1}{H_0^2} + \frac{4F}{3\mu\pi R_0^4} t \qquad \text{Eq. 2.7}$$

Squeeze flow model for different fluid behaviors have been reported in the literature, including Newtonian [116], Power-Law [115, 116], and Herschel Bulky liquids [113]. Most of the previous models have been developed for squeeze flow between parallel circular disks in cylindrical coordination and cannot be directly applied to heat sealing in which squeeze flow occurs between two rectangular parallel plates. This is due to the symmetry in circular disk geometry which makes obtaining an analytical solution much easier. Gupta [117] attempted to derive an analytical solution for a Newtonian fluid with kinematic viscosity of ν between two parallel rectangular plates separated by a distance (a) and approaching at a variable velocity of Vw(t). He considered velocity in both x- and y- directions and assumed a linear decency of V(x) in x-direction. By assuming that the variation of plates approaching velocity with time, Vw(t), is known, he obtained the following equation for the velocity dependency (f) in the thickness direction (shown as η in the equation):

$$f = f_0(\eta) + Rf_1(\eta) + R^2 f_2(\eta) + \ldots \qquad \text{Eq. 2.8}$$

where $\frac{av_w}{\nu} = R$ and,

$$f_0(\eta) = \frac{3\eta}{2} - \frac{\eta^3}{2}$$

$$f_1(\eta) = \frac{\eta^5}{10} - \frac{\eta^7}{280} - \frac{53}{280}\eta^3 + \frac{13}{140}\eta$$

$$f_2(\eta) = E_3\eta + \frac{E_1\eta^3}{6} + \frac{53}{1400}\eta^5 - \frac{579}{58\,800}\eta^7 + \frac{\eta^9}{2016} + \frac{\eta^{11}}{92\,400}$$

Here E_1 and E_2 were determined as constant values of -0.2892701 and 0.0196946, respectively. As the model is derived based on the assumption of a known approaching velocity function, $V_w(t)$, it can be seen that the final model is independent of the pressure gradient between plates.

Morris and Scherer [118] modeled squeezing flow of a Newtonian liquid between two rectangular plates held at a constant pressure. Their main assumptions were: (i) Newtonian fluid for polymer melt, (ii) isothermal condition, (iii) the lubrication assumption, and (iv) quasi-steady state condition, and (v) no slip conditions at the walls. Using these assumptions, they developed an equation for reduced height between plates as a function of time which indicates the volume of squeeze flow.

$$\frac{1}{h^2} - \frac{1}{h_0^2} = \frac{2Pt}{w^2\mu} \qquad \text{Eq. 2.9}$$

In this equation h, h_o, P, w,L and μ are the film thickness at any time (t), initial film thickness, applied sealing pressure, width of the jaw, length of the jaws and the viscosity of the polymer at sealing temperature. The percentage of squeezed out polymer then was determined from:

$$\%\ \text{Squeeze} - \text{out} = 100\ (h_0 - h)/h_0) \qquad \text{Eq 2.10}$$

Figure 2.38 shows the comparison between their experimental data and model prediction for heat sealing of a Plastomer and Ionomer with zero-shear viscosities of 37700 and 774000 Pa.s, respectively.

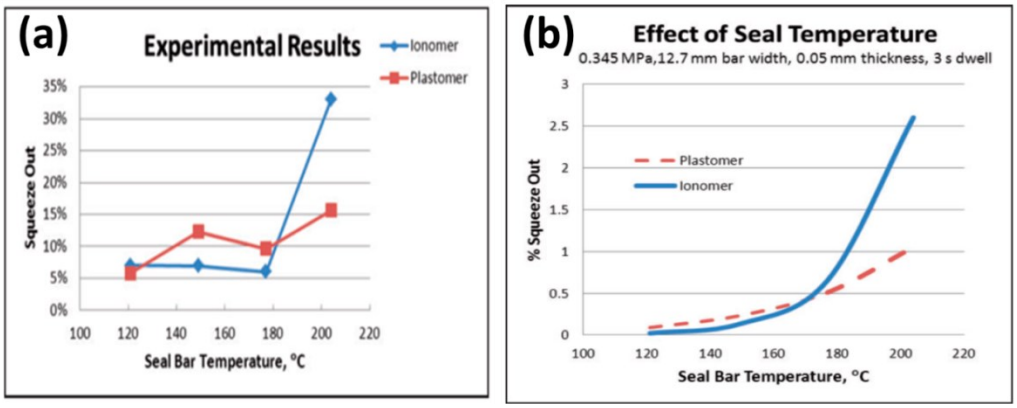

Figure 2.38 Percentage of squeezed-out material versus seal bar temperature for Ionomer and Plastomer at 0.345 MPa, 12.7mm bar width, 0.05mm sealant thickness, and 3 s dwell time: (a) experimental results (b) model prediction curve [118].

It can be seen that their model significantly underestimated the squeeze flow compared to the experimental results. They attributed the poor predictions of their model to the model limitations such as the assumption to Newtonian fluids and isothermal condition. However, by replacing the velocity profile they obtained into equations of motions, it can be seen that the presented velocity profiles do not satisfy the differential equations.

When much complicated fluid behavior was used for squeeze flow between parallel rectangular plates, it has been shown that the obtained non-linear differential equations do not allow achieving an explicit analytical solution and the velocity profile could only be obtained by numerical modeling [119-121]. For example, Shuler and Advani [119] studied squeeze flow in compression molding of a polymer/fiber laminate between two parallel rectangular plates. They used Carreau fluid model for rheological behavior and assumed the lubrication approximation and quasi-steady state assumption and obtained the following non-linear differential equation for the fluid flow between plates:

$$\frac{\partial}{\partial y}\left\{\eta_0\left[1+\left(\lambda\frac{\partial V_x}{\partial y}\right)^2\right]^{(n-1)/2}\frac{\partial V_x}{\partial y}\right\}=\frac{\partial P}{\partial x} \qquad \text{Eq 2.11}$$

Where η_o, λ, n, V_x and P are the zero-shear viscosity of fluid, the relaxation time, Power-law index of fluid, the velocity of the fluid in the x-direction and the pressure within the fluid, respectively. By considering a linear pressure gradient in the x-direction and assuming that the approaching

velocity of the plates is known, they used finite difference and modeled fluid flow by coupling the above equation with mass balance. They determined the pressure gradient across the plate lengths and by integrating the pressure profile, they estimated the force required to achieve the given plate approaching velocity. Figure 2.39 shows their experimental results and model predictions for force exerted on the plate with approaching velocity of 0.254 cm.min^{-1}.

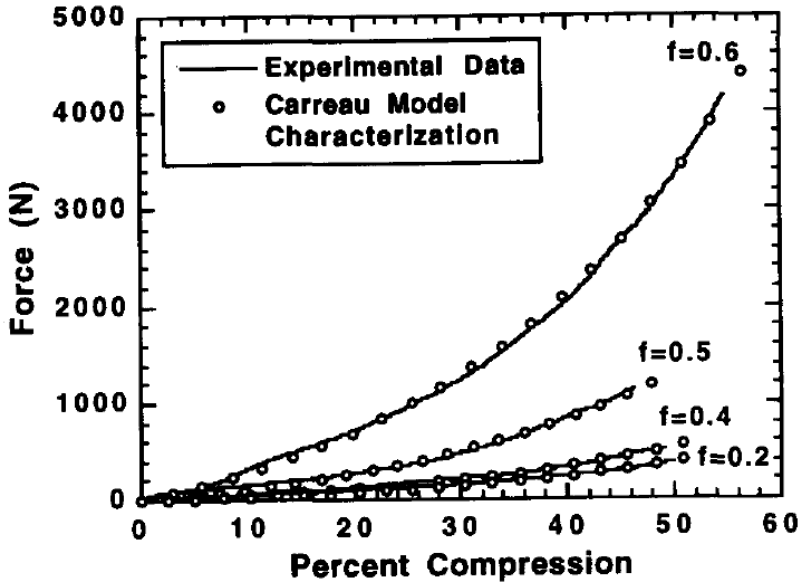

Figure 2.39 Comparing experimental results and numerical modeling results for the force required at an approaching plate velocity of 0.254 cm.min^{-1} as a function of percent compression. f indicates the fiber weight content of the laminate [119].

Despite their interesting results, as they assumed that $\frac{\partial P}{\partial x}$ varies in x-direction, it is expected that $\frac{\partial V_x}{\partial x} \neq 0$ which implies that the flow in the y-direction should have also been considered in the model to satisfy the continuity condition.

It can be seen that the complexity of analyzing squeeze flow in heat sealing due to the non-Newtonian behavior of polymer, caused this subject to be poorly studied in the literature and a comprehensive study on modeling of squeeze flow in heat sealing process is lacking in the literature.

2.7.3 Modeling of Seal Strength

In addition to modeling of a heat sealing process, some authors have attempted to present models to predict the seal strength. Seal strength is a result of intermolecular diffusion of polymer chains across the interface between two sealant layers. Therefore, determining the diffusion distance at which a seal reaches its highest strength is an approach to determine the required dwell time to reach the maximum seal strength. Morris [1] defined a dimensionless diffusion length called W* as:

$$W^* = \frac{W}{R_g} = \frac{4\sqrt{Dt}}{4\sqrt{Dt_d}} = \sqrt{\frac{t}{t_d}} \qquad \text{Eq 2.12}$$

Where W, R_g, D and t_d are diffusion depth at time t, radius of gyration of polymer chains, diffusion coefficient and terminal relaxation time of polymer chains, respectively. By assuming that the plateau seal strength occurs at a critical penetration depth (W_c) and using experimental data to find plateau seal strength in different temperatures and dwell times, he proposed a general value for critical dimensionless diffusion length as W_C^* =0.1. However, his results show that for ionomer films, the proposed W_C^* value over-predicts seal plateau and therefore generalization should be done with caution. Moffitt [122, 123] tried to predict seal properties by defining combination of multiple functions to consider the effects of amorphous content, interfacial wetting and chain diffusion. He considered the effect of amorphous content by defining the probability of forming an amorphous-amorphous contact at the interface as $P_{am}(T) = (1-X_c)^2$ where T is the temperature and X_c is the percentage of crystallinity. To describe the kinetics of wetting at the interface, he used nucleation model described by Wool and O'Connor[14] and finally chain interdiffusion was considered using the de Gennes model [124]. His model (called HEATSEAL) predicts relative fracture energy for peeling of the seal. He used Meka and Stehling [9] data to validate his model and mentioned that his model shows a strong influence of crystal melting distribution (Figure 2.40).

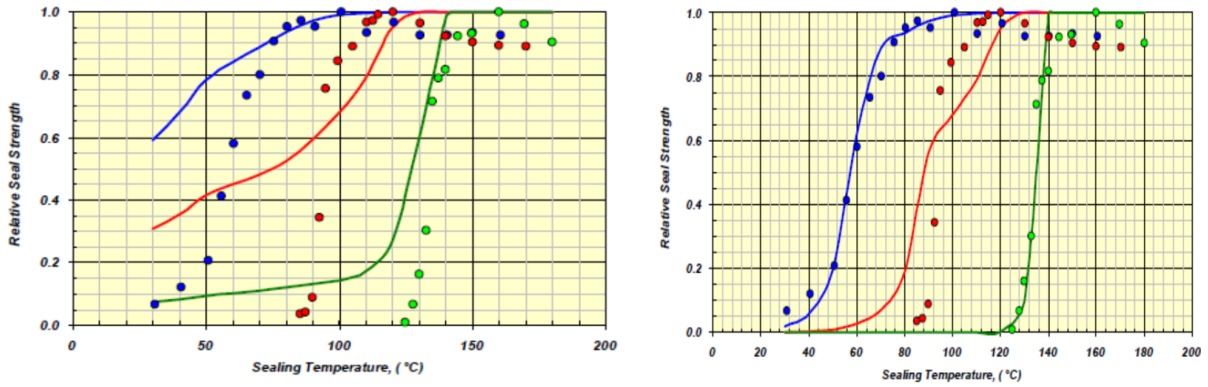

Figure 2.40 Relative seal strength of HEATSEAL model in comparison with Meka and Stehling's data[9] for LLDPE resins (with(●) 0.880 g/cm3, 2.0 MFI and (●) 0.915 g/cm3, 2.0 MFI) and HDPE resin (with(●) 0.949 g/cm3, 0.04MFI) versus sealing temperature. (*left*) Instantaneous wetting is assumed, (*right*) wetting rate is assumed as 62.5 s^{-1} [122].

He also demonstrated HEATSEAL model with some case studies [123] and concluded that a range of melt index between 2 to 10 dg/min for polyethylene resins are the most suitable to be used in packaging industries to minimize dwell time and maximize the production rate (Figure 2.41). However, an MFI below 2 g/10 min is also very common in blown film polyethylene due to the high melt strength required for processing.

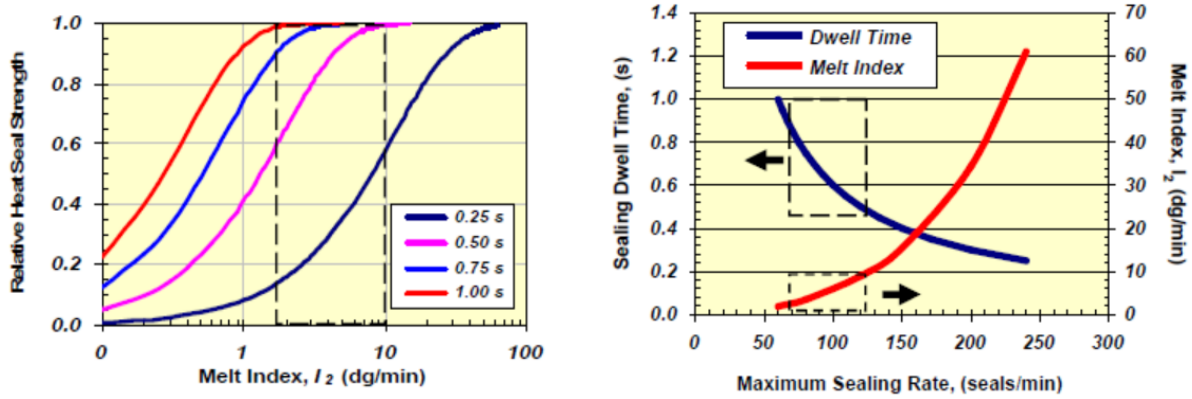

Figure 2.41 (*left*) relative seal strength versus Melt Index for LLDPE (0.915 g/cm^3) at different dwell times. Dashed line section shows preferred melt index operating range. (*right*) Maximum production rate (sealing rate) as a function of dwell time and melt index for LLDPE (0.915 g/cm3) computed by HEATSEAL model. Dash line sections are the preferred operating ranges [123].

2.7.4 Modeling of Hot Tack Strength

Shekhar[30] presented an empirical model for temperature dependency of hot tack strength evolution of ethyl methacrylic acid (EMA) and ethyl acrylic acid (EAA) copolymer using statistical regression of their hot tack data. By studying 17 copolymers and using Stratgraphics software (by STSC, Inc.) and doing multiple regressions, they reached the following empirical equation:

$$HT = EXP(c_1 + c_2T + c_3T^2 + c_4T^3 + c_5A + c_6AT + c_7AT^2) \quad \text{Eq 2.13}$$

Where HT is the hot tack strength (N/25.4mm), T is the seal temperature (℃) and A is the acid content (wt%). He found the following values for the parameters of this model for their studied systems:

c_1=-44.167255, c_2=1.009, c_3=-0.007134, c_4=0.00001624, c_5=1.280342, c_6=-0.019064, c_7=0.00007285

He found that the model predicts well the correlation between peak hot tack strength as a function of acid content (Figure 2.42, a) but it was not able to predict accurately the lowest temperature where hot tack occurs (Figure 2.42, b). Obviously, the proposed model is limited to the studied materials and generalizing the model for other polymers will be limited.

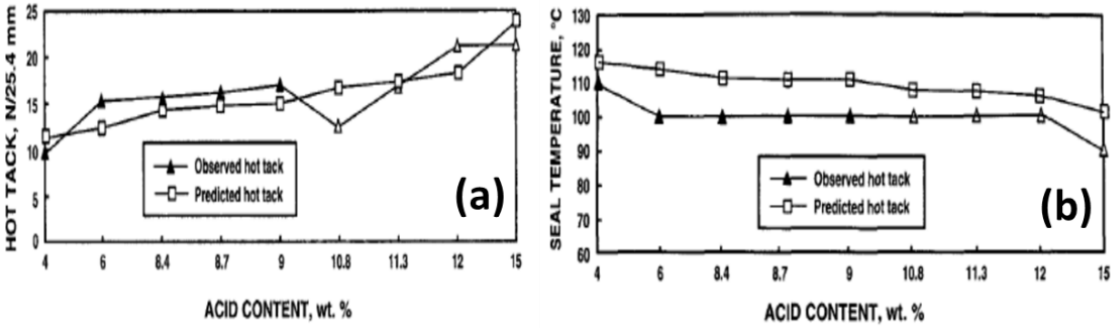

Figure 2.42 (a) Comparison of model predicted and observed hot tack peak at different acid contents. (b) Comparison of seal temperature of model and observed data for different acid content [30].

2.8. Problem Identification

Despite the importance of heat sealing in plastic packaging industry, some of its important aspects have not been studied in detail yet. Previous studies in the literature indicated the significant importance of sealing temperature and heat transfer in controlling seal performance. Increasing sealing temperature improves seal performance up to a certain temperature, but further increase in sealing temperature reduces seal strength due to seal area distortion or easy chain pull out. This indicates the importance of optimization of sealing temperature and modeling of heat transfer in heat sealing process. However, several previous studies on modeling of heat transfer in heat sealing used important parameters such as convective heat transfer coefficient as the fitting factor in their model. This avoids using previous models as predictive tools in design and optimization of heat sealing process. Therefore, a precise predictive model for heat transfer in heat sealing is lacking in the literature.

Squeeze out flow (SOF) is another aspect of heat sealing which has been poorly studied in the literature. During packaging of grainy or liquid products, SOF is an essential requirement that allows encapsulation of the product residue in the seal area to avoid channeling, leaking and in extreme cases, seal failure. Few authors have attempted to establish a relationship between SOF and sealant material properties through either experimental investigations or modeling approach. They could not find a relation between SOF and material properties and modeling results showed poor agreement with experimental SOF data. These indicate the lack of a comprehensive study on SOF in heat sealing and the need for a model to estimate SOF based on the material properties and sealing condition.

Multilayer sealant films have been used widely in industrial applications as an approach to reduce the sealant material cost and improve its processability and mechanical properties. However, effects of sealant film structure on seal properties have not been studied systematically in the literature. A systematic study on effects of sealant structure and back-layer material on seal performance of multilayer sealant allows a better understanding of the contribution of the film structure and materials in final sealing properties.

2.9 Objectives

Considering the mentioned points in the introduction and literature review, the main objective of this project was defined as "***Determining Effects of Sealing Conditions and Film Structure on Seal and Hot Tack Performance of Multilayer Polymeric Films***"

To this aim, the following specific objectives were defined as milestones in this project.

I) Simulation of the heat transfer in heat seal process and comparison of the simulation results with experimental data to optimize processing conditions.

II) Experimental evaluation of squeeze out flow during heat sealing of multilayer polymeric films and its modeling to be able to predict the effects of material properties on squeeze out flow.

III) Investigate the effects of back-layer on seal performance of multilayer sealant films in order to improve seal performance of multilayer sealant films.

CHAPTER 3 ORGANIZATION OF THE ARTICLES

The main results of this project will be presented in chapters 4 to 6 as three research articles. Each chapter contain an article which is published or submitted to a scientific journal.

In chapter 4, the results of the first phase of this project are presented as a research paper entitled "Simulation of Heat Transfer in Heat Sealing of Multilayer Polymeric Films: Effect of Process Parameters and Material Properties". This chapter discusses the effect of different sealing conditions and film structure on the interface temperature between seal sides. To this aim, experimental measurement results of the interface temperature will be compared with a simulation of heat transfer. The results of this phase of the project will allow a better understanding of the important parameters in heat transfer during heat sealing.

In Chapter 5, a second research article entitled "Squeeze Flow in Multilayer Polymeric Films: Effect of Material Characteristics and Process Conditions" will be presented. In this part of the project, effects of sealing condition, sealant thickness and viscosity on squeeze out flow will be experimentally investigated. Three modeling approaches will be used to provide new insight into the squeeze out flow in heat sealing. The obtained results will provide new knowledge and understanding of squeeze out flow in heat sealing and can provide new tools for material selection in packaging design.

In Chapter 6, third scientific contribution of this work will be presented in the form a scientific paper entitled "Effect of Back-layer on Seal Performance of Multilayer Polyethylene-based Sealant Films". In this part of the project, a systematic study was done on the effects of back-layers on seal performance of multilayer sealant using three different back-layers (HDPE, LLDPE and LDPE) and a metallocene polyethylene (m-PE) layer. Effects of backlayer material and metallocene layer thickness as well as sealing condition on seal performance of multilayer sealant films will be presented. A new mechanism will be presented to explain the observed effects of back-layer material on seal properties.

General discussion in Chapter 7 gives challenging faced during the project and finally, Chapter 8 briefly reviews the most important results and conclusions of the thesis and presents recommendations for the future works.

CHAPTER 4 ARTICLE 1:

SIMULATION OF HEAT TRANSFER IN HEAT SEALING OF MULTILAYER POLYMERIC FILMS: EFFECT OF PROCESS PARAMETERS AND MATERIAL PROPERTIES

Zahra Kanani Aghkand, Ebrahim Jalali Dil, Abdellah Ajji,* and Charles Dubois

3SPack, CREPEC, Department of Chemical Engineering, École Polytechnique de Montréal, Montréal, Québec H3C 3A7, Canada

Published in Journal of *Industrial &Engineering Chemistry Research*

Ind. Eng. Chem. Res. 2018, 57, 14571−14582

4.1 Abstract

In this study, heat transfer in a heat-sealing process was simulated using COMSOL Multiphysics software. To this aim, variations of thermal conductivity, specific heat and density of polymers with temperature were measured in a wide temperature range. In addition, the temperature profile at the interface between two sealing films was measured using a very fine thermocouple. Comparing the experimental and simulation results clearly indicate the high accuracy of the simulation and points to the significant role of considering thermal contact resistance (TCR) as the boundary condition between the jaw and the films. These results show that the present simulation, for the first time, can successfully predict heat transfer and temperature evolution in a heat sealing process without any fitting parameter obtained from interface temperature profile measurements. In addition, the obtained results showed that the simulation model can predict the effect of jaw

temperature, sealing time, film thickness and polymer crystallinity in a wide range of temperatures from below to much higher temperatures than the melting point of the sealant.

***Keywords*:** Heat sealing, Interface temperature, Heat transfer, Simulation, Thermal contact resistance, Thermal conductivity

4.2 Introduction

The flexible packaging industry has been progressing constantly due to the wide range of application of polymeric packages [1]. Considering the wide range of properties that are expected from a package, multilayer structures have been widely used in polymer packaging industry. These structures allow tuning properties by controlling the package structure. In every package, sealing is one of the most delicate parts that requires much attention as failure of sealing means failure of the whole package and product loss. Heat sealing is the most commonly used technique in which two sides of the seal are placed between two jaws (bars), either one or both jaws is electrically heated. The jaws apply a certain pressure (sealing pressure) for a given period of time (dwell time) to seal the films together. Finally, the sealed films will be removed after opening of the jaws. If the seal strength is measured right after jaws opening when seal material is still molten, the obtained result is referred to as hot tack strength. On the other hand, the seal properties evaluated after complete cooling to room temperature correspond to the seal strength. Hot tack is very important during filling of the package while seal strength is important during transportation, handling and costumer use.

The most important process parameters that affect seal performance are temperature, pressure and dwell time [1-7]. All these parameters need to be carefully adjusted to achieve a balance between properties and cost of the package. It has been shown that a minimum pressure is required to bring seal layers to close contact and overcome micro-roughness between surfaces [1, 8, 9]. This increases the contact area and enhances chains diffusion. On the other hand, applying excessive pressure will squeeze-out the molten fraction of sealing material from the seal area and distort the seal [8, 10].

In order to achieve a good seal or hot tack strength, two phenomena need to occur during the dwell time [1]: (i) the interface temperature should be high enough to allow chain ends diffusion across the interface, (ii) Brownian motion of the chain ends across the interface should occur to an extent

that results in chain entanglement at the interface. As longer dwell times result in greater heat transfer to the seal interface and longer diffusion depth of the chain ends, increasing dwell time enhances the seal performance. On the other hand, increasing dwell time reduces the production rate and increases the final production cost.

Previous researchers showed that temperature is the most critical parameter to achieve a good seal performance [1, 3, 8]. It should be noted that, due to the difficulties in measuring temperature at the interface between two seal layers (known as the interfacial temperature) in most of the previous studies, the effect of temperature was studied by changing jaw temperatures instead of considering the interface temperature. It is known that increasing sealing temperature increases seal strength [1, 4-6, 8, 11-16] and increasing sealing temperature is a common approach to reduce the required dwell time. However, increasing sealing temperature increases the power consumption and the final production cost. In addition, increasing temperature is always limited by the thermal stability of the materials in the polymeric film.

All aforementioned issues emphasize the significant importance of optimizing seal temperature and dwell time in order to achieve desired seal strength at a minimal production cost [2-4, 8, 17, 18].

Considering the material and processing cost, time and energy required for optimizing of a heat sealing process, modeling and simulation tools can significantly reduce the cost of designing structure of polymer packages and setting heat sealing process parameters. Determining the time required for the sealant surfaces to reach the jaws temperature is critical to optimize the sealing temperature and dwell time and achieve a high seal performance and high production rate. Few studies have been done on modeling of heat transfer in heat sealing process. For example, Meka and Stehling [2] presented a heat transfer model using finite element analysis (FEA) and found a good agreement between experimental data and modeling results at temperatures below melting point of sealant. However, above melting temperature, the predicted temperature by their model deviated considerably from the experimental results. This was attributed to neglecting the endothermic heat of fusion of polymers in their model and thinning of the polymer films due to the squeeze-out of sealant during heat-sealing process. Mihindukulasuriya et al. [19] also predicted interface temperature in sealing of low density polyethylene (LDPE) films using COMSOL Multiphysics software. By determining the specific heat (Cp) of the polymer at different

temperatures from DSC curves of LDPE films and using thermal contact resistance (TRC) as a fitting parameter obtained from interface temperature measurements, their model showed a good agreement with experimental results for both clean and contaminated surfaces. It should be emphasized that all previous studies in literature on modeling of heat transfer in heat sealing used fitting parameters determined from experimental interfacial temperature measurements. These fitting parameters changed by changing process conditions such as jaw temperature or material properties such as melting temperature, density and polymer crystallinity. This indicates the significant limitations of previous works in presenting a model that can predict interface temperature in a heat sealing process without any temperature measurement.

Therefore, the objective of this paper is to present a simulation procedure that can directly predict the effect of different processing conditions and material properties on the interface temperature in a heat sealing process. To this aim, a common three layer film composed of polyamide (PA6) as the abuse layer, polyethylene grafted maleic anhydride (PE-g-MA) as the tie layer and a metallocene linear low density polyethylene (mLLDPE) as sealant layer will be used. The effect of temperature on thermal conductivity, specific heat and density of polymers will be studied. Simulation of the heat sealing process will be performed using COMSOL Multiphysics software. The role of material properties and processing conditions in heat sealing process will be discussed in detail by comparing simulation results and measured interface temperatures.

4.3 Experimental

4.3.1 Materials

Metallocene linear low density polyethylene (mLLDPE) with commercial name of Exact 3131 and High density polyethylene (HDPE) with commercial name of HDPE7925.30 were purchased from ExxonMobil. Polyamide Ultramide B36 (PA) was provided by BASF. Polyethylene-grafted maleic anhydride (PE-g-MA) with commercial name of Bynel 4125 was purchased from DuPont and used as adhesive layer between polyethylene and PA layers. In order to eliminate moisture content of PA, it was dried at 100℃ overnight under vacuum before experiments.

4.3.2 Film preparation

Multilayer films composed of a PA abuse layer, a tie layer (PE-g-MA) and a sealant layer (m-LLDPE or HDPE) were prepared using co-extrusion. Three single screw extruders with 20 mm screw diameter and L/D=30 were used in the co-extrusion of the samples. Temperature profiles of 215 to 240^{o}C, 220 to 235^{o}C and 230 to 250 ℃ were used for sealant extruder, tie extruder and PA extruder, respectively. The screw speeds of the extruders were set to reach the desired thickness of the layers and total thickness of the film. In addition, an air knife at the die exit and a chilled roll calendar were used to control cooling rate of the film. The total film thickness was maintained at 100 μm with average thicknesses of 50 μm for sealant, 10 μm for PE-g-MA, and 40 μm PA layer. To study the effect of sealant thickness, samples with different mLLDPE thicknesses were prepared while the thickness of tie and PA layers were kept at 10 μm and 40 μm, respectively.

4.3.4 Light Microscopy

In order to determine the thickness of the layers, samples were cut using a razor blade and their machine direction (MD) cross-section was observed under a light microscope (Spotlight 200i, PerkinElmer). The thickness of the layers was then determined using an image analysis software (ImageJ).

4.3.5 Scanning Electron Microscopy (SEM)

The squeeze out of materials from sealed area was investigated using a tabletop SEM equipment (TM3030plus, Hitachi,). To this aim, the sealed area was cut using a razor blade and its cross-section close to the sealed area was observed using the SEM.

4.3.6 Heat Sealing

Heat sealing of the samples was performed using a heat sealing machine (SL10 LakoTool, Lako Tool & Manufacturing Inc) at the desired temperature and pressure. The time resolution of the heat sealing machine was 100 ms. Based on the results of a previous study [16], a pressure of 40 psi (2.75 atm or 0.275 N/mm^2) was used in all sealing experiments.

4.3.7 Interface Temperature Measurement

To measure the temperature between two films (interface temperature), a fine bare wire thermocouple with the diameter of 75 µm (CHROMEGA® Constantan) was purchased from Omega Engineering Inc. The fast response time of this thermocouple (<5 ms) ensures the high resolution for non-isothermal studies and recording interface temperature changes during sealing. An eight channel USB data acquisition module (OM-DAQ-USB-2401, Omega Engineering Inc.) was used to connect the thermocouple to a computer to record the data. Figure 4.1 shows how the thermocouple was placed between two sides of the sealed film. It should be noted that, if not specified, in all temperature measurements, the thermocouple was centered with respect to the length and width of the sealed area. The reported temperatures are an average of three measurements. The maximum standard deviation in the measurements was determined to be less than 3.1 ^{o}C.

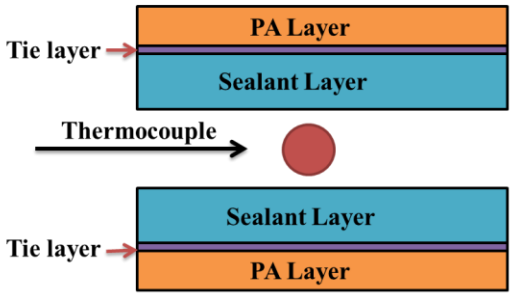

Figure 4.1 Schematic showing the position of thermocouple between two sides of the seal.

4.3.8 Density Measurement

The density of the polymers at different temperatures and pressures were measured using a high pressure piston-type dilatometer (PVT100, ThermoHaak). The procedure, after melting mLLDPE, HDPE and PE-g-MA samples, was: temperature was raised to 160^{o}C and then cooled down with the rate of 10^{o}C/min. For PA, the temperature was increased to 240^{o}C and then the sample was cooled down at 10^{o}C/min and the results were recorded from 160^{o}C. Volume measurement and, consequently, density estimation were done for 10^{o}C steps at each pressure.

4.3.9 Differential Scanning Calorimetry (DSC)

Temperature Modulated DSC (TMDSC) was used to determine the specific heat of the polymers. TMDSC tests were performed using a DSC Q2000 machine (TA Instruments) in the temperature range of 25 to 150 ℃. All TMDSC experiments were carried out using an oscillation amplitude of ±1.27 ℃ and oscillation period of 60 s with a heating rate of 2℃/min. An average of three different measurements was used in this work. The standard error in the measured values was always less than 3%. The following equation was used to determine the crystallinity:

$$\mathbf{X_C} = \frac{\mathbf{\Delta H_f}}{\mathbf{\Delta H_{f(100\%)}}} \times \mathbf{100} \qquad \text{Eq. 4.1}$$

ΔH_f and $\Delta H_{f(100\%)}$ are the heat of fusion of PE and the heat of fusion for 100% crystalline PE, respectively. The later was taken from the literature as 290 J/g[20]. $\Delta H_{f(100\%)}$ of PE was also used in calculation of the crystallinity of PE-g-MA.

4.3.10 Thermal Conductivity Measurement

Thermal conductivity of polymers was determined using a commercial machine (PVT100, ThermoHaak) equipped with a thermal conductivity cell. The polymer was added to a cylindrical cell with heating from the walls. After polymer melting, a probe containing a heater element and a thermocouple was introduced in the middle of the sample. The thermocouple and element in the probe were vertically parallel and 0.5 mm apart from each other. A known voltage was applied to the heater element in the probe for 30 s and the thermocouple recorded the temperature during this period. Thermal conductivity was calculated from the linear part of temperature profile vs. time. For higher resolution in the transition region of 80^{o}C to 120^{o}C, data was recorded with 5^{o}C steps while out of this region 10^{o}C steps were used. A detailed procedure for the measurement of thermal conductivity by this approach can be found in the paper published by Dawson and M Rides [21].

4.3.11 Atomic Force Microscopy (AFM)

Surface roughness of the of PA side of films was measured using an AFM machine (Nanoscope V Dimension Icon/Fastscan AFM, Bruker, USA) operated in tapping mode in air. In order to acquire images, 125 µm TappingMode™ ScanAsyst Air probes were used. Roughness measurements were

performed on an area of 50 × 50 μm^2 and the reported roughness values are an average of four different measurements.

4.3.12 Micro-Hardness

Micro-hardness of PA side of the film samples was determined according to ASTM E 384 using a micro-hardness machine MMT-X7B from MATSUZAWA. The reported values are an average of five different measurements.

4.4 Modeling strategy

A schematic of the geometry that was used in the simulation is shown in Figure 4.2. As can be seen, the geometry is composed of two sides of a multilayer film with outer PA layer, a middle PE-g-MA layer and a PE layer as the sealant layer. The two sides of the film are pressed together under certain heat and pressure. As co-extrusion process was used to prepare multilayer film samples, perfect interface assumption between layers can be applied and, therefore, continuity was assumed as boundary conditions between PA-tie and tie-PE layers. For interface of PA layer and jaw surface, thermal contact resistance (TCR) was used as the boundary condition. The importance of considering TCR in the simulation will be discussed later in this paper. As the film on top and bottom part of the sealed area have the same structure and both jaws are at the same temperature, symmetric boundary condition can be used at the interface of the sealant layers of top and bottom sides.

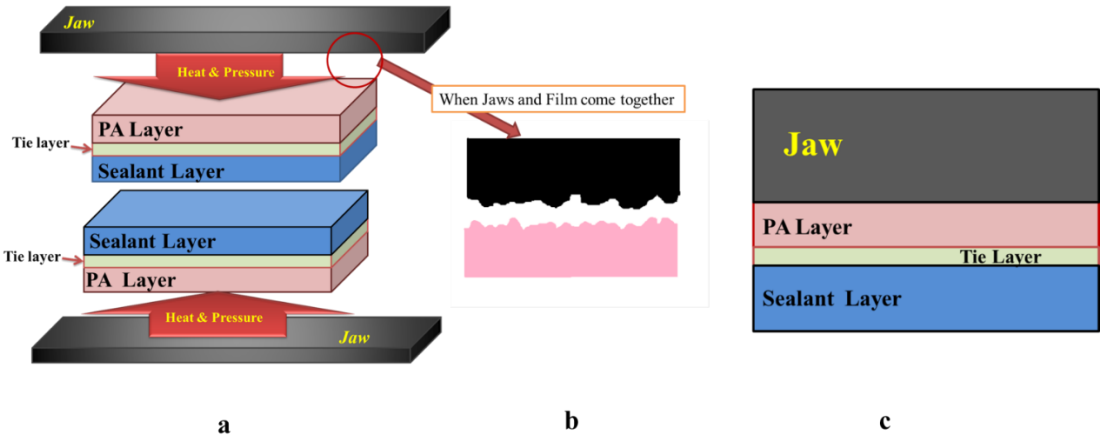

Figure 4.2 Schematic of (a) the film structure used in measurements, (b) Surface roughness of Jaw and PA layer when come together, (c) the structure used in simulation model.

As will be shown later, it was found that the squeeze out flow (SOF) was negligible in the studied conditions and, therefore, only the heat transfer was considered in this simulation. The simulation was done using COMSOL Multiphysics (5.2a, COMSOL Inc.) with parameters listed in Table 4.1.

Table 4.1 Parameters used in the COMSOL simulation

Parameter	Value
Sample length	25.4mm
Thickness of seal layer	50μm unless specified otherwise
Thickness of tie layer	10μm
Thickness of PA layer	40μm
Specific heat (Cp)	From DSC measurements
Thermal conductivity (k)	From thermal conductivity measurements
Density (ρ)	From density measurements
Pressure	0.27 N/mm^2
Jaw temperature	Constant
Mesh type	Free Triangular
Time expand	10ms
Jaw material	Stainless steel

4.5 Results and Discussion

4.5.1 Heat transfer direction

In order to confirm that heat transfer direction in the heat sealing process is mainly in the film thickness direction, three sets of experiments were done in which, three thermocouples were placed in the longitudinal, width and thickness in the center and close to edges of sealed area as illustrated in Figure 4.3. The measured temperatures for each set of thermocouples are shown in Figure 4.3

under the schematic of each direction. A large gradient between the recorded temperatures can be obviously seen in the experiment where thermocouples are placed at different positions in the thickness direction. These results clearly indicate a much significant temperature gradient in the thickness direction compare with the two other directions. The observed results can be explained by considering the much larger length and width (L, W) of the sealed area compared with the film thickness.

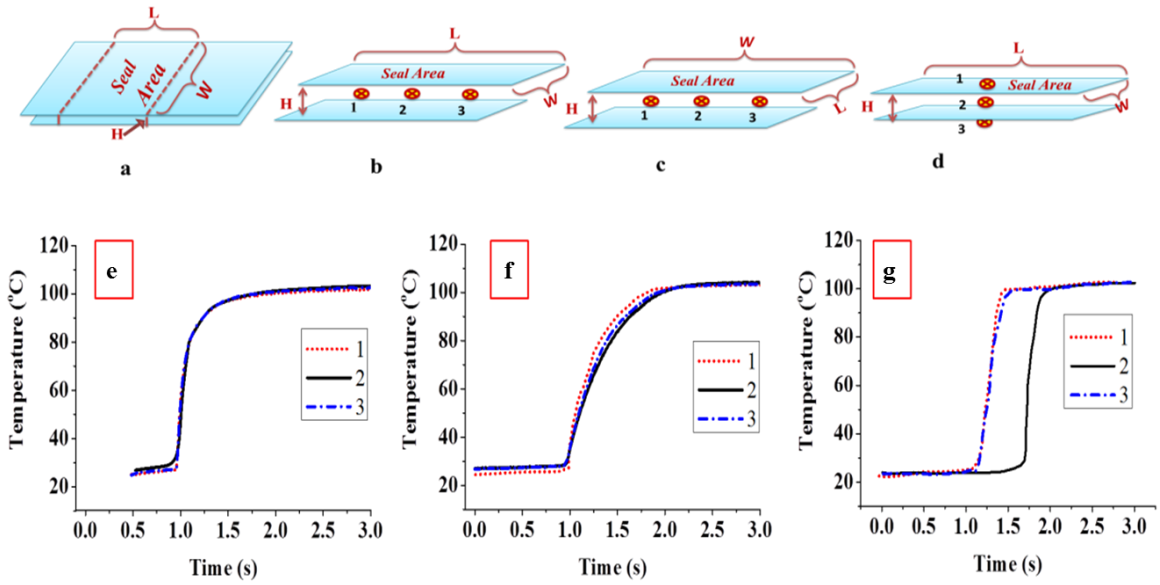

Figure 4.3 Top: positioning of thermocouples for determining heat flow direction: (a) seal area dimensions, (b) in longitudinal direction, (c) width direction and (d) thickness direction. (e), (f) and (g) show the recorded temperature profiles for thermocouples in (b), (c) and (d), respectively.

Based on these results, a one dimensional heat transfer model (in the thickness direction) was used in the simulation of the heat sealing process in this study.

4.5.2 Evaluation of Squeeze-out Flow

Meka and Stehling [3] found a deviation between their heat seal model and experimental data which they attributed to the squeeze out of sealant from the sealed area and reduction of the film thickness. Morris et al. [10] presented an experimental approach to measure the amount of squeeze-out flow and found that, the amount of squeeze-out flow increases with increasing pressure, dwell

time, temperature, film thickness and width of the jaws. They also presented a mathematical model to estimate the squeeze out flow using a one dimensional quasi steady-state condition, a Newtonian polymer melt under isothermal conditions. However, they observed a disagreement between experimental data and model predictions which they attributed to the assumptions mentioned above. Considering the two dimensional nature of squeeze-out flow and the non-isothermal and transient condition during heat sealing process, quantification of squeeze out flow in heat sealing is still a challenge.

In order to quantify the squeeze out flow in this work, after sealing a sample under the desired conditions, the thicknesses of the layers were measured from SEM images of the cross-section of the sealed area and at the regions close to the sealed area. Figure 4.4 shows a typical image of a 100 μm thick film with 50 μm sealant layer of mLLDPE sealed at T=140 ^{o}C, P= 2.7 N/mm^2 and dwell time of 0.5 s. The thickness of mLLDPE layer in the seal area was determined to be double of its thickness in the initial film which points to the lack of squeeze-out flow in this sample. In addition, no distortion of the boundaries between the layers in or out of the seal area was observed. Similar results were observed for the same film at lower temperatures and pressures. These results clearly confirm the negligible squeeze-out flow for the sealing conditions used in this study.

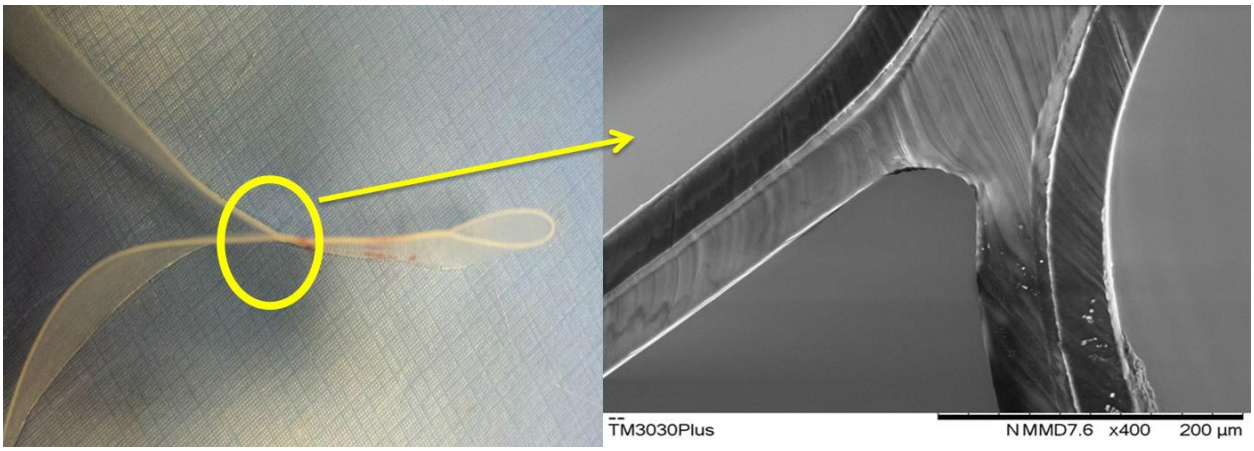

Figure 4.4 Left) A sample with 50μm thick mLLDPE sealed at 140^{o}C, 2.7 N/mm^2 and 0.5 s dwell time, Right) SEM image of marked area.

Figure 4.5 shows SEM images of cross-section of film with thickest sealant (130 μm) sealed at 105^{o}C and 140^{o}C jaw temperatures and 0.5, 1 and 2 s dwell times under 0.27 N/mm^2 sealing

pressure. As can be seen, no sign of squeeze-out was observed in these samples. Regarding that squeeze-out is much pronounced in thicker sealants[10], these results indicate that squeeze-out of sealant is negligible in the studied range of temperature, dwell time and pressure.

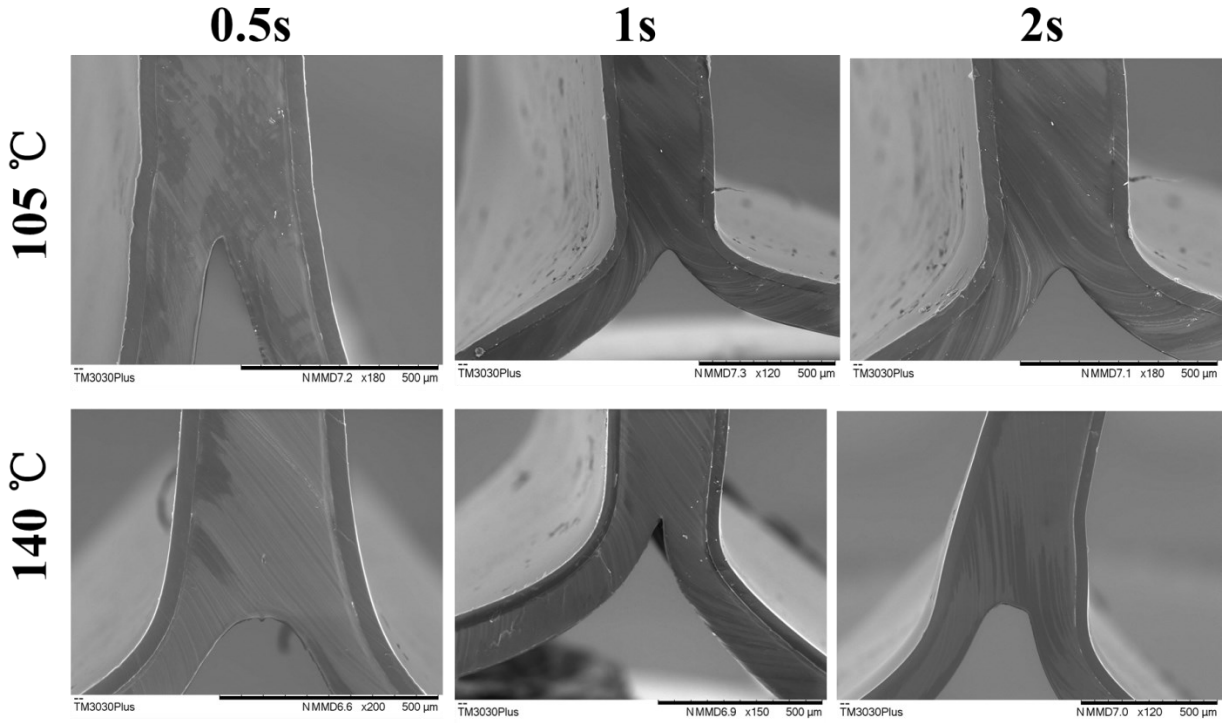

Figure 4.5 SEM images of film samples with thickest sealant (130µm) sealed at 105 ^{o}C and 140 ^{o}C jaw temperatures with 0.5, 1 and 2 s dwell times and sealing pressure of 0.27 N/mm^2.

4.5.3 Material Characterization

As previously mentioned in the modeling strategy, the variations of materials characteristics with temperature need to be determined before simulation of heat transfer in the heat sealing process. To this aim, variations of specific heat (Cp), density (ρ) and thermal conductivity of polymeric materials with temperature were investigated. Figure 4.6 shows the variation of Cp of polymer materials with temperature, measured using TMDSC. In addition, a summary of TMDSC results is presented in Table 4.2. For mLLDPE, HDPE and PE-g-MA in the temperature range of interest, TMDSC results show an increase in Cp by melting of the crystalline regions and a drop after complete melting of crystals. It should be noted that, as DSC determines Cp based on the difference between the heat applied to the sample and the reference pans, the change in the Cp in the phase

transition region in these graphs indicates the heat absorbed by the material due to the phase transition rather than the change in Cp. However, using the obtained values of Cp from TMDSC in the phase transition region allows considering the heat absorbed by the material during phase transition and, consequently, the difference between melting behaviour of materials. On the other hand, as the heat sealing is done at much lower temperature than melting of PA, only a smooth linear increase in Cp of PA can be seen in the studied temperature range. It should be mentioned that, molecular weight distribution of polymers results in different sizes of crystalline regions and broad melting peaks in contrast to the sharp phase transition in low molecular weight materials.

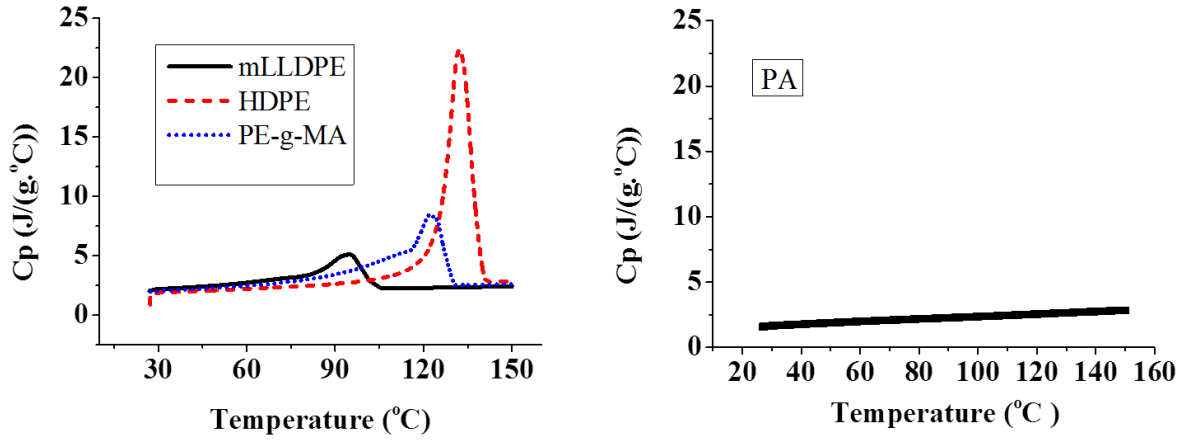

Figure 4.6 Specific heat capacity of (Left) mLLDPE, HDPE and PE-g-MA; (right) PA

Table 4.2 Peak temperature and heat of fusion of the polyethylene based polymers.

Material Name	Peak Temperature(^{0}C)	Heat of fusion(J/g)	Crystallinity (%)
mLLDPE	95	56	19.3
PE-g-MA	122	117	40.3
HDPE	132	205	70.7

The variation of density of materials with temperature at the heat sealing pressure (0.27 N/mm^2) was also determined and the results are shown in Figure 4.7.

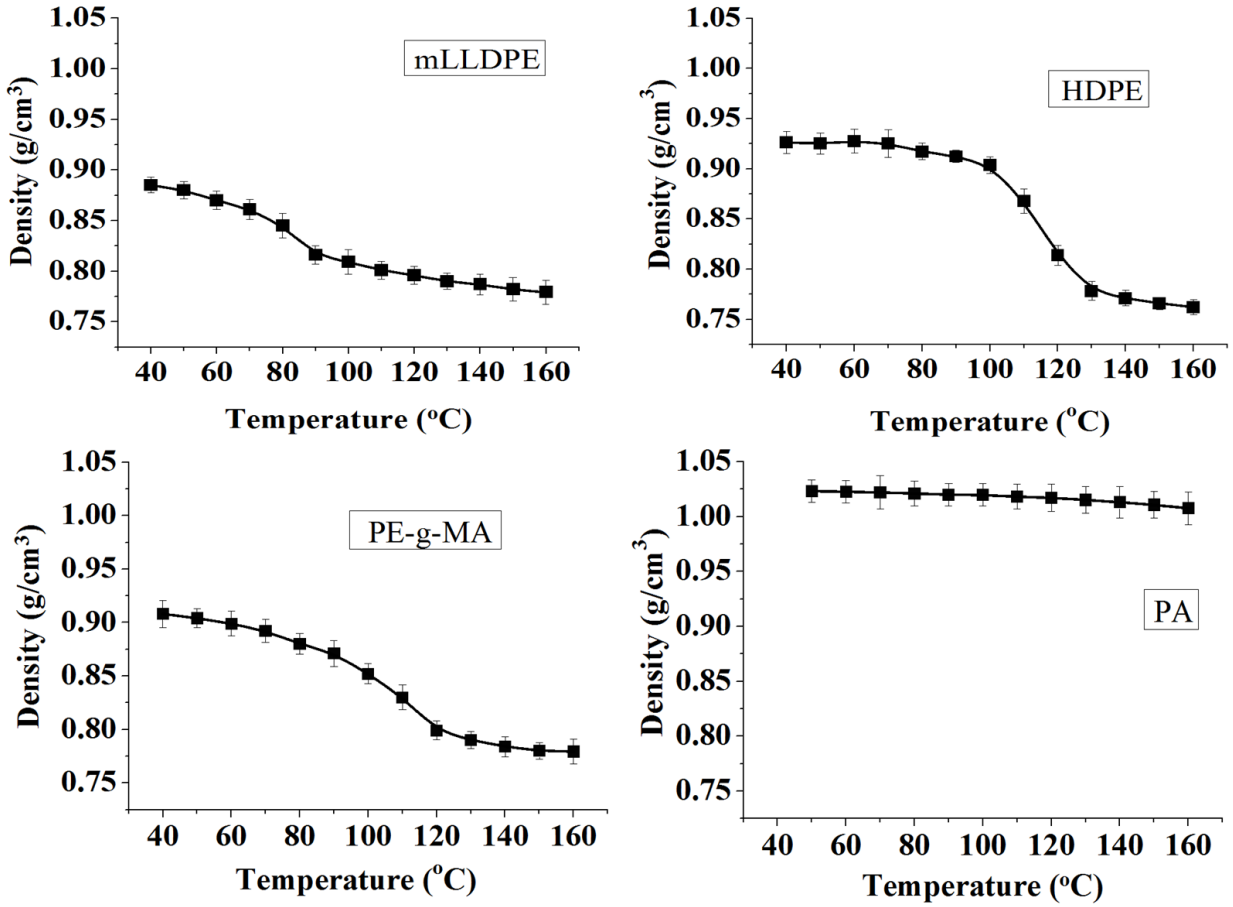

Figure 4.7 Variation of density of mLLDPE, HDPE, PE-g-MA and PA by temperature at P=0.27 N/mm^2.

By comparing Figure 4.6 and Figure 4.7, it is visible that the density of polyethylenes and PE-g-MA decreases remarkably close to the peak temperature observed in Cp graphs in Figure 4.6. The observed drop in the density is attributed to the increase in chain disorder and free volume after melting of crystals. Small discrepancies between the peak temperature in Cp and temperatures of density drop are related to the time that each sample took to reach to the desired temperature in density measurement tests. As pointed by Dos Santos et al. [22], this can lead to melting some crystals before the peak temperature and shifts the density drop temperature toward lower temperatures.

Thermal conductivity (k) of mLLDPE at a temperature of 105°C and different pressures was measured and the results are shown in Figure 4.8. Previous studies showed that increasing pressure

increases thermal conductivity of polymers [21, 23, 24] but, considering the error bars in Figure 4.8, no noticeable pressure dependency was observed in the studied range of pressure (0.27 N/mm^2 up to 40 N/mm^2). As a result, in this study, the thermal conductivity is assumed to be constant with pressure.

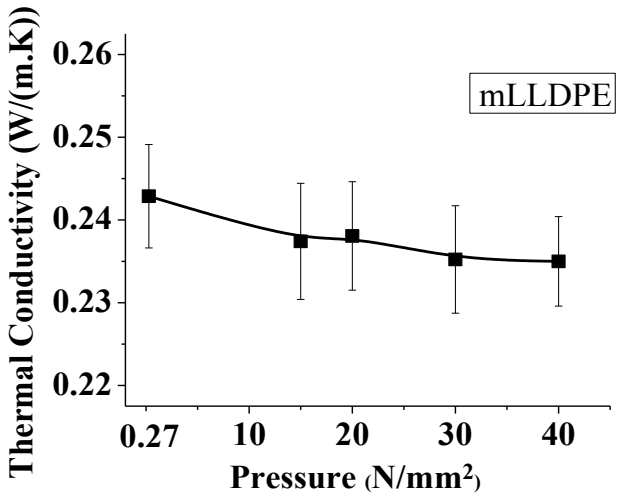

Figure 4.8 Effect of pressure on thermal conductivity of mLLDPE at 105^{o}C.

Figure 4.9 shows variation of thermal conductivity as a function of temperature for different materials used in this study. For mLLDPE and PE-g-MA, thermal conductivity increases with increasing temperature and reaches a plateau at temperatures above their melting temperature. On the other hand, as the temperature reaches the melting point of HDPE, its thermal conductivity decreases and finally reaches a plateau. Dependency of thermal conductivity to temperature has been associated to two opposing mechanisms [22, 25, 26]: (i) increasing the free volume which reduces thermal conductivity, (ii) increasing segmental mobility which increases thermal conductivity. In highly crystalline materials such as HDPE, melting crystals increase the free volume significantly and, as a result, the first mechanism becomes dominant and thermal conductivity decreases with temperature. On the other hand, in lower crystalline materials such as mLLDPE and PE-g-MA, the change in the free volume is not as significant as the change in the segmental mobility. Therefore, thermal conductivity of these materials increases with increasing temperature.

In the case of PA, due to its high melting point, the curve of thermal conductivity shows a very slight increase in the studied range of temperature, which is related to the increase in segmental mobility with temperature.

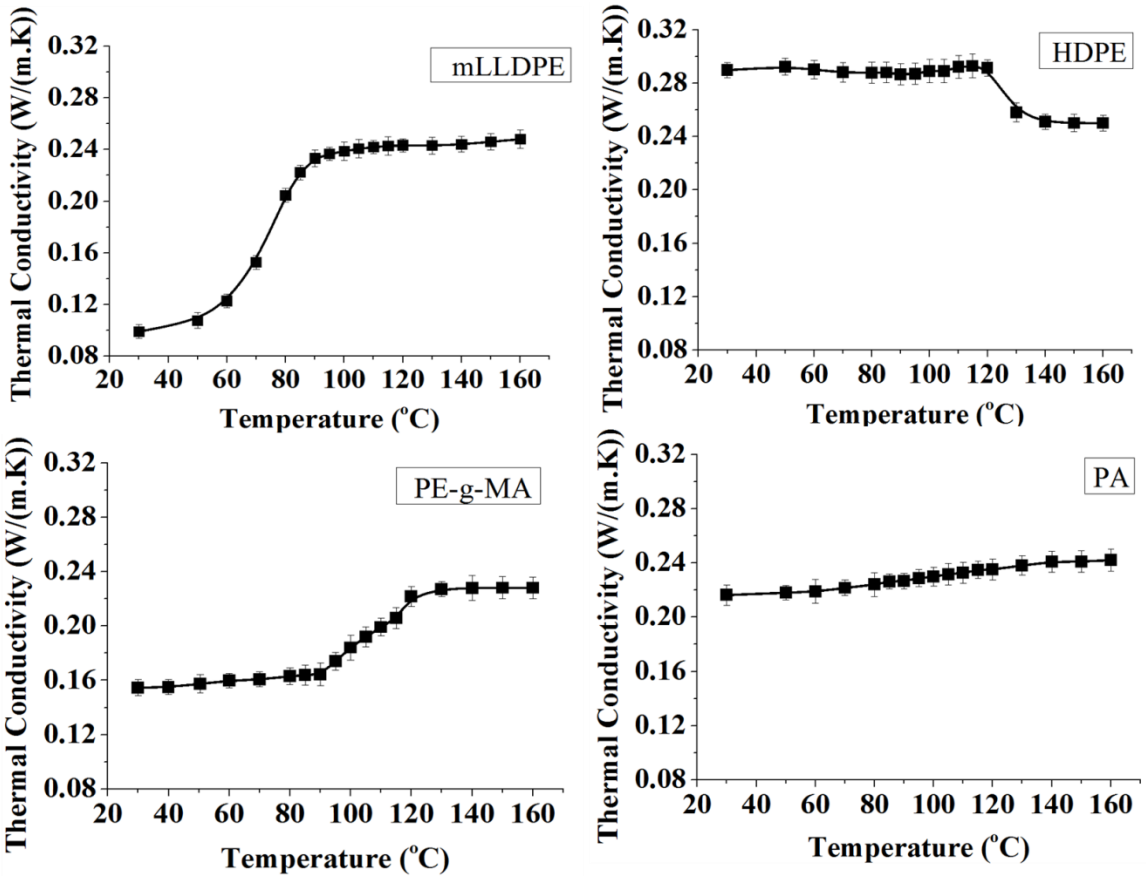

Figure 4.9 Variation of thermal conductivity with temperature, error bars indicate the standard error.

4.5.4 Thermal contact resistance (TCR)

Taking into account that heat sealing is done at temperatures much below the melting temperature of the abuse layer (PA in this case), micro-roughnesses of the PA layer surface do not allow a full contact between jaws and the films. Therefore, thermal contact resistance (TCR) (defined as the inverse of the overall heat transfer coefficient) should be used as the boundary condition between the PA layer and the jaw. Figure 4.10 compares the interface temperature predicted from simulation results without TCR (constant temperature at PA surface) and the experimental results

measured at two different sealing pressures. A gap between experimental results and the simulation exists, especially from 0.1 to 0.3 s which is slightly reduced by increasing pressure. Knowing that increasing the contact pressure reduces effect of TCR by increasing the contact between jaw and films [27-29], this indicates the significant importance of using TCR boundary condition to achieve a reliable simulation. This is in agreement with previous studies in literature that emphasized the importance of considering TCR in simulation of the heat sealing process [19]. In addition, TCR boundary condition allows including effects of surface roughness, surface hardness and applied pressure on the heat transfer and the interface temperature.

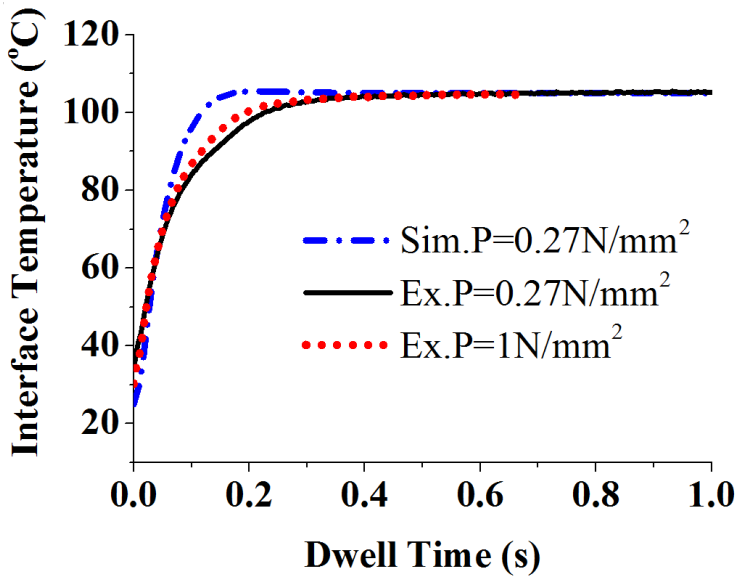

Figure 4.10 Comparison of simulation (Sim) results without TCR assumption and experimental (Ex.) results of interface temperature at jaw temperature (Tjaw) 105℃ and sealing pressures of 0.27 N/mm^2 and 1 N/mm^2.

Thermal contact resistance models exist in literature and can be categorized into plastic, elastic and elasto-plastic models based on the type of deformation of surface asperities [27, 28, 30, 31]. When the contact pressure is much greater than the surface micro-hardness of softer surface, a plastic deformation of asperities on the soft surface occurs. On the other hand, at pressures lower than surface micro-hardness, surface asperities undergo an elastic deformation. Elasto-plastic models consider both plastic and elastic deformations. In order to use TCR boundary condition, models in the literature estimate heat transfer coefficient between contact surfaces (h_c). Two predefined equations for estimation of h_c available in COMSOL software are Cooper-Mikic-

Yovanovich [27] and Mikic elastic[32] correlations that consider plastic and elastic deformation, respectively. Keep in mind that heat sealing is done at much higher temperatures than glass transition temperature of PA (~ 60 ^{o}C), the plastic Cooper-Mikic-Yovanovich model (CMY) model was used in this study.

CMY model uses Eq.2 to calculate h_c, which is affected by contact pressure (P), micro hardness of softer material (H_C), surface roughness (σ_{asp}) and asperities average slope (m_{asp}).

$$\boldsymbol{h_c = 1.25 K_{contact} \frac{m_{asp}}{\sigma_{asp}} \left(\frac{P}{H_c}\right)^{0.95}} \qquad \text{Eq. 4.2}$$

In addition, this model includes thermal conductivity between two contact surfaces which is calculated as $K_{contact} = \frac{2K_1K_2}{K_1+K_2}$. Surface roughness of the PA side of film samples was measured using AFM and the results are shown in Figure 4.11. The average value of surface roughness was determined as 59± 17 nm.

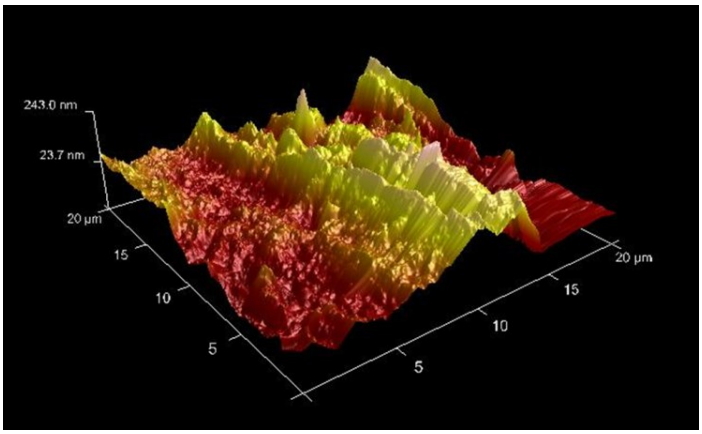

Figure 4.11 AFM images of the surfaces of PA side of the multilayer film before heat sealing.

The overall heat transfer coefficient is defined as the sum of h_c and gap conductance (h_g). Among various thermal gap conductance models [33, 34], "parallel plate gap gas conductance" was used in this study as it is a simple but effective model in predicting gap conductance. This model assumes two parallel plates with a gap filled by a gas phase. The gap conductance in this model is represented by: $h_g = {}^{k_g}/_{\delta}$ where δ is the effective gap thickness and is related to surface roughness, micro-hardness and contact pressure.

Using the values of thermal conductivities and the thermal contact resistance calculated based on CMY model by COMSOL, the bulk resistance (defined as $\sum l_i/k_i$ where l_i and k_i are thickness and thermal conductivity of each layer) and TCR can be estimated to be in order of 10^{-3} m^2.K/W and 10^{-5} m^2.K/W. These values show that the value of TCR is much lower than the bulk resistance. However, it should be noted that despite the lower value of thermal contact resistance compared to the bulk resistance, the effect of TCR cannot be neglected due to its different nature. TCR is known to affect temperature profile by introducing a discontinuity in the heat transfer shown as a step in temperature profile at the contact between two surfaces [27, 29, 35, 36]. This situation is in analogy with the Biot number problem [37, 38] where the surface of a solid exchanging heat with a fluid will never be at the fluid temperature. Therefore, despite the lower values of TCR, the relative importance of the solid thermal conductivity to the heat transfer coefficient affects the shape of the temperature distribution in the solid similar to the one shown in Figure 4.10.

4.5.5 Simulation results

4.5.5.1 Effect of Dwell Time and Jaw Temperature

The simulation was run based on the strategy described in the modeling strategy section by considering air as the trapped gas between jaw and film surface. Figure 4.12 (a,b,c) shows the comparison of simulation and experimental results for different jaw temperatures. In addition, Figure 4.12 (d) shows a comparison between the simulation results presented in Figure 4.12 (a, b, c). A good agreement can be seen between experimental and simulation results in all studied jaw temperatures, especially above the melting point of the sealant layer. Comparing Figure 4.12 (a) with Figure 4.10 clearly indicates that using TCR boundary condition is critical in achieving a reliable simulation. In addition, these results indicate that the selection of the CMY and parallel-plate gap gas conductance models was appropriate choices in modeling strategy. It is worth mentioning that Mikic elastic model was also examined but the simulation results deviated from experimental results. The obtained results show that the interface temperature reaches the jaw temperature after 0.45 s, 0.4 s and 0.25 s for jaw temperatures of 80°C, 105°C and 140°C, respectively. It is observed that increasing jaw temperature, in addition to reducing the time of reaching jaw temperature, increases the slope of the curves before the plateau markedly. These results are especially important in optimizing dwell time to reduce time and energy at the industrial scale. This point will be discussed in more detail later in this paper.

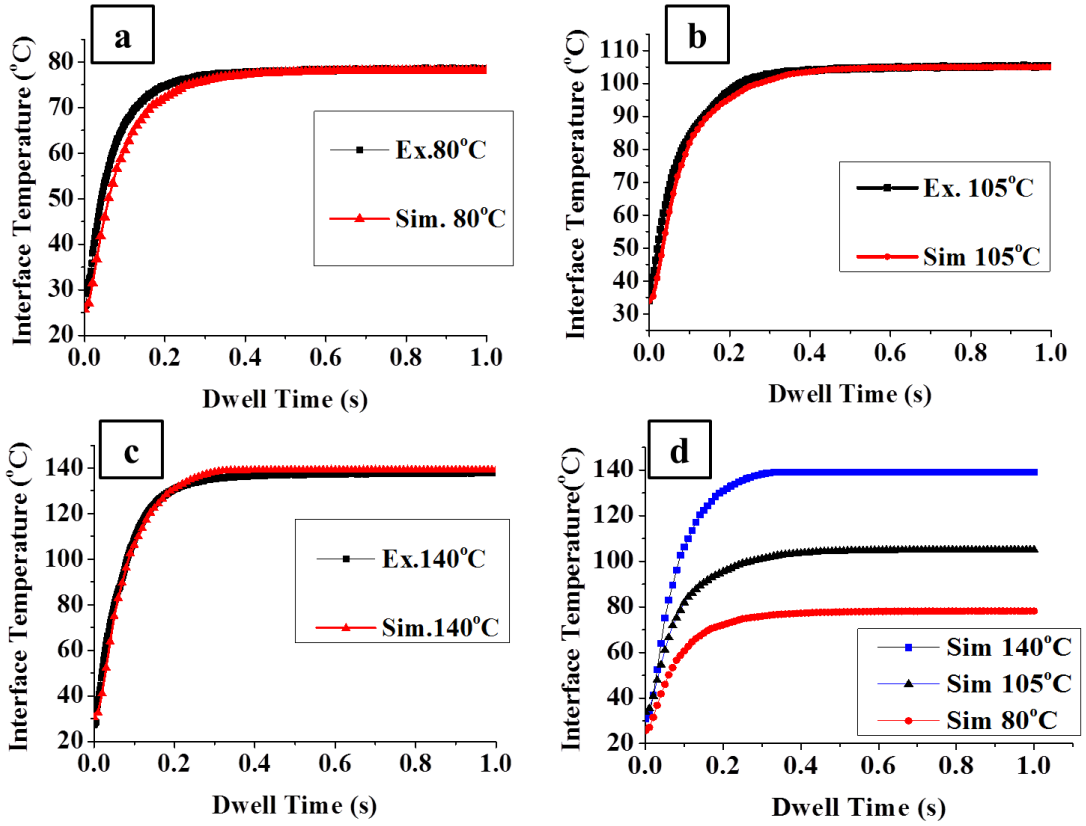

Figure 4.12 Simulation (Sim.) and experimental(Ex.) resutls at jaw temperature of (a) 80ºC,(b) 105℃, (c) 140 ºC,(d) comparing simulation results in different jaw temperatures. Sealing was done at 0.27 N/mm^2

As the studied jaw temperatures begins at 80ºC (below melting of mLLDPE) and continue to 140ºC (above melting of mLLDPE), these results clearly confirm that the presented simulation can predict well the interface temperature below and above the melting temperature of the sealant. As discussed previously, squeeze-out sealant material was negligible in the studied condition. The good agreement between experimental and simulation results indicate that considering both TCR boundary condition and the variation of material properties with temperatures are essential in achieving a simulation with a very high level of accuracy over a wide range of temperature.

4.5.5.2 Effect of Different Sealant Materials

Figure 4.13 shows the experimental and simulation results of the film sample with HDPE as the sealant layer.

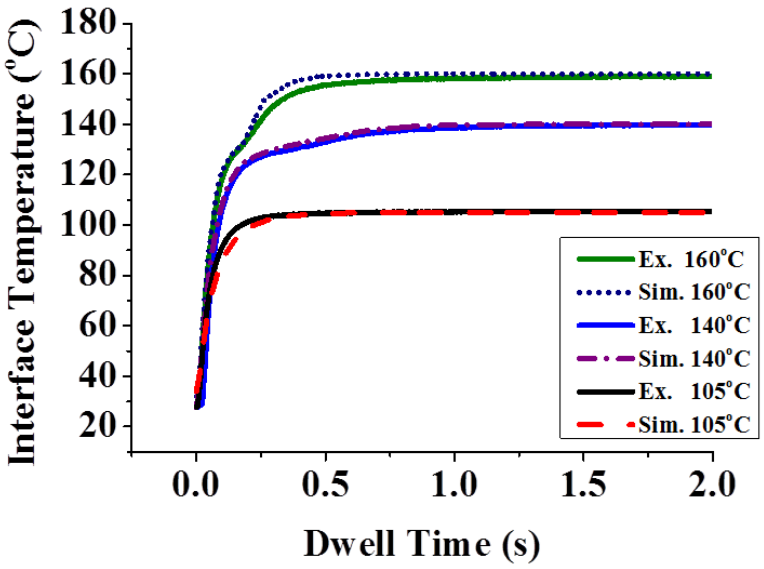

Figure 4.13 Comparison of experimental (Ex.) and simulation (Sim.) results for HDPE as sealant for different jaw temperatures.

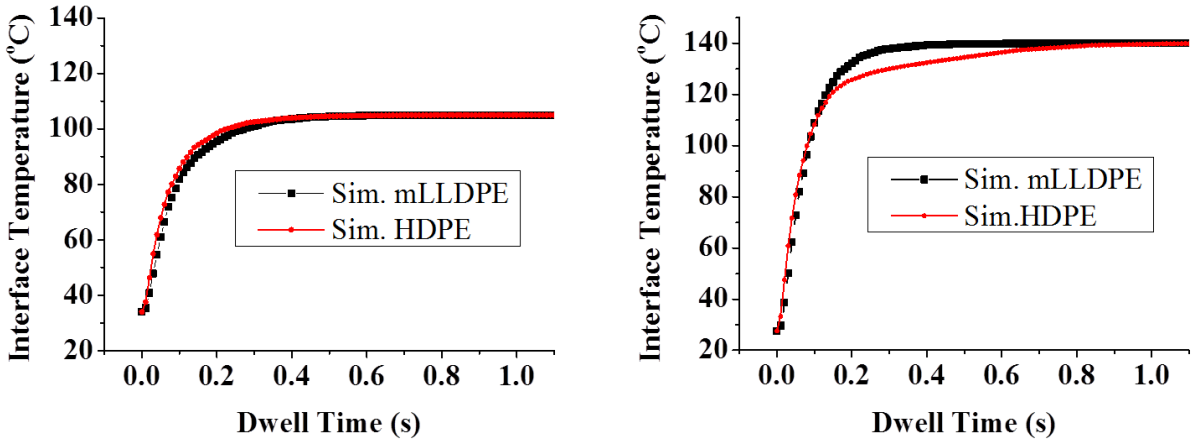

Figure 4.14 Comparison of simulation (Sim) results of mLLDPE and HDPE as sealants: Left, at 105°C; Right, at 140°C.

As illustrated, in all cases, the simulation results are in a very good agreement with experimental data. At temperatures below melting of HDPE (T_m=136°C), a profile similar to the mLLDPE is observed and interface temperature reaches jaw temperature after 0.5 s. By increasing jaw temperature to 140°C, the time required to reach the jaw temperatures increased to 0.84s. This can be better seen in Figure 4.14, which compares the simulation results of mLLDPE and HDPE for

jaw temperatures of 105°C and 140°C. This is in contrast with what was observed for mLLDPE, where increasing jaw temperature reduced the time required for interface temperature to reach the jaw temperature.

Interestingly, when jaw temperature is at 160°C, a completely different behaviour with a step in interface temperature profile is observed in both experimental and simulation results and the interface temperature reached the jaw temperature after 1 s. The temperature window in which the step-like behaviour is observed (120-140°C) corresponds well with the temperature window in which melting of HDPE occurs. The difference between the temperature profile in HDPE and mLLDPE can be attributed to two parameters: (i) The effect of temperature on thermal conductivity and (ii) absorbed heat during melting of crystals. In the case of mLLDPE, melting of polymer crystals reduces the heat transfer toward the inner layers by absorbing heat but, in contrary, melting also increases the thermal conductivity of the polymer. In the case of HDPE, the heat of fusion is much larger than that of mLLDPE, Table 4.2, and therefore retardation effect of heat absorbed during melting is more pronounced. In addition, melting reduces thermal conductivity of HDPE. Therefore, the observed step-like behaviour in interface temperature profile of HDPE can be attributed to its much larger heat of fusion and the decrease in its thermal conductivity during melting.

It should be noted that, the most important application of simulation in heat sealing is eliminating or reducing the trial and error in designing of a package. To this aim, a reliable simulation needs to be able to consider the differences between sealant materials. Regarding previous studies on simulation of heat sealing in literature [3, 19, 39], the obtained results clearly indicate that the presented simulation has the ability to see the complex effect of melting on the interface temperature profile. This can be attributed to the fact that in previous studies, the effect of temperature on material properties such as thermal conductivity, specific heat and density were not perceived [3, 19]. In addition, in some cases TCR was not used as the boundary condition [3] or was taken only as a fitting parameter obtained from the experimental results [19], which limits the application of the presented models.

4.5.5.3 Effect of Sealant Thickness

Thickness of the sealant layer is one of the parameters that its optimization has many practical uses. Very thin sealant layer does not provide good sealing properties. On the other hand, a thick

sealant layer increases the final cost of the package. In addition, increasing thickness of the sealant layer also delays the heat transfer to the interface and increases the required sealing time. Therefore, application of the presented simulation in optimizing dwell time and temperature especially in thick sealants in order to reduce the sealing time is of interest.

In order to examine the effect of sealant thickness, the simulation results of interface temperature in a 180 μm multilayer film with 130 μm thick sealant of mLLDPE, was compared with the experimental results in Figure 4.15. It should be noted that in flexible packaging, sealant layers thicker than 100 μm are not usual and therefore this thickness can be assumed as an ultimate thickness. It is observed that even at such a thick sealant layer, the simulation results are in a very good agreement with the experimental results. In addition, it can be seen that in the thick 130 μm sealant layer, the interface reaches the jaw temperature after 1.8 s which is much longer compared to 0.35 s for the sample with 50 μm sealant layer. Despite the fact that some previous studies [3, 40, 41] estimated the effect of thickness on heat transfer, this is the first study that shows a very good agreement between experimental and simulation results in such a wide range of sealant thicknesses.

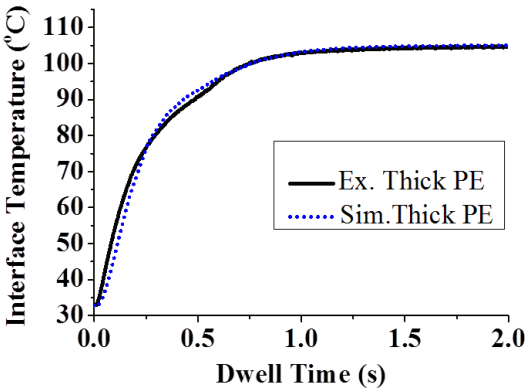

Figure 4.15 Experimental (Ex.) and simulation (Sim.) results of interface temperature of film with 130 μm sealant layer

As discussed in section 3-2, at 0.27 N/mm^2, no squeeze out flow was observed up to 2 s of dwell time at jaw temperature of 140°C. Based on the experimental and simulation results, the maximum

time for interface temperature to reach the jaw temperature was 2 s for the film with 130µm thick sealant. It should be noted that even if squeeze out flow occurs at longer dwell times, it will not affect the interface temperature as interface temperature already reached the jaw temperature. Therefore, as mentioned previously, ignoring squeeze out flow is a valid assumption in this study.

4.5.5.4 Effect of pressure

Sealing pressure is another important processing parameter in heat sealing. Figure 4.16 shows the effect of applied pressure on a 50 µm thick sealant. It can be observed that both experimental and simulation results indicate that increasing pressure up to ten times did not have a significant effect on interface temperature. These results are in-line with previous results reported by Najarzadeh et al. and Theller [1, 8]. For instance, Najarzadeh et al. found that only a minimum pressure between 0.1-0.5 N/mm^2 is required to establish the contact between the film and jaws and increasing pressure above 0.5 N/mm^2 did not have a considerable effect on sealing properties.

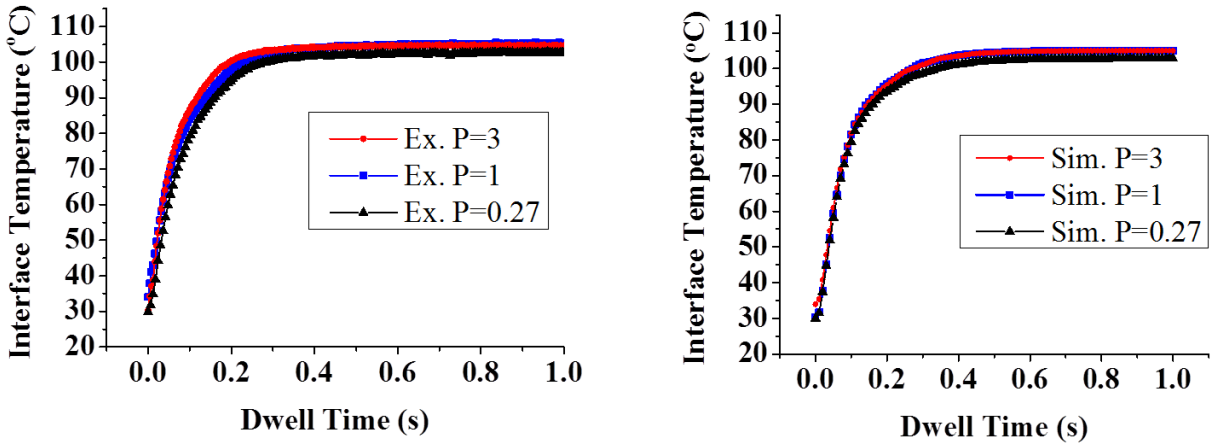

Figure 4.16 Comparison of (Left) Experimental results for different sealing pressures; (Right) Simulation results for different sealing pressure, at 105°C as jaw temperature. The unit of pressure is [N/mm^2].

4.6 Conclusion

In this work, simulation of heat transfer in heat sealing of a multilayer polymeric film was done using COMSOL Multiphysics software. The multilayer structure was composed of a metallocene linear low density polyethylene (mLLDPE) or a high density polyethylene (HDPE) as sealant layer, a polyethylene grafted maleic anhydride (PE-g-MA) as the tie layer and a polyamide (PA)

layer as the abuse layer. In order to determine the variation of material properties with temperature, thermal conductivity, specific heat capacity and density of polymers were measured at different temperatures. Thermal contact resistance was used as the boundary condition between the jaws and PA layer. It was shown that the Cooper-Mikic-Yovanovichmodel model, due to considering the plastic deformation of surface asperities, predicts much better the boundary condition in this system. In addition, it was revealed that squeeze out of sealant from the sealed area was negligible in the studied condition. The simulation results were in very good agreement with experimental data over a very wide range of temperature. When the jaw temperature was below the melting temperature of mLLDPE and HDPE, a sharp increase in the interface temperature followed by a plateau at longer times was observed in all samples. On the other hand, when the jaw temperature was set above the melting point of the sealants, lower crystalline mLLDPE sealants showed similar behaviour as observed for lower temperatures but in highly crystalline HDPE, a step-like delay was observed when the interface temperature reached melting temperature of HDPE. The origin of the observed step-like behaviour was discussed in detail and it was found that the much greater heat of fusion of HDPE and the decrease in its thermal by temperature are responsible for the observed delay. In addition, it was found that in mLLDPE, increasing the jaw temperature reduces the time required for the interface temperature to reach the jaw temperature while in highly crystalline HDPE (due to the above mentioned step-like delay), the time required to reach the jaw temperature increases as temperatures approaches melting point of HDPE. These results indicate the critical role of crystallinity of the sealant layer in determining the dwell time required to achieve desired seal strength. The effect of sealant thickness was also studied and it was found that increasing mLLDPE sealant thickness from 50 μm to 130 μm increased the dwell time required to reach the jaw temperature from 0.35 s to 1.8 s. Effect of pressure on interface temperature evolution was also examined and it was found that increasing sealing pressure from 0.27 N/mm^2 to 2.7 N/mm^2 did not have a significant effect on the interface temperature evolution. The obtained results have very important implications in packaging industry as the present simulation results clearly indicated the critical roles of the interface between film/jaw and the role of material properties especially material crystallinity in heat sealing of a multilayer film.

4.7 Reference

1. Theller, H.W., *Heat sealability of flexible web materials in hot-bar sealing applications.* Journal of Plastic Film and sheeting, 1989. **5**: p. 66-93.
2. Stehling, F.C. and P. Meka, *Heat sealing of semicrystalline polymer films. II. Effect of melting distribution on heat-sealing behavior of polyolefins.* Journal of Applied Polymer Science, 1994. **51**(1): p. 105-119.
3. Meka, P. and F.C. Stehling, *Heat sealing of semicrystalline polymer films. I. Calculation and measurement of interfacial temperatures: Effect of process variables on seal properties.* Journal of Applied Polymer Science, 1994. **51**(1): p. 89-103.
4. Tetsuya, T., et al., *The effect of heat sealing temperature on the properties of OPP/CPP heat seal. I. Mechanical properties.* Journal of Applied Polymer Science, 2005. **97**(3): p. 753-760.
5. Hashimoto, Y., et al., *Effect of heat-sealing temperature and holding time on mechanical properties of heat-sealed Poly(Lactic acid) films.* ANTEC, 2006.
6. Mazzola, N., et al., *Correlation between thermal behavior of a sealant and heat sealing of polyolefin films.* Journal of Polymer Testing, 2012. **31**(7): p. 870-875.
7. Mueller, C., et al., *Heat sealing of LLDPE: relationships to melting and interdiffusion.* Journal of Applied Polymer Science, 1998. **70**(10): p. 2021-2030.
8. Najarzadeh, Z. and A. Ajji, *A novel approach toward the effect of seal process parameters on final seal strength and microstructure of LLDPE.* Journal of Adhesion Science and Technology, 2014. **28**(16): p. 1592-1609.
9. Selke, S.E.M., J.D. Culter, and R.J. Hernandez, *Plastics Packaging: Properties, Processing, Applications, And Regulations*, ed. 2nd. 2004: Hanser Gardner Publications.
10. Morris, B.A. and J.M. Scherer, *Modeling and experimental analysis of squeeze flow of sealant during hot bar sealing and methods of preventing squeeze-out.* Journal of Plastic Film and Sheeting, 2015. **32**(1): p. 34-55.
11. Morris, B.A., *PREDICTING THE HEAT SEAL PERFORMANCE OF IONOMER FILMS.* Plastic Film and sheeting, 2002. **18**.
12. Aithani, D., et al., *Heat Sealing measurement by an innovative technique.* Packaging Technology and Science, 2006. **19**(5): p. 245-257.
13. Poisson, C., et al., *Optimization of PE/Binder/PA extrusion blow-molded films. I. Heat sealing ability improvement using PE/EVA blends.* Journal of Applied Polymer Science, 2006. **99**(3): p. 974-985.
14. Yuan, C.S., et al., *Heat sealability of laminated films with LLDPE and LDPE as the sealant materials in bar sealing application.* Journal of Applied Polymer Science, 2007. **104**(6): p. 3736-3745.
15. Planes, E., S. Marouani, and L. Flandin, *Optimizing the heat sealing parameters of multilayers polymeric films.* Journal of Materials Science, 2011. **46**(18): p. 5948-5958.
16. Robertson, G.L., *Food Packaging ,Principles and Practice*. Third ed. 2012: CRC Press.
17. Najarzadeh, Z., *Control and optimization of sealing layer in films*, in *chemical engineering*. 2014, École Polytechnique de Montréal. p. 165.
18. Kim, S., et al., *Enhanced Interfacial Adhesion between an Amorphous Polymer (Polystyrene) and a Semicrystalline Polymer [a Polyamide (Nylon 6)].* ACS Applied Materials & Interfaces, 2011. **3**(7): p. 2622-2629.

19. Yuan, C. and H. A, *Effect of bar sealing parameters on OPP/MCPP heat seal strength.* eXPRESS Polymer Letters, 2007. **1**(11): p. 773-779.
20. Mihindukulasuriya, S.D. and L.-T. Lim, *Heat sealing of LLDPE films: Heat transfer modeling with liquid presence at film–film interface.* Journal of Food Engineering, 2013. **116**(2): p. 532-540.
21. Wunderlich, B. and G. Czornyj, *A Study of Equilibrium Melting of Polyethylene.* Macromolecules, 1977. **10**(5): p. 906-913.
22. Dawson, A., et al., *Thermal conductivity of polymer melts and implications of uncertainties in data for process simulation.* Cerca con Google, 2000.
23. Dos Santos, W.N., J.A. De Sousa, and R. Gregorio Jr, *Thermal conductivity behaviour of polymers around glass transition and crystalline melting temperatures.* Polymer Testing, 2013. **32**(5): p. 987-994.
24. Dawson, A., M. Rides, and J. Nottay, *The effect of pressure on the thermal conductivity of polymer melts.* Polymer Testing, 2006. **25**(2): p. 268-275.
25. Lobo.Hubert and B.J. V., *Thermal conductivity and diffusivity of polymers*, in *Handbook of Plastics Analysis*. 2003, Marcel Dekker Inc.
26. Choy, C.L., *Thermal conductivity of polymers.* POLYMER, 1977. **18**.
27. Dashora, P. and G. Gupta, *On the temperature dependence of the thermal conductivity of linear amorphous polymers.* Polymer, 1996. **37**(2): p. 231-234.
28. Cooper, M.G., B.B. Mikic, and M.M. Yovanovich, *Thermal contact conductance.* Heat Mass Transfer, 1968: p. 279-300.
29. Babu, K.N., *Thermal Contact Resistance:Experiments and Simulation*, in *Applied Mechanics*. 2015, Chalmers university of technology.
30. Zheng, J., et al., *Measurements of interfacial thermal contact conductance between pressed alloys at low temperatures.* Cryogenics 2016. **80**: p. 33-43.
31. Gibbins, J., *Thermal Contact Resistance of Polymer Interfaces*, in *Mechanical Engineering*. 2006, University of Waterloo.
32. Sridhar, M.R. and M.M. Yovanovich, *Review of Elastic and Plastic Contact Conductance Models: Comparison with Experiment.* Journal of Thermophysics and Heat transfer 1994. **8**(4).
33. Mikik, B., *Thermal Contact Resistance*. 1966, Belgrade.
34. Song, S., M.M. Yovanovich, and F.O. Goodman, *Thermal gap conductance of conforming surfaces in contact.* Heat Transfer, 1993. **115**: p. 533.
35. Song, S., M.M. Yovanovich, and K. Nho, *Thermal Gap Conductance: Effects of Gas Pressure and Mechanical Load.* THERMOPHYSICS 1992. **6**(1).
36. Bahrami, M., M.M. Yovanovich, and E.E. Marotta, *Thermal Joint Resistance of Polymer-Metal Rough Interfaces.* Journal of Electronic Packaging, 2006. **128**(1): p. 23.
37. Fieberg, C. and R. Kneer, *Determination of thermal contact resistance from transient temperature measurements.* International Journal of Heat and Mass Transfer, 2008. **51**(5-6): p. 1017-1023.
38. Grewal, N.S., T.K. Cheung, and S.C. Saxena, *Heat transfer between horizontal finned tubes and a gas-solid fluidized bed.* Industrial & Engineering Chemistry Process Design and Development, 1985. **24**(2): p. 458-471.
39. Prasher, R., *Predicting the Thermal Resistance of Nanosized Constrictions.* Nano Letters, 2005. **5**(11): p. 2155-2159.

40. Morris, B.A., *Application of modeling to speed flexible package development.* Journal of Plastic Film and Sheeting, 2013. **29**(3): p. 249-270.
41. Morris, B.A., *Predicting the performance of ionomer films in heat-seal processes.* Paper, Film and Foil Converter, 2003. **77**(3): p. 207.
42. Morris, B.A., *Predicting the Heat Seal Performance of Ionomer Films (75)*, in *ANTEC 2002 Plastics: Annual Technical Conference, Volume 2: Materials*. 2002, Society of Plastics Engineers.

CHAPTER 5 ARTICLE 2:

SQUEEZE FLOW IN MULTILAYER POLYMERIC FILMS: EFFECT OF MATERIAL CHARACTERISTICS AND PROCESS CONDITIONS

Zahra Kanani Aghkand, Abdellah Ajji*

3SPack, CREPEC, Department of Chemical Engineering, École Polytechnique de Montréal, Montréal, Québec H3C 3A7, Canada

*Corresponding Author: abdellah.ajji@polymtl.ca

Submitted to ASC Applied Polymer Materials

5.1 Abstract

This work studies squeeze out flow (SOF) of thin sealant layers in multilayer polymeric films during heat sealing. Effects of sealing temperature, time, pressure, as well as sealant thickness and viscosity on SOF were examined. SOF was quantified using scanning electron microscopy (SEM) images. Experimental results showed that SOF increased with time and temperature. When sealant thickness was reduced from 130 to 50 µm, no SOF was observed even at high sealing pressure and time. Reducing viscosity of the sealant was found to be a promising approach only at high pressure and long sealing times. Increasing sealing pressure was found to have a marginal effect on SOF. Three approaches were used to model SOF: analytical one-dimensional model, numerical one-dimensional model using finite difference method (FDM), (iii) Numerical two-dimensional model using finite element analysis (FEA). The phenomena involved in SOF were discussed in detail and it was shown that the presented FDM model could predict SOF with good precision. Modeling results also showed that squeeze flow occured in shear rates between the Newtonian and Power-law regions. This highlights the complexity of SOF in thin sealant layers and the importance of the presented FDM model in designing multilayer polymeric films.

Keywords: Squeeze flow, Multilayer polymeric films, modelling, heat sealing

5.2 Introduction

Flexible plastic packaging plays a critical role in handling and keeping packaged products safe from contamination and spoilage, while allowing presenting product information and promoting products and brands [1, 2]. In addition, much less package to product weight ratio in flexible packaging reduces their environmental impact compared to alternative packaging options [3]. Nowadays and by increasing the demand for multifunctional flexible packaging, different aspects need to be considered in package design. Defect free sealing ensures a hermetic sealing that provides package integrity and protects products during packaging, handling and delivery steps [4]. Heat sealing is the most common process in sealing of flexible plastic packaging. Channeling in the seal area is a common defect in heat sealed packages which can originate from non-optimized sealing conditions such as temperature, pressure, and dwell time [2, 5, 6]. In addition, channeling can occur in the wrinkled area, three-point junctions or in the presence of contaminations in the seal area. It has been shown that numerical modeling of heat sealing process allows optimize sealing condition and improving seal quality [7-10]. The effect of wrinkles, junctions or contaminations can also be minimized by selecting sealants with good caulkability[5, 6]. Caulkability is the ability of a sealant material to flow and fill gaps in the wrinkles and junctions or encapsulate contaminations in the seal area [125]. Caulkability is a necessary characteristic of sealant materials especially in the packaging of powders, grainy or shredded products such as coffee powder or shredded cheese [11, 12]. Considering the physics of heat sealing process, caulkability can be seen as the ability of a sealant to flow under the squeezing sealing pressure during heat sealing process. This phenomenon is known as squeeze out flow or in short, SOF [2, 6, 13]. Despite the significant importance of SOF in heat sealing of plastic packaging, few attempts have been made to study the effects of sealant material properties and sealing condition on SOF in heat sealing process. Dan and Li [5] examined SOF of a wide range of different sealant materials. They used scanning electron microscopy (SEM) images taken from the cross-section of the sealed area in the presence of solid particles and expressed SOF as the ability of the sealant material to encapsulate the solid particles. The size of the gap between the surface of solid particles and the polymer matrix in SEM images was considered as the ability of sealant to show SOF and caulkability. As a poor interface between a polymer matrix and particles can cause debonding of the interface and gap formation during cooling and cutting the sample, this method can cause

considerable error in examining the caulkability of sealants. They also assumed that the shear rate during SOF in heat sealing falls within the Newtonian region but could not find a relation between SOF wand zero-shear viscosity of sealant materials. Some previous works have also examined seal through contaminations, by attempting to correlate caulkability to seal strength. For example, Mesnil et al. [11] examined the seal through contamination properties of different sealant materials, but only compared their seal initiation temperature and seal strength. As the seal strength can be affected by many material properties and sealing conditions, this approached cannot provide a reliable tool in examining the caulkability of sealants.

Due to the lack of the knowledge on the effects of sealing parameters and sealant characteristics on SOF and caulkability of sealants, selecting a proper sealant material in industrial applications can be very costly as it requires trials involving all steps of package production chain from the film production step to converting and, finally, packaging of products. This indicates the significant importance of modeling SOF during heat sealing as a promising solution to reduce the cost of sealant selection. Squeeze flow of liquids between solid surfaces has been studied extensively due to its wide range of applications. The compression moulding of polymers is a squeeze flow of molten polymer inside the mold [10, 14]. Valves and diarthrodial joints are examples for squeeze flows in biology and bioengineering [15]. SOF has also been studied in polymer welding [2, 16-18], interface healing of polymers [19] and estimation of the rheological properties of polymers [20-22] and foods [23, 24]. Analytical models have been presented to estimate SOF in different geometries such as parallel rectangular plates [25], circular discs [21, 26], or even non-parallel surfaces [27] for both Newtonian and non-Newtonian fluids [28-30]. SOF can be defined as:

$$SOF\% = (1 - \frac{h}{h_0}) \times 100 \qquad \text{Eq. 5.1}$$

where h/h_o is the ratio of the final gap to the initial gap between solid surfaces. The previous works on modeling SOF in the literature can be categorized into two main groups: (i) constant volume mode [18, 26], and (ii) constant contact area mode [21, 25]. In the first group, the liquid does not fill the gap between plates and squeezing of the plates increases the contact area between solid surfaces and the liquid, but the liquid remains always between solid surfaces and no liquid is squeezed out. In the constant contact area mode, the liquid always fills completely the gap between plates and squeezing of the plates leads to squeeze out of the liquid from the gap. SOF in heat

sealing should be modeled using constant contact area assumption because the contact area between the solid and liquid surfaces remains constant during the process. Most of the previous studies on squeeze flow in this category, focused on SOF between two parallel circular disks in cylindrical coordination and the experimental results were presented in much thicker polymeric sheets. Therebefore, they cannot be directly applied to squeeze flow within sealant layers during heat sealing which occurs between two rectangular plates with a very thin gap. Gupta [25] derived an analytical formula to estimated SOF of a Newtonian fluid between two parallel rectangular plates. His formula was obtained based on the assumption that the approaching velocity of the plates at any time is known. However, in heat sealing process only the applied pressure is controlled, and models based on approaching velocity cannot be considered as predictive models. Morris and Scherer [125] developed the following analytical model to predict SOF during heat sealing process of plastic materials:

$$\frac{h_0}{h} = \left(1 + \frac{F \times t \times h_0^2}{\eta \times w \times L^3}\right)^{1/2} \qquad \text{Eq. 5.2}$$

where F, t, η, W and L are the applied force, time, viscosity, width of the seal area and the length of the seal area, respectively. Their model was based on the Newtonian fluid, Quasi-steady state and isothermal assumptions. They attempted to measure SOF experimentally based on the cross-sectional area of squeezed out sealant material. By comparing model predictions with experimental data, they found that the model significantly underestimated SOF which they attributed to the Newtonian fluid and isothermal assumptions. It should be noted that replacing the obtained velocity profiles by the authors do not satisfy the equations of motions used in developing their model. When a much more complicated fluid behavior was used for modeling squeeze flow between parallel rectangular plates in isothermal conditions, it has been shown that the obtained non-linear differential equations do not allow achieving an explicit analytical solution and therefore numerical methods have been used to estimate the velocity and pressure profiles [10, 14, 31, 32]. The previous works used computational flow dynamics (CFD) software to model SOF and they considered the approaching velocity of the solid surfaces as a model input. These have considerably limited the practical application of the available models in predicting SOF in heat sealing process.

In this work, first, effects of sealant material characteristics and sealing condition on squeeze out flow of different sealants in multilayer polymeric films will be examined experimentally. To this aim, a procedure for measurement of SOF will be presented based on SEM image analysis. Then, the effects of different processing conditions such as sealing temperature, sealing time (dwell time), sealing pressure, will be examined at two different sealant thicknesses. The effect of sealant viscosity as the main material characteristic of the sealant will also be investigated. One analytical model and two numerical models based on finite difference method (FDM) and finite element analysis (FEA) will be used to model SOF in heat sealing. The mechanism of SOF in heat sealing will be discussed in detail using the experimental data and models results.

5.3 Experimental

5.3.1 Materials

Two metallocene linear low density polyethylene (m-LLDPE) with commercial names of Exact 3131 and Exact 3139 were purchased from ExxonMobil. Polyamide (PA) and Polyethylene-grafted maleic anhydride (PE-g-MA) with commercial names of Ultramid B36 and Bynel 4125 were purchased from BASF and DuPont, respectively. PE-g-MA was used as adhesive layer between m-LLDPE and PA layers. PA granules were dried at 100℃ overnight under vacuum to eliminate its moisture content before experiments.

5.3.2 Film preparation

Multilayer films containing of a sealant layer (m-LLDPE), a tie layer (PE-g-MA) and a PA outer layer, were prepared using cast film co-extrusion. Three single screw extruders with 20 mm screw diameter and L/D=30 were used in the co-extrusion process. Temperature profiles of 215 to 240^{o}C, 220 to 235^{o}C and 230 to 250 ℃ were used for the extrusion of sealant layer, tie layer and PA layer, respectively. An air knife and a calendar at the die exit were used for cooling and collection of film samples. To investigate the effect of sealant thickness, multilayer film samples with two different sealant thicknesses of 50 and 130 μm were prepared while the thickness of the tie and PA layers were maintained at 10 μm and 40 μm, respectively.

5.3.3 Melt density

Melt density of polymers at the sealing temperatures were measured using a high-pressure piston-type dilatometer (PVT100, ThermoHaak). The detail of measurement procedure can be found in our previous publication [9]. In summary, 0.5 to 0.7 g of polymer granules were fed into the cylinder of the dilatometer. Temperature was raised to 160^{o}C and degassing was done to avoid bubble entrapments into the melt. Then polymer melt was cooled down with the rate of 10^{o}C/min. The instrument determines density variation by measuring the variation of volume at 10^{o}C steps.

5.3.4 Differential Scanning Calorimetry (DSC)

DSC tests were performed using a DSC machine (Q2000 machine, TA Instruments) under nitrogen atmosphere. Thermal history of the samples was eliminated by heating the samples to 180^{o}C and then cooling them to the room temperature at 10^{o}C/min. Then temperature was then again increased from the room temperature to 180 ℃ at 10^{o}C/min and the data was recorded for analyses.

5.3.5 Rheological Characterization

Samples were prepared by compression molding at 180 °C and 300 kPa under a nitrogen blanket. Samples were in disk shape form with thickness of 1.2 mm and diameter of 25 mm. The rheological analysis was performed using a controlled-stress rheometer (Physica MCR 301, Anton Paar) with 25 mm parallel plate geometry at 1 mm gap. The measurements were done at temperatures of 105°C and 140°C under nitrogen atmosphere. The zero-shear viscosity and Power-Law parameters were obtained by fitting Carreau-Yasuda and Power-law models on the obtained data using the machine software (RheoPlus V2.65).

5.3.6 Heat Sealing

An automated heat-sealing machine (SL10 LakoTool, Lako Tool & Manufacturing Inc) was used to seal the samples at the desired temperature, pressure and dwell time. The machine had a time resolution of 100 ms. Strips of films with a width of 25.4 mm and the length of 100 mm were cut. The sealing bars had dimensions of 25.4 mm in 19.4 mm.

5.3.7 Scanning Electron Microscopy (SEM)

Cross-sections of sealed area was observed using a SEM equipment (TM3030plus, Hitachi,). To this aim, samples were cut using a razor blade and their cross-section was observed by the SEM machine.

5.3.8 Measurement of SOF

SOF measurements were done based on image analyses of SEM images of cross-section of sealed area in two regions: between the films and on the edges of sealed area. These two regions are shown below.

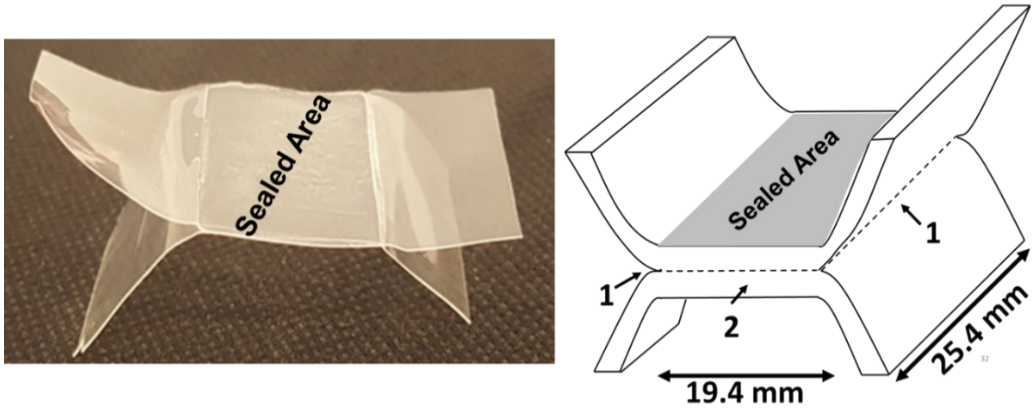

Figure 5.1 (Left) a sealed sample, (right) schematic showing the regions where SOF was measured from SEM images of the cross section of sealed area: 1. between films, 2. on the edges. The dashed lines in the schematic show the interface between two sides of the seal.

Depending on the amount of SOF, different shapes can be seen in the sealed area especially between sealed films region (region 1 in Figure 1.1). To measure SOF in the samples after sealing, the film thickness was traced back into the sealed area until the traced lines reach each other in the center, see Figure 5.2. The traced lines reach each other in the center at a point where sealed area should begin in the absence of SOF. Three different shapes of the sealed area between were observed that are shown in Figure 5.2. In samples similar to Figure 5.2(a1), it can be seen that the point where the traced lines reached each other is the same as the point where sealed area begins. This indicates that this type of samples did not have SOF during sealing. In the samples similar to Figure 5.2(b1) and Figure 5.2(c1), it can be seen that the points where traced lines reached each

other are inside of the sealed area, which indicates considerable SOF in these samples. To calculate the amount of SOF, the area of the highlighted regions in Figure 5.2(b) and (c) was multiplied by the width of the sealed strips (25.4 mm).

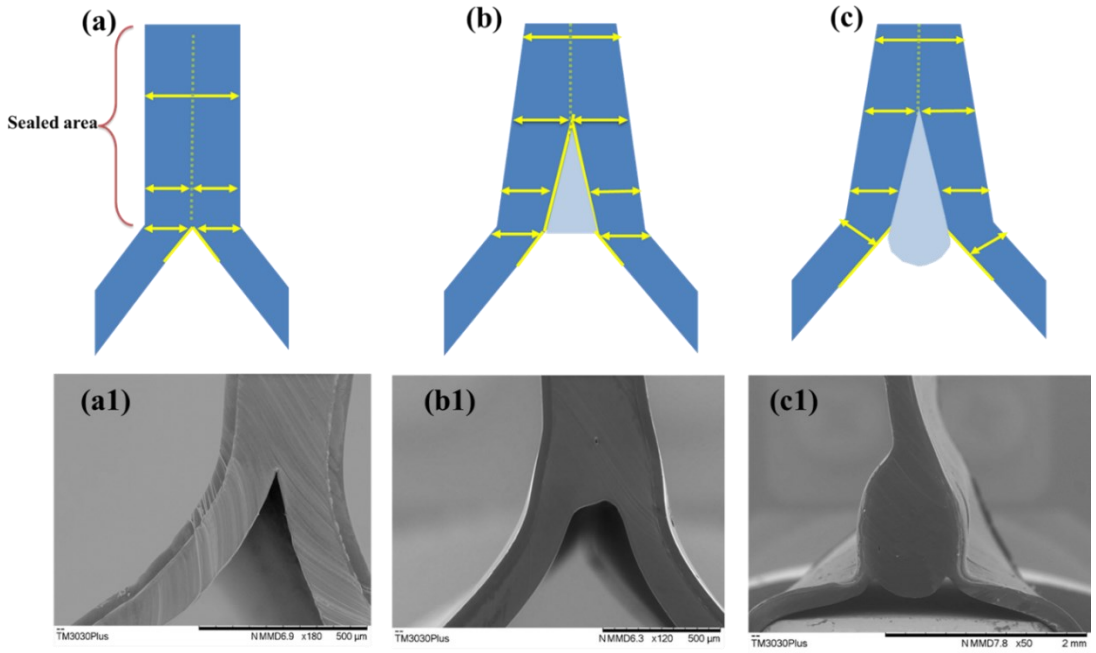

Figure 5.2 Schematic and SEM images of different possible shapes of the cross-section of sealed area between sealed films, (a) and (a1): No SOF in a film with 130µm sealant sealed at P=0.2N/mm^2, dwell time=1s and T=140^{o}C ,(b) and (b1) low SOF in a film with 130µm sealant sealed at P=0.2N/mm^2, dwell time=2s and T=140^{o}C, (c) and(c1) high SOF or poly ball shape in a film with 130µm sealant sealed at P=3 N/mm^2, dwell time=3s and T=140^{o}C. The dashed lines show the interface between sealed sides.

In addition, SOF was also measured on the edges of the sealed area (indicated as region 2 in Figure 1.1). Figure 5.3 shows the procedure of measuring SOF in the edge side. SOF in the edge side was calculated by multiplying the area of the squeezed-out region by the length of the sealed area (19.4 mm). Finally, the total amount of SOF is obtained by adding the calculated amount of SOF in region 1 and 2. It should be noted that as SOF occurs in the melt state and the above mentioned measurements were done in the solid state, the obtained values from the image analyses were multiplied by the ratio of the density of sealant in solid state to its melt density at the sealing temperature.

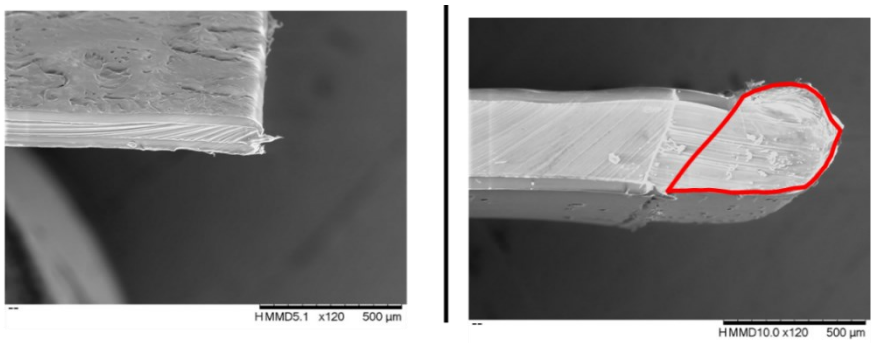

Figure 5.3 SEM images of SOF from edge of the sealed area: (lef) no SOF in the film with 50µm sealant thickness sealed at t= 2s, P= 3 N/mm^2 and T= 140 ^{o}C, (right) SOF in film with 130µm sealant thickness sealed at t= 3s, P= 0.27 N/mm^2 and T= 140^{o}C. The red line in the right image shows the SOF region.

5.3.9 Simulation of Heat Transfer

Heat transfer during heat sealing was modeled using COMSOL Multiphysics. The heat transfer model was described in detail in our previous study [9]. In brief, heat transfer from the heated jaws to three-layer films composed of PA, PE-g-MA and mPE was modeled using the following assumptions: (i) perfect interface and continuity between polymer layers, (ii) symmetry at the interface between two seal sides, (iii) thermal contact resistance (TCR) boundary condition between the jaw and PA layer described using the plastic Cooper−Mikic−Yovanovich (CMY) model, (iv) temperature variations of density, specific heat (C_p) and thermal conductivity (k) were considered.

5.4 Modeling Strategy

In order to model the sealant flow during heat sealing, a geometry similar to the one shown in Figure 5.4 was considered.

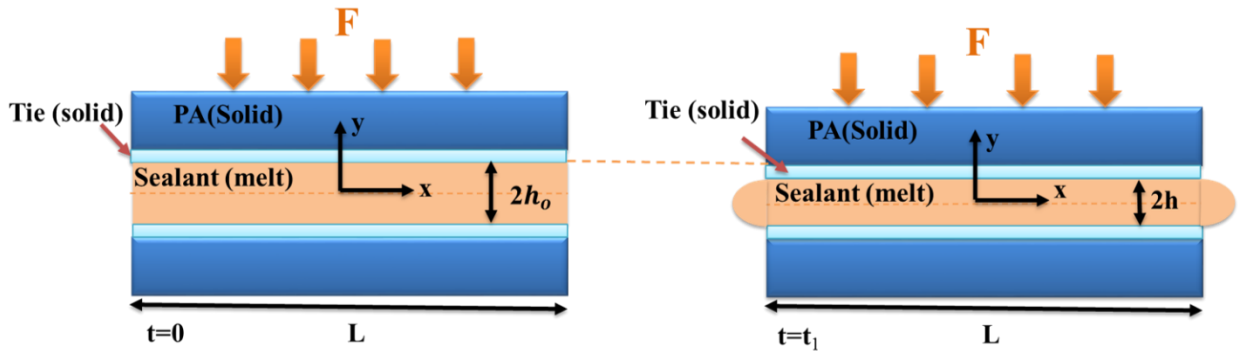

Figure 5.4 Squeeze flow during heat sealing process: (left) before, and (right) after squeeze flow

Three modeling approaches were used: (i) one-dimensional modeling using Power-law fluid, (ii) one-dimensional modeling using Carreau-Yasuda fluid and finite difference method (FDM), (ii) two-dimensional modeling using Carreau-Yasuda fluid and finite element analysis (FEA) using COMSOL Multiphysics software

5.4.1 One-dimensional model based on Power-law fluid

The power-law model was derived based on the geometry and coordination system shown in Figure 5.4, and the following assumptions: (1) symmetry in both x- and y- directions (2) creep flow, inertia effects are negligible, (3) quasi-steady state condition, (4) thickness of the sealant is much smaller than its other dimensions, (5) incompressible fluid, (6) complete melting of the sealant (single phase flow), (7) sealant viscosity follows power-law model, (8) constant applied pressure to the jaws, (9) one dimensional fluid flow in x-direction, (10) no slip condition at the walls, and (11) isothermal flow. The mass balance, continuity and the Navier-Stokes equations then can be written as:

$$\frac{\partial V_x}{\partial x} = 0 \qquad \text{Eq.5.3}$$

$$-\frac{dh}{dt} = \frac{4}{L}\int_0^h V_x(y)dy = \frac{4}{L}\int_0^h y\left(-\frac{\partial V_x}{\partial y}\right)dy \qquad \text{Eq. 5.4}$$

$$-\frac{\partial P}{\partial x} = m\frac{\partial}{\partial y}\left(-\frac{dV_x}{dy}\right)^n \qquad \text{Eq. 5.5}$$

The relation between pressure gradient and the applied force to the films can be written as:

$$F = 2W\int_0^{L/2} P(x)\,dx = 2W\int_0^{L/2} x\left(-\frac{\partial P}{\partial x}\right)dx \qquad \text{Eq. 5.6}$$

Solving this system of equations using the assumption of a linear pressure profile ($\frac{\partial P}{\partial x} = \text{constant}$) within the sealant layer leads to the following analytical solution:

$$\frac{h_0}{h} = \left(1 + t\,\frac{4(n+1)}{L(2n+1)}\,h_0^{\frac{1}{n}+1}\left(\frac{2F}{mL^2W}\right)^{1/n}\right)^{\frac{n}{n+1}} \qquad \text{Eq. 5.7}$$

5.4.2 One-dimensional FDM model

The following assumptions were used to build the model: (1) symmetry in both x- and y- directions (2) creep flow, inertia effects are negligible, (3) quasi-steady state condition, (4) thickness of the sealant is much smaller than its other dimensions, (5) incompressible fluid, (6) complete melting of the sealant (single phase flow), (7) sealant viscosity follows Carreau-Yasuda model, (8) constant applied pressure to the jaws, (9) one dimensional fluid flow in x-direction, (10) no slip condition at the walls, and (11) isothermal flow.

In this model, the Navier-Stokes equation based on Carreau-Yasuda fluid assumption can be written as:

$$\frac{\partial P}{\partial x} = \frac{\partial}{\partial y}\left(\eta_0\left(1 + (-\lambda\frac{\partial V_x}{\partial y})^a\right)^{\frac{n-1}{a}}\frac{\partial V_x}{\partial y}\right) \qquad \text{Eq. 5.8}$$

Equation 8 is a non-linear equation without an explicit analytical solution for the velocity gradient. Therefore, solving system of equations 3, 4, 6 and 8 using the applied force as the only input data is not possible. Shuler and Advani [31] solved a system of equations 4, 6 and 8 using experimental dh/dt data as a model input. Their method was based on initial guessing of $\frac{\partial P}{\partial x}$ at each x- location, then estimation of $\frac{\partial V_x}{\partial y}$ at any y-node in that x-location using Equation 8, and finally estimating

dh/dt using Equation 4 at each x-location. By comparing the estimated dh/dt with the experimental data, they corrected $\frac{\partial P}{\partial x}$ until the estimated dh/dt converged to the experimental data. In addition to the long computation time for their approach, assuming that $\frac{\partial P}{\partial x}$ is a function of x, indicates that in their model V_x depends on the x-location. This implies that $\frac{\partial V_x}{\partial x} \neq 0$ which does not satisfy the continuity condition (Equation 3). In addition, considering that they assumed the approaching velocity (dh/dt) as a known parameter leads to a model which cannot predict SOF and rather can only be used to examine velocity, and pressure profile within liquid.

In order to achieve a predictive model based on the above system of equations, Equation 6 can be simplified using a linear pressure profile assumption. Using this assumption, Equation 6 can be reformed to estimate the pressure gradient as:

$$\frac{\partial P}{\partial x} = -\frac{4 \times F}{L^2 W} \qquad \text{Eq. 5.9}$$

A numerical method now can be used to solve the system of equations consisting of equation 5 and 3 to estimate dh/dt. Figure S-1 in the supplementary information shows the flow chart for the program written in Octave software to solve this system of equations.

5.4.3 Two-dimensional FEA model

Squeeze flow during heat sealing was modeled using COMSOL Multiphysics by considering the following assumptions: (1) incompressible fluid, (2) transient laminar flow in the sealant layer, (3) isothermal condition, (4) known approaching jaws velocity, (5) thickness of sealant is much thinner than its other dimensions, (6) sealant is completely melted (single phase flow), (7) sealant viscosity follows Carreau-Yasuda model, and, (8) no slip condition at the walls. It should be noted that, as shown in the supplementary information, 2D modeling of SOF without the knowledge of squeezing velocity (dh/dt) or pressure gradient is not possible. Considering these assumptions, a simulation consisting of three main physics was built in COMSOL Multiphysics: (i) laminar flow mode to simulate the flow in the sealant, (ii) solid mechanics mode for simulation of solid surface movement, and (iii) Multiphysics mode for simulation of interactions of solid surfaces with the fluid. In addition, the Carreau-Yasuda model was defined as a material function for the viscosity

of the sealant materials. The jaw velocity was also defined as a function of time based on the experimental measurements. The moving mesh and a deforming fluid domain were used to consider the movement of jaws and deformation of the sealant layer during squeeze flow. The geometry was considered to be surrounded by air at ambient pressure and temperature.

5.5 Results and Discussion

5.5.1 Material Characterization

Figure 5.5 shows the complex viscosity of the sealant materials measured as a function of angular frequency at two different temperatures of 105°C and 140°C for Exact 3131 and at 140°C for Exact 3139.

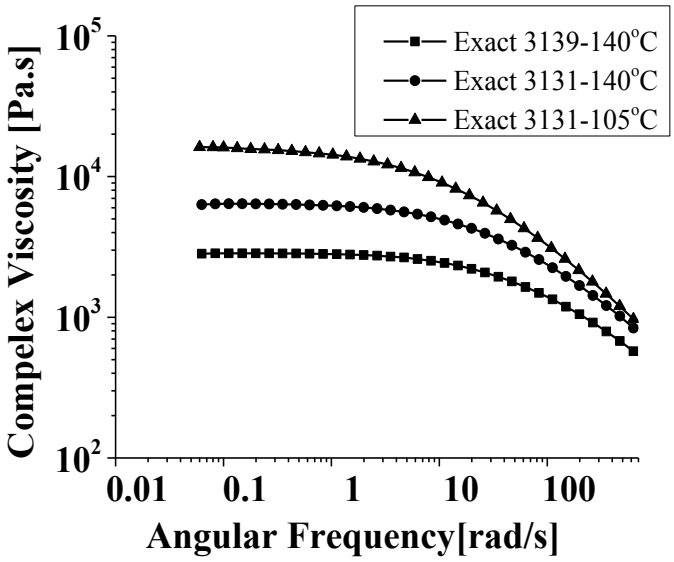

Figure 5.5 Complex viscosity versus angular frequency for Exact 3131 at 105°C and 140°C and Exact 3139 at 140°C.

Both sealant materials showed a Newtonian plateau at low angular frequencies followed by a transition region and a power-low behavior at higher frequencies. Increasing temperature in Exact 3131 considerably reduced the length of the Newtonian plateau region which is in-line with previous findings on the effect of temperature on rheological properties of polymer melts [33]. Polyethylene melts have been shown to obey the Cox-Merz rule [34] which indicates that the

complex viscosity at different angular frequencies is proportional to the shear viscosity at different shear rates [35]. Carreau-Yasuda and Power-law models [36] were fitted on complex viscosity data of sealant materials to determine their rheological characteristic parameters and the obtained results are listed in Table 5.1 In addition to rheological characterization, understanding melting behavior of sealant materials is another important aspect needed for analyzing their SOF behavior. Results of the DSC analysis, Figure 5.6, Exact 3131 and 3139 show peak melting temperatures of 94.1 and 95.1°C. In addition, the melting peak of Exact 3131 and 3139 ends at 103 and 104°C.

Table 5.1 Rheological parameters determined from fitting Carreau-Yasuda and Power-law models on experimental data.

	Power -Law model		Carreau-Yasuda model			
Equation	$\eta = m\dot{\gamma}^{n-1}$		$\eta = \eta_0(1 + (\lambda\dot{\gamma})^a)^{\frac{n-1}{a}}$			
Sample	n	m (Pa.s^n)	η_0(Pa. s)	τ (s)	a	n
Exact 3131 at 105°C	0.45	37153	14660	0.18	2	0.45
Exact 3131 at 140°C	0.48	25118	6473	0.029	0.82	0.32
Exact 3139 at 140°C	0.57	9862	2870	0.02	0.86	0.39

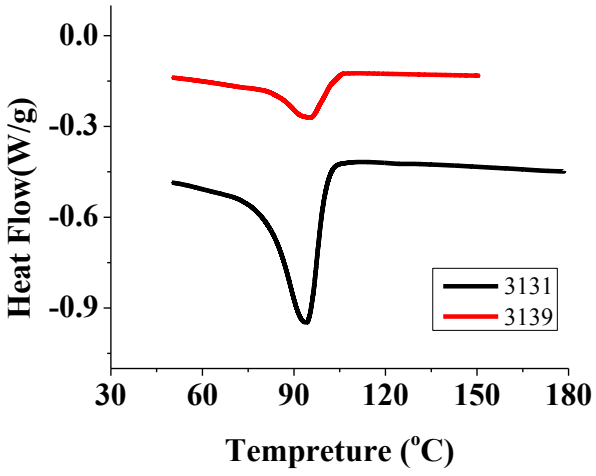

Figure 5.6 DSC heating curves of Exact 3131 and Exact 3139

These results confirmed that both sealing temperatures of 105 and 140°C used in this study are located above the melting peak temperatures of the sealants. In addition, the variation of specific

heat of sealant materials with temperature was also measured for modeling of heat transfer during the sealing process. SOF measurements based on image analysis are done in the solid state while SOF occurred in the melt state, therefore, the variation of density between melt and solid state needs to be considered in determining SOF. The variation of density with temperature was considered for modeling of heat transfer during the sealing process. Figure 5.7 shows the variation of densities of Exact 3131 and Exact 3139 measured in the range of 40 to 160^{o}C. It should be mentioned that the variation of the density within the studied pressure range in this study, 0.27 to 3 N/mm^2, was found to be negligible.

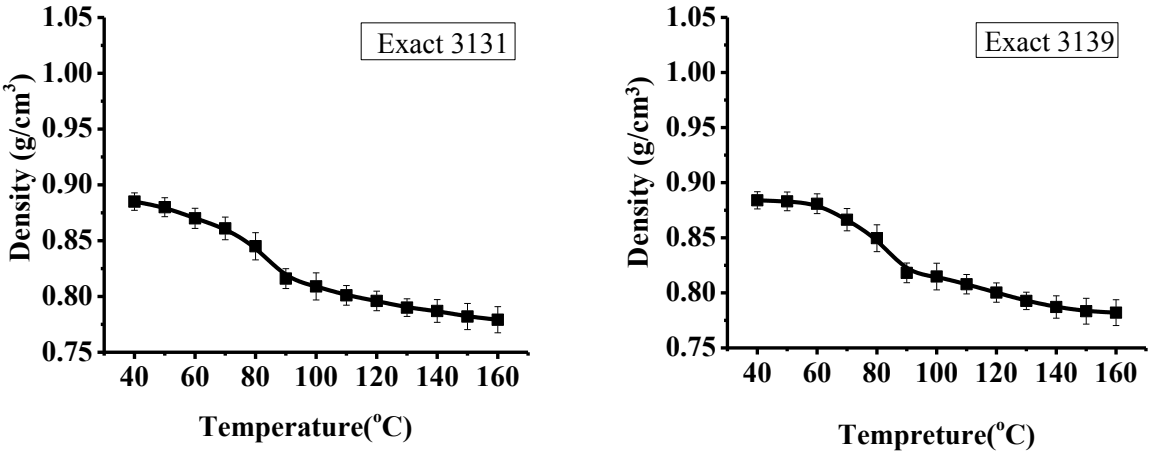

Figure 5.7 Variation of density of Exact 3131 (taken from our previous study[9]) and Exact 3139 with temperature.

By increasing temperature and approaching the melt temperature of sealants, the density of both materials decreased rapidly and reached a value of 0.8 g/cm^3 at 105^{o}C and 0.78 g/cm^3 at 140^{o}C. Considering the density of sealants at room temperature (~ 0.88 g/cm^3), the measured SOF data at room temperature were multiplied by 1.11 to compensate for density variation.

5.5.2 Effect of Jaw Temperature and Dwell Time on SOF

Before discussing experimental results, it should be mentioned that SEM images showed that SOF occurred in the sealant layer during heat sealing and the tie layer remained intact and inside the seal area. This can be attributed to the higher melting temperature (T_m= 122 ^{o}C [9]), higher viscosity (see Figure S-2 in the supplementary information) and the thinner layer thickness of tie compared to the sealant materials

Figure 5.8 shows the evolution of SOF at different dwell times in two studied jaw temperatures of 105°C and 140°C for a thick sealant (130µm) of Exact 3131. It should be noted that all samples were sealed at sealing pressure of 3 N/mm^2. When samples were sealed at 140°C, SOF increased continuously at short times and the SOF variation by time decreased considerably at dwell times longer than 2 s. These results indicate that increasing dwell time cannot always lead to enhanced SOF and caulkability. A much lower SOF was observed when samples were sealed at 105°C. In addition, decreasing the jaw temperature reduced considerably SOF dependency to dwell time at short sealing times. These results can be attributed to the increased viscosity of the sealant by reducing temperature. It should be noted that 3s of heat sealing is considered as a very long sealing time and most heat sealing processes in plastic packaging are done with dwell times shorter than 1s. Considering the negative effect of increasing dwell time on production rate in industrial scale, these result clearly indicate that increasing jaw temperature is a much more prominent approach in improving SOF and caulkability.

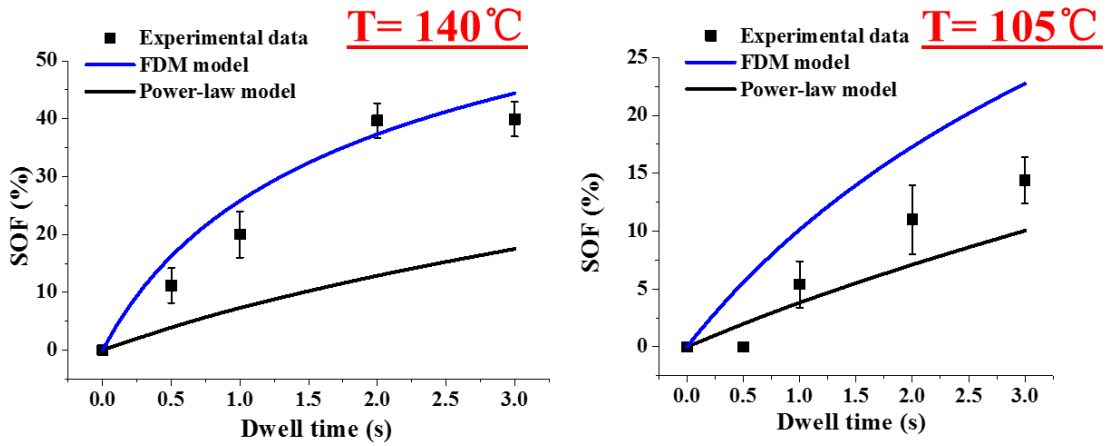

Figure 5.8 Comparing SOF at different dwell times in samples sealed at 105°C and 140°C with the predictions of the FDM and power-law models.

Figure 5.8 also shows the predictions of the FDM model, and the power-law model. At both jaw temperatures, power-law model underestimates considerably the SOF and shows a continuous increase in the SOF by time. The origin of underestimation of SOF by the power-law will be discussed later in this paper. On the other hand, the FDM models tends to overestimate SOF especially at jaw temperature of 105°C. But it can be seen that the FDM model predicts well the trend of the experimental data. As mentioned earlier, two-dimensional FEA model requires the

knowledge of the squeezing velocity of the jaws. Using Equation 1, the sealant layer thickness at any time can be determined from SOF data. Figure 5.9 shows the calculated h/h_o curve based on the measured SOF data in Figure 5.8. The derivative of the obtained results is in fact the squeezing jaw velocities which can be used in the FEA model. The velocity profile across the sealant thickness predicted by the FEA model at two different jaw temperatures are shown in Figure 5.10 . In addition, the velocity profiles predicted by the FDM model are also shown in this Figure.

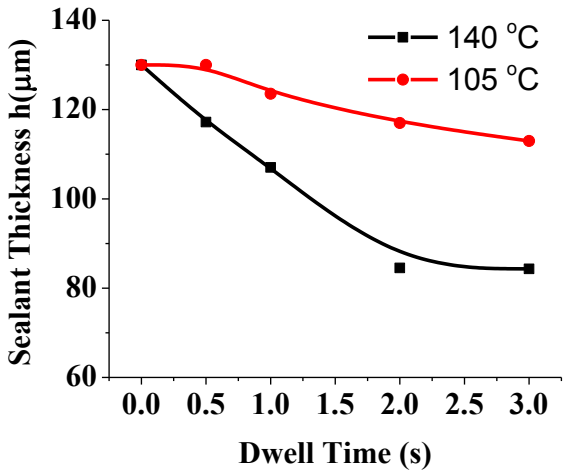

Figure 5.9 Reduction of sealant thickness with dwell time at sealing temperatures of 105°C and 140°C determined from SOF data in Figure 8.

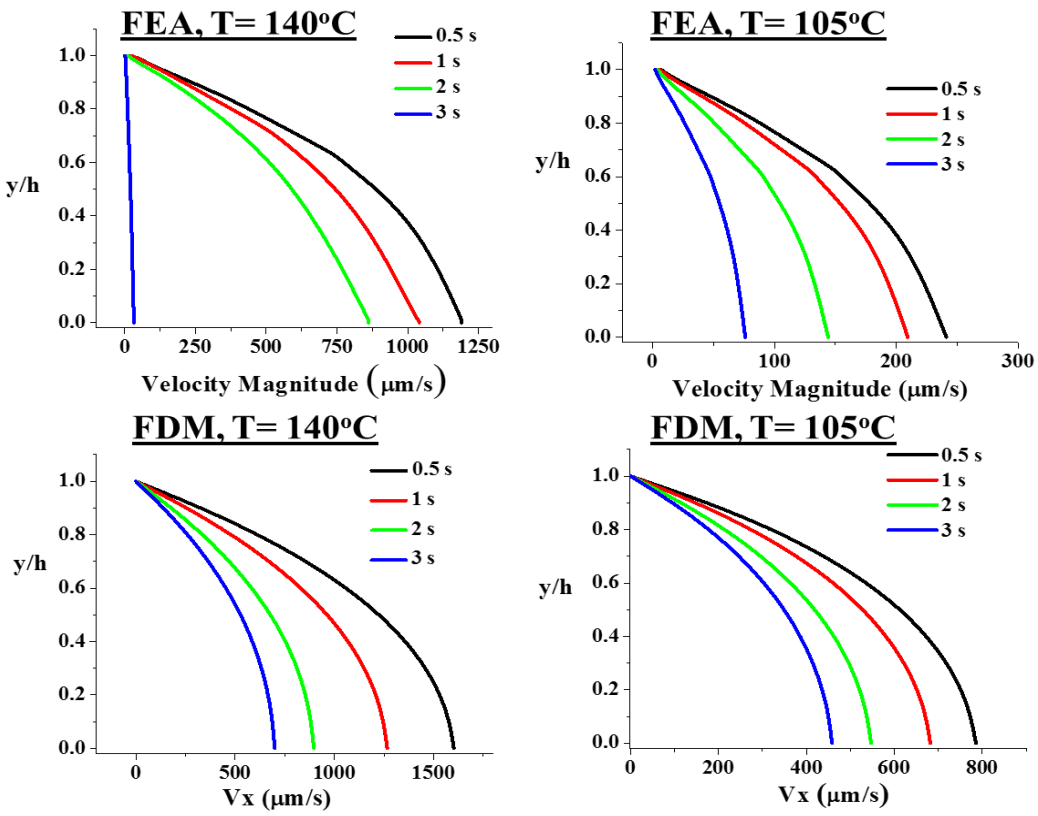

Figure 5.10 Velocity profile across the half thickness of the sealant layer at different dwell times. The sealant thickness was normalized for the ease of comparing the profiles. Legends show the dwell time for each profile.

Both FEA and FDM models predict a parabolic velocity profile but the FDM model predicts higher fluid velocities compared to the FEA model, especially at low sealing temperature. This can explain why the FDM model overestimated experimental SOF data. To better understand the origin of this difference, pressure distribution and pressure gradients inside the sealant layer predicted by FEA model at each dwell time is shown below.

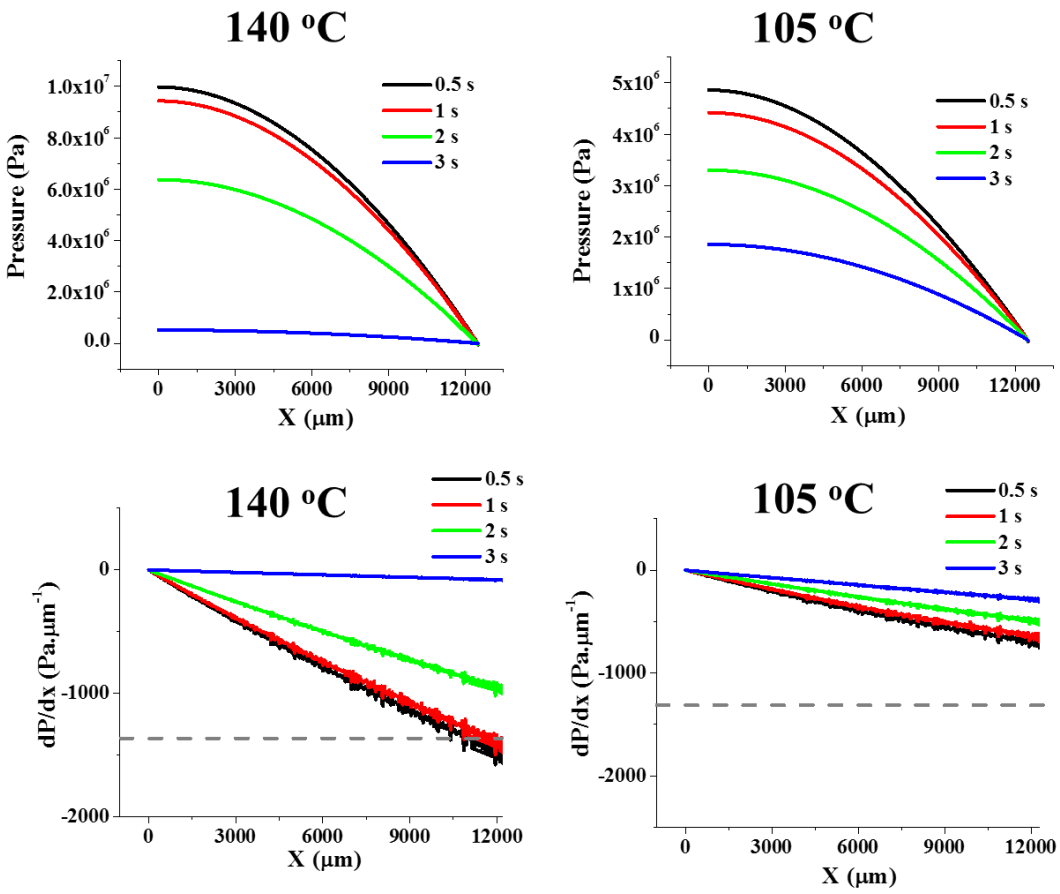

Figure 5.11 Pressure profile (top) and pressure gradient (bottom) estimated by the FEA model at different dwell times and Jaw temperatures. The dashed lines in the pressure gradient profiles show the constant pressure gradient used in the FDM model.

Pressure distributions along the x-axis estimated by FEA model clearly shows a non-linear pressure profile in the x-direction. In addition, the estimated pressure gradients by FEA model in all dwell times are always below the constant pressure gradient considered in the FDM model (the dashed line in Figure 5.11). In addition, heat transfer from the heated jaws toward the interface was not considered in the FDM model. In a previous study [9], a comprehensive heat transfer simulation was done on heat sealing process of multilayer films with the same film structure as in this study and it was shown that the simulation predictions were in a very good agreement with the experimental temperature measurements at the interface between two seal sides. As the heat transfer to the sealed area is done from outside, it is expected that the outer side of the sealant layer melts first, and then the melt layer thickness increases by increasing dwell time until the whole sealant layer is melted, Figure 5.12 (a). Using the heat transfer simulation, the evolution of the

thickness of the melt layer for 130 µm Exact 3131 sealant at 140°C and 105°C sealing temperatures was predicted and the results are shown in Figure 5.12 (b). It should be noted that, reaching the peak melting temperature of the sealant s considered as the melting criterion.

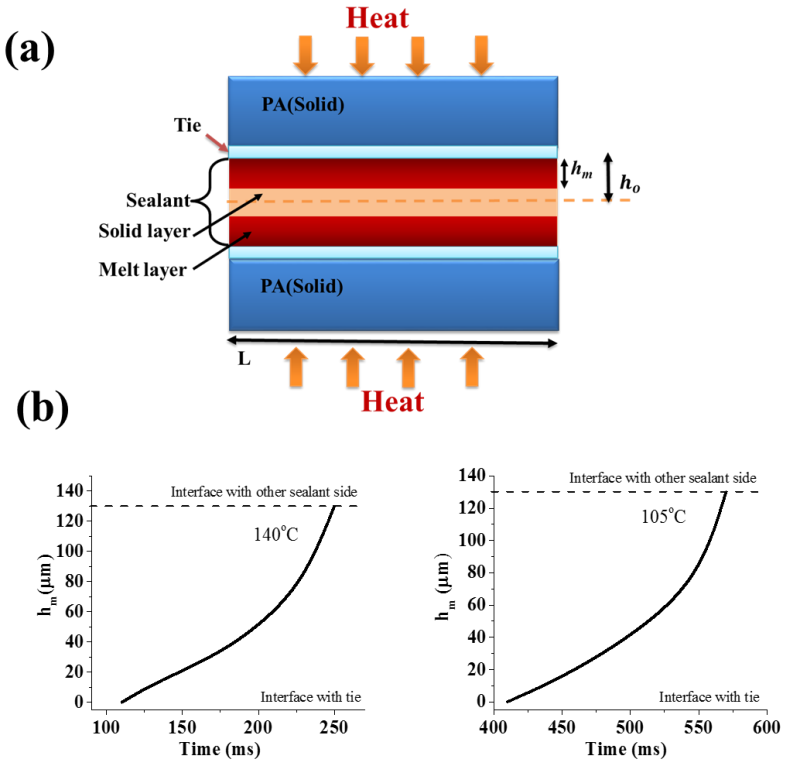

Figure 5.12 (a)Schematic of melt layer thickness evolution during heat sealing, and (b) Exact 3131 melt layer thickness(h_m) at different times during heat sealing process at jaw temperatures of 140°C and 105°C. The total thickness of the sealant layer was 130 µm

The simulation results show that at the jaw temperature of 140°C, the whole sealant layer is in the solid state at dwell times below 110 ms. After 130 ms, 12 µm of the sealant layer is melted and the thickness of the melt layer increases rapidly and finally the whole sealant layer is melted after 250 ms. On the other hand, when the jaw temperature was set to 105°C, simulation results showed that melting of the sealant layer begins after 410 ms and the whole sealant layer is melted after 560 ms. The longer time needed for melting of the sealant layer in the sample sealed at 105°C is related to the slower heat transfer in this sample due to smaller temperature gradient between jaws and films. These results can explain why when the film was sealed at 105°C, no SOF was observed after 0.5s of dwell time but considerable SOF was observed at the same condition and sealing

temperature of 140°C. The observed times required to melt the whole sealant layer can be considered as a horizontal shift factor in the FDM model results. Figure 5.13 shows the FDM model predictions using the shift factors of 0.25 and 0.56 s for SOF of the thick sealant at seal temperatures of 140 and 105°C, respectively.

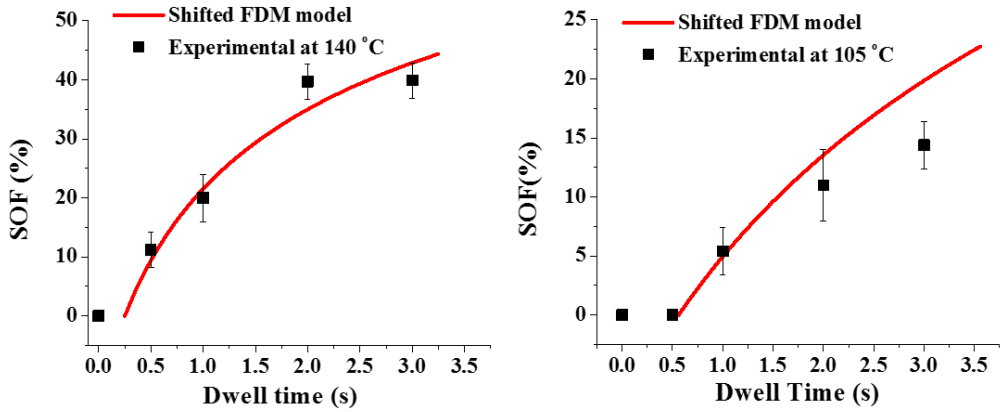

Figure 5.13 Comparing the shifted FDM model predictions based on heat transfer simulation results with the experimental results

By comparing the shifted predictions with Figure 5.9, one can see that shifting using the horizontal shift factor reduced the difference between model predictions and experimental data. This indicates that heat transfer acts as a delaying mechanism in SOF and therefore, considering heat transfer is necessary in improving model predictions. The better model predicting by shifting based on heat transfer model also show that SOF is likely to be negligible before complete melting of the sealant layer and therefore considering phase transition during SOF is very unlikely to enhance SOF predictions and only increases the complexity of the models.

As shown in Figure 5.9, the Power-law model underestimated SOF results. It is clear that using the horizontal shift factor for the power-law prediction, increases the gap between predictions and experimental data. To better understand the origin of underestimation of SOF by the Power-law model, average shear rate and maximum shear rate estimated by FEA and FDM models are shown in Figure 5.14.

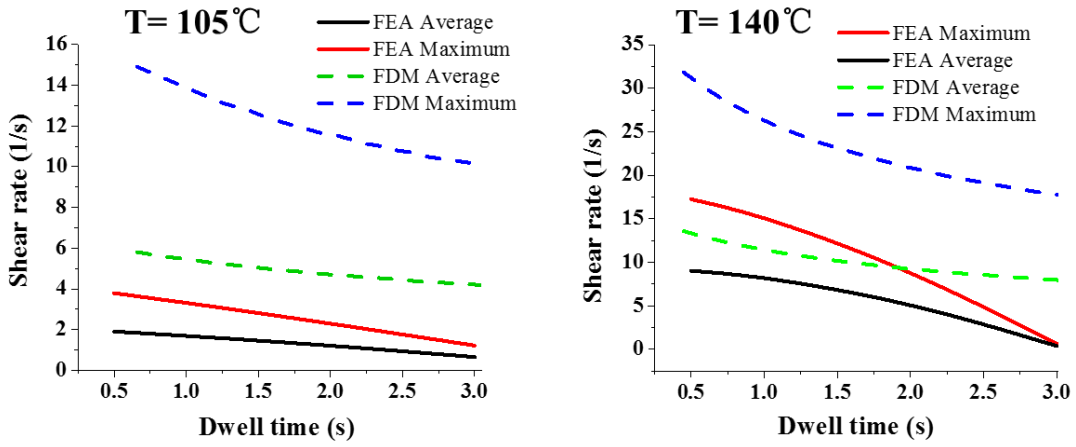

Figure 5.14 Average and maximum shear rates at the middle length of the plate (x=L/4) in the FEA and FDM modeling

The Power-law model can also be used to estimate the shear rate using Equation 5. Using this approach, an average shear rate of 4.32 s^{-1} can be estimated. Although the FDM model always predicts higher shear rates compare to FEA model (which is in-line with the overestimation of the velocity predicted by this model) but the estimated average shear rates by FEA and FDM in both temperatures fall within the transition region between Newtonian and Power-law regions according to the rheological characterization of sealants, Figure 5.5. As the shear rate during the SOF in in the transition region, using Power-law model results in overestimation of viscosity and, consequently, underestimation of SOF. This also can explain why Ward and Li [5] could not find a relation between SOF and zero-shear viscosity of sealant materials in their study.

Despite the difference between experimental SOF data and the FDM model predictions, considering that FEA model requires the approaching velocity of jaws, the much lower computation time and flexibility of using a free software (Octave) to run the FDM model, indicate the potential of the FDM model as a tool for initial screening of sealant materials during the packaging design process. Considering the predictive advantages of FDM model, this model will be used mainly used in the rest of the paper.

5.5.3 Effect of thickness of sealant layer on SOF

Thickness of the sealant layer is one of the most important design parameters that is commonly used when SOF and caulkability is needed in plastic films. Finding an optimum thickness is essential in achieving a good caulkability at a reasonable sealant layer cost. In addition, thick sealant layer requires higher sealing temperature and/or longer dwell times which both lead to higher production cost. In order to examine the effect of sealant thickness, SOF was measured in a film with a sealant layer of 50 µm of Exact 3131. Figure 5.15 shows the variation of SOF at different dwell times in two studied jaw temperatures of 105°C and 140°C for this film sample.

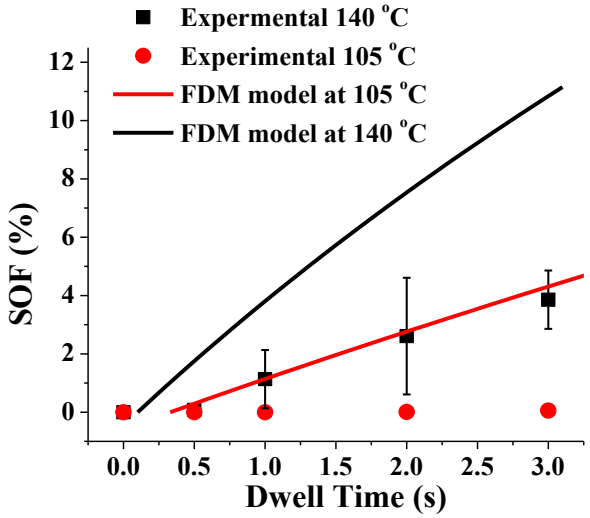

Figure 5.15 SOF at different dwell times and sealing temperature for a 50 µm thick sealant of Exact 3131

By comparing Figure 5.15 and Figure 5.8, it can be clearly seen that reducing the sealant thickness by 2.6 times reduced SOF by almost 10 times at 3s dwell time. In addition, combining reducing sealant thickness by 2.6 times and reducing sealing temperature by 30°C, prevented SOF. It should be noted that the large error bars in the measured data in Figure 5.15 are due to the small SOF values in these samples. Using the same approach for simulation of heat sealing, horizontal shift factor of 0.1 and 0.33 were used to shift the FDM predictions. Despite the overestimation of SOF values by the FDM model, the small SOF amount in these samples and the considerable error in the measurements should also be considered when comparing the FDM model results and the experimental data.

5.5.4 Effect of polymer viscosity on SOF

In order to study the effect of polymer viscosity on SOF, SOF of a film sample prepared with 50μm sealant layer of Exact 3139 was examined at P= 3 N/mm^2 and 0.5 N/mm^2 with dwell times of 3s and 0.5s. These two conditions were selected as they represent the most favored and the least favored conditions for SOF to occur. Measurements showed SOF of 11.1% for the sample sealed at high pressure and long dwell time while no SOF was observed for the sample sealed at low pressure and short dwell time. It was shown in the previous section that a film with 50μm sealant of Exact 3131 showed about 4% of SOF at 3 N/mm^2 and dwell time of 3s. Considering the viscosity of Exact 3139 compare to Exact 3131, Figure 5.5, it can be seen that while decreasing viscosity of the sealant layer could enhance SOF at high pressure and long dwell time, but it didn't have an effect at low sealing pressure and short dwell time. The obtained results clearly indicate that reducing viscosity cannot always lead to enhanced SOF and caulkability and the effect of viscosity can be suppressed at low sealing pressures and short dwell times. Using the FDM model, the SOF in the sample with 3139 was estimated as 20.8%, which is about two times of the experimental value. The overestimation of the SOF can again be attributed to the higher-pressure gradient in FDM model.

5.5.5 Effect of Sealing Pressure on SOF

Although effect of pressure on seal strength has been previously studied in the literature [37], but the effect of pressure on SOF in heat sealing has not been experimentally examined yet. Effect of applied pressure during sealing on SOF was studied in the pressure range of 0.27 to 3 N/mm^2 for both films with thin (50 μm) and thick (130 μm) sealant layers and the obtained results are shown in Figure 5.16.

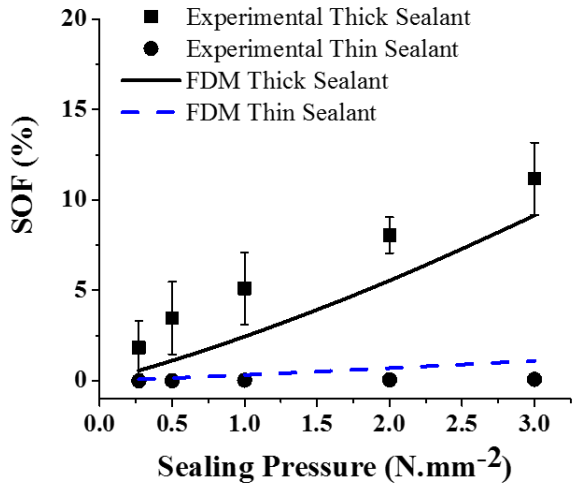

Figure 5.16 Effect of sealing pressure on SOF in films with thick(130µm) and thin (50µm) sealants. Heat sealing was done at 0.5s and T=140ºC for all samples. The lines show shifted FDM model predictions

In the film with 50 µm thick sealant layer (names as thin sealant in Figure 5.16), increasing sealing pressure up to 3 N/mm^2 did not result in any squeeze out flow. It should be noted that 3N/mm^2 is a high pressure for heat sealing and most heat sealing processes in the industry are done in the range of 0.27 to 1 N/mm^2 [37]. When the sealant thickness was increased to 130 µm, increasing pressure by almost 10 times increased the SOF to 12%. It is known that increasing pressure can damages the seal appearance and shortens the service lifetime of jaws. These results clearly indicate that increasing pressure at short dwell times did not improve considerably SOF in heat sealing. The shifted FDM model results, Figure 5.16, show good agreements with the experimental results which shows the ability of the model to demonstrate the effect of sealing pressure on SOF.

5.6 Conclusions

Squeeze out flow (SOF) was studied in multilayer films composed of an outer polyamide (PA) layer, a tie layer and a sealant layer based on metallocene polyethylene. SOF in heat sealing was modeled using three approaches: (i) one-dimensional model using power-law fluid behavior, (ii) one-dimensional model using Carreau-Yasuda fluid and finite difference method (FDM), (iii) two-dimensional model using Carreau-Yasuda fluid and finite element analysis (FEA). Experimental SOF values were estimated based on image analysis of SEM images

taken from the cross-section of sealed area. The effect of dwell time on SOF was examined at two different sealing temperatures of 140ºC and 105ºC. SOF measurements showed that at the higher jaw temperature, increasing dwell time increased SOF continuously until 2s but the SOF variation by time reduced significantly after that. Reducing jaw temperature reduced considerably the amount of SOF and its dependency on dwell time. Effect of sealant thickness was examined, and it was found that decreasing sealant thickness from 130μm to 50μm suppressed SOF and negligible amount of SOF was observed even at long sealing times and high sealing pressures. Effect of sealant viscosity was also studied by using a lower viscosity sealant and it was found that in thin sealants reducing viscosity could enhance SOF only at high pressures and long dwell times. Effect of sealing pressure was also examined at two different sealant thicknesses of 130 μm and 50 μm. It was found that increasing pressure by almost 10 times did not induce SOF in the thin sealant film while it only caused 12% SOF in the thick sealant. The phenomena involved in SOF during heat sealing were discussed in detail using the obtained experimental data and models' predictions. Comparing the experimental results power-law model showed that power-law model always underestimated SOF values. By comparing FEA and FDM models, it was found that considering a non-linear pressure profile within the sealant layer in essential in precise prediction of SOF. However, the FDM model results based on linear pressure profile were also in good agreement with experimental data. It was shown that considering the time required for melting of the whole sealant layer as a horizontal shift factor could improve considerably the FDM model predictions. Estimation of the shear rate in SOF during heat sealing showed that SOF occurred within the transition region between the Newtonian and power-law regions. The obtained results indicate the complexity of analysis of SOF in heat sealing and highlights the importance of the FDM model presented in this work.

5.7 Acknowledgement

The authors would like to thank Dr. Ebrahim Jalali Dil and M. Reza Fasihanifard for their valuable comments.

5.8 References

1. Robertson, G.L., *Food Packaging ,Principles and Practice*. Third ed. 2012: CRC Press.
2. Morris, B.A., *The Science and Technology of Flexible Packaging: Multilayer Films from Resin and Process to End Use*. 2016: Elsevier Science & Technology Books.
3. Cinelli, P., et al., *Cosmetic packaging to save the environment: future perspectives.* Cosmetics, 2019. **6**(2): p. 26.
4. Wagner Jr, J.R., *Multilayer flexible packaging*. 2016: William Andrew.
5. Ward, D. and M. Li, *Seal-through-contamination and "caulkability"an evaluation of sealants' ability to encapsulate contaminants in the seal area*, in *TAPPI PLACE Conference*. 2016: Fort Worth, Texas.
6. Morris, B.A. and J.M. Scherer, *Modeling and experimental analysis of squeeze flow of sealant during hot bar sealing and methods of preventing squeeze-out.* Journal of Plastic Film and Sheeting, 2015. **32**(1): p. 34-55.
7. Meka, P. and F.C. Stehling, *Heat sealing of semicrystalline polymer films. I. Calculation and measurement of interfacial temperatures: Effect of process variables on seal properties.* Journal of Applied Polymer Science, 1994. **51**(1): p. 89-103.
8. Mihindukulasuriya, S.D. and L.-T. Lim, *Heat sealing of LLDPE films: Heat transfer modeling with liquid presence at film–film interface.* Journal of Food Engineering, 2013. **116**(2): p. 532-540.
9. Kanani Aghkand, Z., et al., *Simulation of Heat Transfer in Heat Sealing of Multilayer Polymeric Films: Effect of Process Parameters and Material Properties.* Industrial & Engineering Chemistry Research, 2018. **57**(43): p. 14571-14582.
10. Levy, A., G.P. Martel, and P. Hubert, *Modeling the Squeeze Flow of a Thermoplastic Composite Tape During Forming*, in *COMSOL Conference*. 2012: Boston, USA.
11. Philippe Mesnil, et al., *Seal Through Contamination Performance of Metallocene Plastomers*, in *TAPPI Polymers, Laminations & Coatings Conference*. 2000.
12. Bamps, B., et al., *Evaluation and optimization of seal behaviour through solid contamination of heat-sealed films.* Packaging Technology and Science, 2019. **32**(7): p. 335-344.
13. Morris, B.A., *Predicting the performance of ionomer films in heat-seal processes.* Paper, Film and Foil Converter, 2003. **77**(3): p. 207.
14. Picher-Martel, G.-P., A. Levy, and P. Hubert, *Compression moulding of carbon/PEEK randomly-oriented strands composites: A 2D finite element model to predict the squeeze flow behaviour.* Composites Part A: Applied Science and Manufacturing, 2016. **81**: p. 69-77.
15. Hou, J., et al., *An analysis of the squeeze-film lubrication mechanism for articular cartilage.* Journal of biomechanics, 1992. **25**(3): p. 247-259.

16. Mueller, C., et al., *Heat sealing of LLDPE: relationships to melting and interdiffusion.* Journal of Applied Polymer Science, 1998. **70**(10): p. 2021-2030.
17. Ting, G., *Polymer Welding: Strength Through Entanglements.* 2012.
18. Grewell, D. and A. Benatar, *Welding of Plastics: Fundamentals and New Developments.* International Polymer Processing, 2007. **22**(1): p. 43-60.
19. David Grewell and A. Benatar, *Coupled tempeature, diffusion and squeeze flow model for interface healing predictions*, in *ANTEC*. 2006. p. 2205-2210.
20. Engmann, J., C. Servais, and A.S. Burbidge, *Squeeze flow theory and applications to rheometry: A review.* Journal of Non-Newtonian Fluid Mechanics, 2005. **132**(1): p. 1-27.
21. Leider, P.J. and R.B. Bird, *Squeezing Flow between Parallel Disks. I. Theoretical Analysis.* Industrial & Engineering Chemistry Fundamentals, 1974. **13**(4): p. 336-341.
22. Chan, T.W. and D.G. Baird, *An evaluation of a squeeze flow rheometer for the rheological characterization of a filled polymer with a yield stress.* Rheologica acta, 2002. **41**(3): p. 245-256.
23. Suwonsichon, T. and M. Peleg, *Rheological characterisation of almost intact and stirred yogurt by imperfect squeezing flow viscometry.* Journal of the Science of Food and Agriculture, 1999. **79**(6): p. 911-921.
24. Campanella, O. and M. Peleg, *Squeezing flow viscosimetry of peanut butter.* Journal of Food Science, 1987. **52**(1): p. 180-184.
25. Gupta, P.S. and A.S. Gupta, *Squeezing flow between parallel plates.* Wear, 1977. **45**(2): p. 177-185.
26. Dienes, G. and H. Klemm, *Theory and application of the parallel plate plastometer.* Journal of Applied Physics, 1946. **17**(6): p. 458-471.
27. Sherwood, J.D., *Squeeze flow of a power-law fluid between non-parallel plates.* Journal of Non-Newtonian Fluid Mechanics, 2011. **166**(5): p. 289-296.
28. Wilson, S.D.R., *Squeezing flow of a Bingham material.* Journal of Non-Newtonian Fluid Mechanics, 1993. **47**: p. 211-219.
29. Sherwood, J.D. and D. Durban, *Squeeze flow of a power-law viscoplastic solid.* Journal of Non-Newtonian Fluid Mechanics, 1996. **62**(1): p. 35-54.
30. Lian, G., et al., *On the squeeze flow of a power-law fluid between rigid spheres.* Journal of Non-Newtonian Fluid Mechanics, 2001. **100**(1): p. 151-164.
31. Shuler, S. and S. Advani, *Transverse squeeze flow of concentrated aligned fibers in viscous fluids.* Journal of Non-Newtonian Fluid Mechanics, 1996. **65**(1): p. 47-74.
32. Ghnatios, C., F. Chinesta, and C. Binetruy, *3D Modeling of squeeze flows occurring in composite laminates.* International Journal of material forming, 2015. **8**(1): p. 73-83.
33. Hieber, C. and H. Chiang, *Shear-rate-dependence modeling of polymer melt viscosity.* Polymer Engineering & Science, 1992. **32**(14): p. 931-938.
34. Wood-Adams, P.M., *The effect of long chain branches on the shear flow behavior of polyethylene.* Journal of Rheology, 2001. **45**(1): p. 203-210.
35. Cox, W. and E. Merz, *Correlation of dynamic and steady flow viscosities.* Journal of Polymer Science, 1958. **28**(118): p. 619-622.
36. Rudolph, N. and T.A. Osswald, *Polymer rheology: fundamentals and applications*. 2014: Carl Hanser Verlag GmbH Co KG.
37. Najarzadeh, Z. and A. Ajji, *A novel approach toward the effect of seal process parameters on final seal strength and microstructure of LLDPE.* Journal of Adhesion Science and Technology, 2014. **28**(16): p. 1592-1609.

CHAPTER 6 ARTICLE 3:

EFFECT OF BACK-LAYER ON SEAL PERFORMANCE OF MULTILAYER POLYETHYLENE-BASED SEALANT FILMS

Zahra Kanani Aghkand, Amir Saffar, Abdellah Ajji *

(1) 3SPack, CREPEC, Department of Chemical Engineering, École Polytechnique de Montréal, Montréal, Québec H3C 3A7, Canada

*Corresponding Author

Email: abdellah.ajji@polymtl.ca

Submitted to Journal of *Applied Polymer Science*.

J Appl Polym Sci. 2021; e50742. https://doi.org/10.1002/app.50742

6.1 Abstract

This work studies effects of back-layer materials, thickness of sealant layer and sealing condition on seal performance of multilayer polyethylene-based films. Multilayer films with back-layers of high-density polyethylene (HDPE), or low-density polyethylene (LDPE), or linear low-density polyethylene (LLDPE) were produced with different thicknesses of the metallocene layer. It was found that increasing the thickness of the metallocene layer improved hot tack properties. In addition, films with back-layers of LLDPE or LDPE showed higher hot tack strength compared to those with HDPE back-layer. Increasing sealing temperature reduced significantly the hot tack strength and its dependency on metallocene layer thickness. It was found that increasing delay time after sealing, before peeling test, increased hot tack strength, but the rate of hot tack evolution and the type of peeling behavior were considerably affected by the type of back-layer material. The effect of dwell time was also examined, and it was observed that increasing dwell time in the studied range did not affect the hot tack evolution. The mechanisms involved in the development of hot tack evolution were discussed, and it was shown that the back-layer effects can be explained by bulk viscoelastic energy dissipation theory.

6.2 Introduction

The wide range of properties expected from plastic films such as barrier, sealing, optical and mechanical properties, as well as reducing final price of the package have been the main motivations for producing multicomponent films in plastic packaging industry [1]. Considering the previous studies in the literature on this subject, multicomponent sealants can be categorized as (i) single layer films composed of a multicomponent polymer blend[2-5], (ii) multilayer films with a single polymer in each layer[6-9], and (iii) multilayer films with a mixture of different polymers in some or all layers[10-13].

It has been well-established that metallocene polyethylene can provide high hot tack and seal strength [10, 14-19]. Therefore, they have been widely used in plastic packaging to improve hot tack and seal performance of films. On the other hand, metallocene polyethylene is expensive and producing films with neat metallocene sealant layer is challenging due to their soft and rubbery nature and tackiness. This results in poor manufacturing process stability, causes blocking issues in the produced rolls and makes the converting process very challenging (if not impossible). Therefore, attempts have been made to reduce the sealant layer cost and overcome the drawbacks of processing films with neat metallocene polyethylene by blending them with polyethylene produced with conventional polymerization methods. Although this approach reduces the cost of the sealant layer, seal performance decreases considerably [2, 10, 17, 20, 21]. This indicates that the optimization of cost and performance is essential when blending metallocene with conventional polyethylene which increases considerably the cost of this blending approach in industrial applications.

In the case of multilayer sealants, despite some previous works on multilayer sealants[6-13, 22], only Viganò [23] examined the effect of back-layer material on seal properties of multilayer sealant films. He studied blends of conventional polyethylene with metallocene linear low-density polyethylene (mLLDPE) in 3-layer co-extruded polyethylene sealant films. He used blends of low-density polyethylene (LDPE) and mLLDPE in both sealing and lamination sides and put blends of LDPE (or HDPE) and mLLDPE in the middle layer. He also used three different mLLDPEs with different comonomers: butene (C4-mLLDPE), hexene(C6-mLLDPE) and octene(C8-mLLDPE). He found that C6-mLLDPE showed highest hot tack and replacing C6-mLLDPE with other polymers in any layer had a negative impact on hot tack strength. Finally, he concluded that the

composition of the blend and mLLDPE type affected significantly the hot tack performance of the films. However, there is no information regarding miscibility of the polymers. Also, type of polymers and their composition were changed at the same time during producing the films. Those reasons make the clear conclusion from the paper very difficult.

It is well known that blending can be a low-cost technique to improve some properties such as toughness. However, controlling the morphology and microstructure of the blend is essential to achieve the desired properties [3, 12, 15, 24]. By increasing the number of components, controlling the morphology and properties of blends become very challenging [25-28].

Considering a multilayer sealant film using metallocene polyethylene as sealant layer and other type of polyethylene in each layer, can be a solution to overcome the drawbacks of single layer metallocene sealant films. The back-layer reduces the final cost and provides process stability during production and converting process. This approach has been used widely in polyethylene film industry, but a comprehensive study on the effect of back-layer material and the thickness of the metallocene sealant layer on seal and hot tack performance of multilayer polyethylene sealant films is lacking in the literature. This has motivated us to study the effect of back-layer materials on hot tack and seal performance of multilayer polyethylene sealant films. In this work, multilayer polyethylene sealant films with a neat metallocene layer and a conventional polyethylene back-layer were produced. The effects of back-layer material and thickness of metallocene layer as well as effects of sealing conditions on hot tack evolution of film samples were examined. Based on the obtained results, different parameters affecting seal strength such as heat transfer will be discussed and, finally, it will be shown that viscoelastic energy dissipation can explain the observed experimental results.

6.3 Experimental

6.3.1 Materials

Three commercial polyethylene polymerized by conventional methods were selected as back-layers: HDPE, LDPE, and LLDPE. In addition, a commercial metallocene polyethylene (mPE) was used for the sealant layer. Table 6.1 presents the information on the specific resins used with some of their properties. All data were provided by the resin manufacturer.

Table 6.1 Summary of the materials used in this study with some of their properties

Nomenclature	Manufacturer	Grade	Density (g/cm^3)	MFI* (g/10min)	Yield Strength (MPa)
mPE	ExxonMobil	Exact 3131	0.9	3.5	5.4
HDPE	Nova Chemicals	Sclair 19A	0.962	0.72	27
LDPE	Nova Chemicals	LF-0219-A	0.918	2.3	11
LLDPE	ExxonMobil	LL3003	0.918	3.2	7.0

*from TDS, at 190°C/2.16 kg

6.3.2 Film preparation

Film samples composed of a back-layer and a sealant layer were prepared using cast film co-extrusion. Two single screw extruders manufactured by LabTech Instruments Inc. with the same general-purpose screw design (20 mm screw diameter and L/D=30) were used in the co-extrusion process. The screws were equipped with a Maddock mixing segment followed by a mixing segment with mixing pins at their ends. The temperature profile along the barrel of both extruders was: 200/210/215/220°C and the die temperature was 220°C. The extruders screw speeds were set to reach the desired thickness of the layers while the total thickness of the film kept at 50μm. For film cooling, an air knife was applied at 20 psi right at the exit of the die to supply air to the film surface. A single layer of 50 μm mPE sealant was also produced as the control sample with the same conditions as mentioned above. The film samples hereafter will be named as XXXX-mPE-YY in which XXXX designates the back-layer material and YY the thickness of the mPE layer in micrometers.

6.3.3 Lamination

In order to examine the seal performance of film samples, they were laminated to a 12 μm polyethylene terephthalate (PET) film using a solvent-less adhesive. The lamination process was done on an industrial scale laminator (Nordmeccanica Group) at 150 m/min at ProAmpac facility. Before lamination, only the

film surface that would adhere to PET film was treated using a corona treatment station installed on the lamination machine which was operated at 3 kW to achieve a good surface modification and adhesion.

6.3.4 Scanning electron microscopy (SEM)

A tabletop SEM (TM3030plus, Hitachi, with software Hitachi TM3030, version.01-05-02) was used to determine the thickness of the layers. Film samples (without lamination) were cut using a razor blade and placed in a sample holder designed for film sample. The cross-section of the film samples was then observed at 15kV acceleration voltage. Layer thicknesses were determined using SEM software. The reported layer thicknesses were averaged over 10 different measurements.

6.3.5 Heat Sealing

Laminated film samples were sealed using a heat-sealing machine (SL10 LakoTool, Lako Tool & Manufacturing Inc.) at different jaw temperatures and dwell times. The dimension of metal jaws is 19.1×25.4 mm and one of them covered by Teflon layer. The time resolution of the heat-sealing machine was 100 ms. Based on our previous studies [29] and in order to obtain a good contact between films while avoiding squeeze out of sealant layer, all tests were done at sealing pressure of 0.27 N/mm^2.

6.3.6 Differential scanning calorimetry (DSC)

DSC Q2000 machine (TA Instruments) was used to examine melting and crystallinity of neat polymers and non-laminated film samples. To this aim, samples of about 7 to 10 mg were cut and encapsulated in an aluminum pan. DSC tests were run under nitrogen flow of 50 ml/min at heating and cooling rates of 10^{o}C/min. The obtained data then were analyzed using TA Universal Analysis 2000 software (version 4.5A). In order to remove the thermal history in the granules of neat polymers, first, the samples were heated to 180^{o}C and were kept at that temperature for 5 minutes. Then they were cooled to room temperature and heated again at the mentioned rates. For film samples, the analyses were done on the first heating cycle as thermal history is important. The heat of fusion in all samples was determined as the area under the melting peaks using TA Universal Analysis software. The following equation was used to determine the crystallinity of polymers from the measured heat of fusion [30]:

$$\%Crystallinity = \frac{\Delta H_f}{\omega \times \Delta H_{f,100\%}} \times 100 \qquad \text{Eq. 6.1}$$

Where ΔH_f, ω and $\Delta H_{f,100\%}$ are the measured heat of fusion, the weight percent of the material in the examined sample and the heat of fusion of completely crystalline polyethylene. For $\Delta H_{f,100\%}$ a value of 293 J/g was used as reported in literature [31]. The reported results are an average of three measurements. The standard deviation in peak melting and crystallization temperatures was always less than 0.7°C and less than 2.7 J/g for the heat of fusion among the measured values.

6.3.7 Dynamic mechanical analysis (DMA)

A dynamic mechanical analyzer (TA Instruments, DMA 2980) was used for measuring storage modulus of film samples at different temperatures. Strip samples with a length of 20 mm and width of 5 mm were cut using a razor blade. The samples were tested using the film tension clamp at frequency of 1 Hz and amplitude of 30μm. Temperature was increased from room temperature to 80°C at a heating rate of 5°C/min.

6.3.8 Simulation of heat transfer

In order to estimate the interface temperature between film samples during heat sealing, heat transfer in laminated multilayer films with HDPE back-layer was simulated using COMSOL Multiphysics software in 2D symmetric mode. Details of the heat transfer model can be found in our previous study on simulation of heat transfer in heat sealing [32]. Figure 6.1 shows schematically the geometry used in the simulation. Material properties for the PET layer (such as density, specific heat capacity and thermal conductivity) were taken from COMSOL material library. Material properties of HDPE and mPE were taken from our previous study [32].

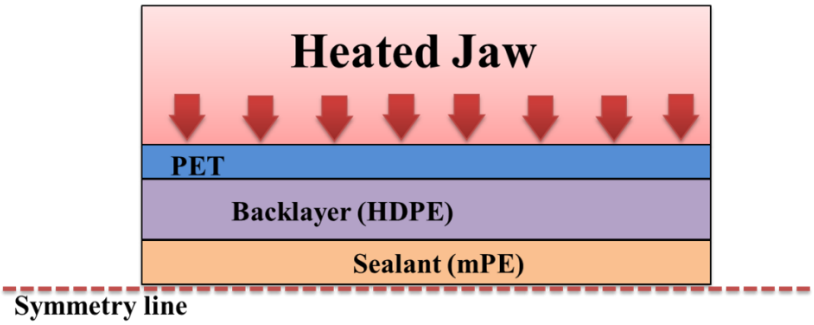

Figure 6.1 Schematic of the geometry used in simulation of heat transfer in laminated multilayer sealant film using COMSOL Multiphysics. The interface (which is the symmetry line) is shown as a dashed line.

6.4 Results and Discussion

6.4.1 Materials characterization

Thermal properties of sealant materials can significantly affect their hot tack and seal performance. It is known that higher melting temperature and crystallinity in polyethylene sealants, resulted in higher seal initiation temperature (SIT). It is believed that seal strength development occurs mainly at temperatures close or above the sealant melting temperature [29, 33-36]. Figure 6.2 shows DSC results of the different polyethylenes used in this study. In addition, Table 6.2 summarizes the important parameters determined from DSC curves.

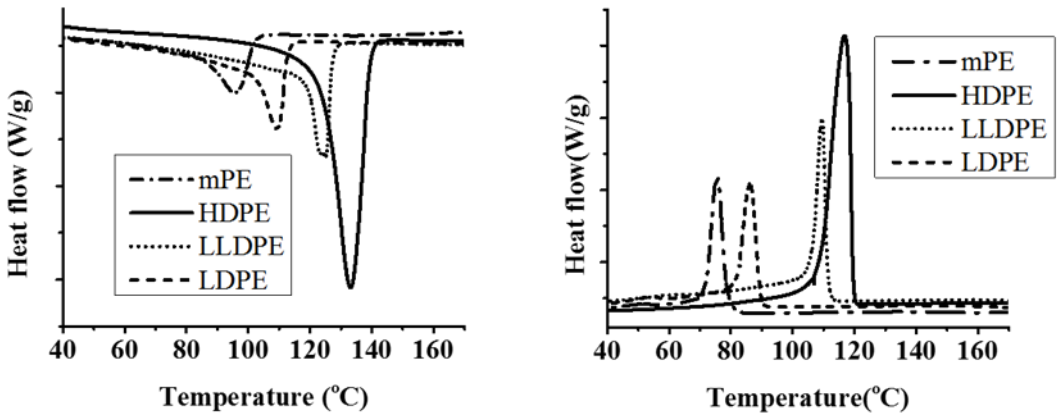

Figure 6.2 DSC results of different polyethylene types used in this study: (left) second heating cycle (right) cooling cycle.

Table 6.2 Thermal properties of neat materials and multilayer sealants obtained from DSC analyses.

Material	Peak melting temperature, T_m (°C)		Crystallinity (%) from Eq.1	Crystallization Temperature, T_c (°C)	ΔH_c (J/g)
mPE	96.4		20.6	75.6	57.6
LLDPE	125.1		30.2	109.5	88.7
LDPE	109.4		22.2	94	61.8
HDPE	133.1		55.5	117.2	171
HDPE-mPE-15	mPE	95.7	17.5	81.8	4.5
	HDPE	131.6	28.2	119.4	63.8
LDPE-mPE-15	mPE	90.7	27.6	82.1	8.4
	LDPE	108	14.7	97.4	32.7
LLDPE-mPE-15	mPE	94.1	23.5	82.6	6
	LLDPE	123.7	14.9	110.6	32.6

mPE had the lowest peak melting temperature, heat of fusion and crystallinity among the polyethylene types. This allows mPE to have a low SIT with high hot tack strength and seal performance [37]. LDPE, LLDPE and HDPE, respectively, show higher melting temperatures and crystallinity compared to mPE. Figure 6.3 shows DSC results of multilayer sealant films with a 35 μm LDPE, LLDPE and HDPE back-layers and a 15 μm mPE sealant layer. A summary of the DSC analyses for these samples is also listed in Table 6.2.

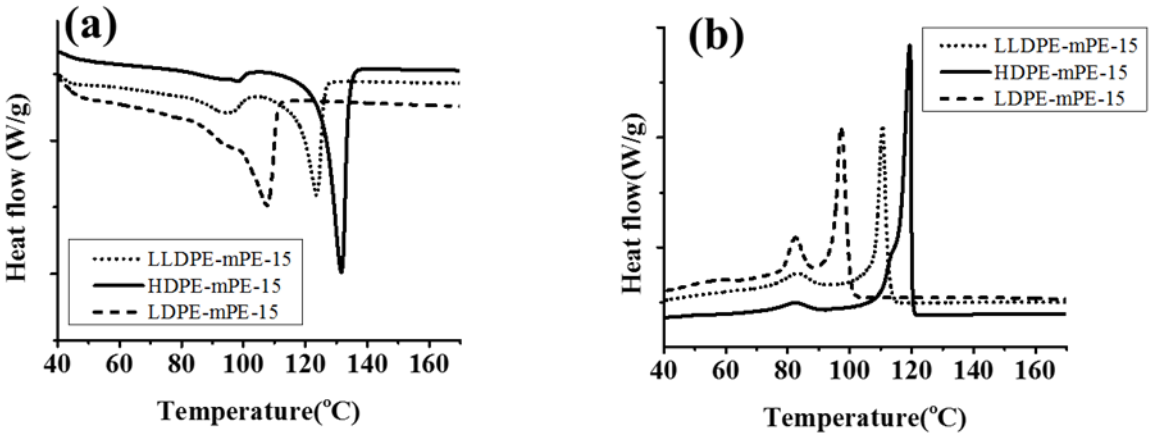

Figure 6.3 DSC curves of multilayer sealant materials with different back-layers: (a) first heating cycle, (b) cooling cycle. All samples had a 35 μm LDPE, LLDPE and HDPE back-layers and a 15 μm mPE sealant layer.

In all samples, back-layers showed considerably lower crystallinity compared to the results of the neat polymers. This can be attributed to the fast cooling that film samples experience after exiting the die. The faster cooling results in a reduced crystallinity in semi-crystalline polymers by reducing the growth rate of the crystalline phase [38]. In addition, in all samples, mPE layers showed higher crystallization temperatures compared to the mPE granules. This can be attributed to the fact that back-layers crystallize at higher temperatures and the formed interface between the molten PE layer (mPE) and solid PE phase (back-layer) at the interface of layers can enhance nucleation of mPE [39]. It can also be seen that the crystallinity of the metallocene layer is affected by the back-layer material, especially when LDPE was used as the back-layer compared to the films prepared with HDPE and LLDPE back-layers. When the film exits from the die, mPE layer experiences the external cooling by the air knife. Considering the crystallization temperatures of back-layers, HDPE will form crystals first and releases the crystallization heat at much higher temperature than the crystallization temperature of mPE. Consequently, as can also be seen in Figure 6.2, no overlap exists between crystallization peaks of HDPE and mPE. However, some overlaps exist between crystallization peak of LLDPE and mPE and to a larger extent between crystallization peaks of LDPE and mPE. Therefore, in these samples, it is likely to expect that the released heat from crystallization of back-layers could reduce the cooling rate of the mPE layer leading to slightly higher crystallinity of mPE in film samples with LLDPE and LDPE back-layers.

In order to examine the effect of the back-layer material on hot tack properties, it is necessary to examine the hot tack performance of the 50 μm single layer mPE film as the control sample. Figure 6.4 reported the hot tack curve of this sample. Hot tack begins at low temperature and reaches a maximum at 105°C which is followed by a decrease hot tack at higher temperatures. The observed increase in hot tack by increasing temperature is attributed to the enhanced molecular diffusion at the interface between seal sides [33] while the reduction in hot tack at high temperatures has been assigned to easier pullout of the diffused polymer chains [35].

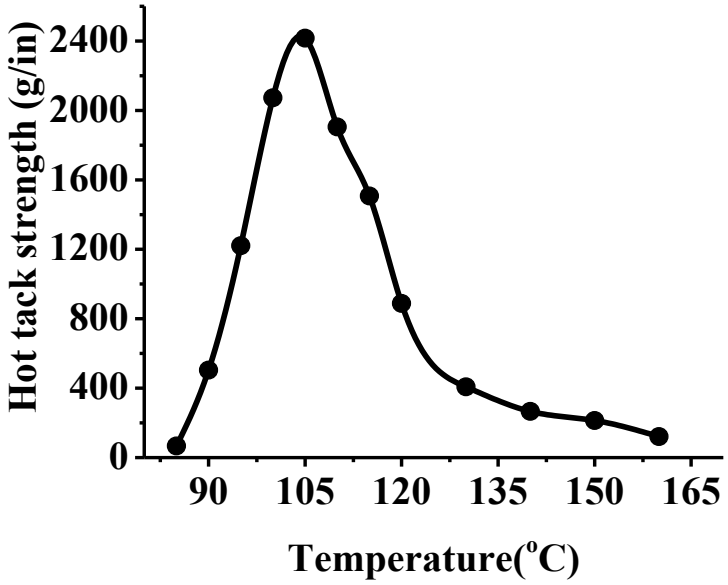

Figure 6.4 Hot tack curve of the laminated 50 μm single layer mPE sealant laminated to 12 μm PET.

6.4.2 Determining layers thicknesses

As explained in the experimental section, the thickness of the layers in the sealant film was controlled by controlling the extruders' flow rate. To confirm the thickness of the layers, the thickness of the layers in HDPE-mPE films were determined using SEM and the results are shown in Figure 6.5. Due to the close density of mPE with LDPE or LLDPE, distinguishing layers in the other two structures were not possible. It should be noted that, as the layer thicknesses were controlled by controlling extruders' flow rate during the process, confirming layer thickness in

HDPE-mPE film can be considered as a confirmation in the two other structures as well. Using the densities of 0.9962 g/cm^3 for polyethylene crystal phase and 0.86 g/cm^3 for amorphous polyethylene phase [31], the difference between density of HDPE, LDPE and LLDPE can be estimated. The obtained results indicate an error of 2.2% in the thickness of the back-layer between HDPE and LDPE or LLDPE.

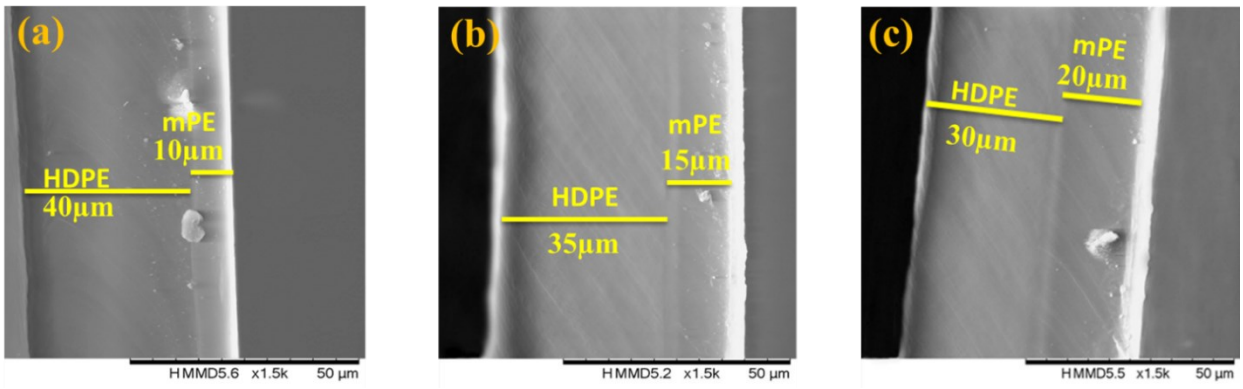

Figure 6.5 SEM microscopy of HDPE-mPE films with different thicknesses of the layers: (a) HDPE-mPE-10, (b) HDPE-mPE-15, (c) HDPE-mPE-20.

6.4.3 Effect of mPE layer thickness and back-layer material on hot tack strength

Figure 6.6 shows the effect of back-layer material on the hot tack strength of prepared films at 105^{o}C. It should be mentioned that hot tack temperature was selected as the single layer mPE sealant showed the maximum hot tack at this temperature. The film sample LDPE-mPE-10 could not be produced due to the instability of the process at this layer ratio.

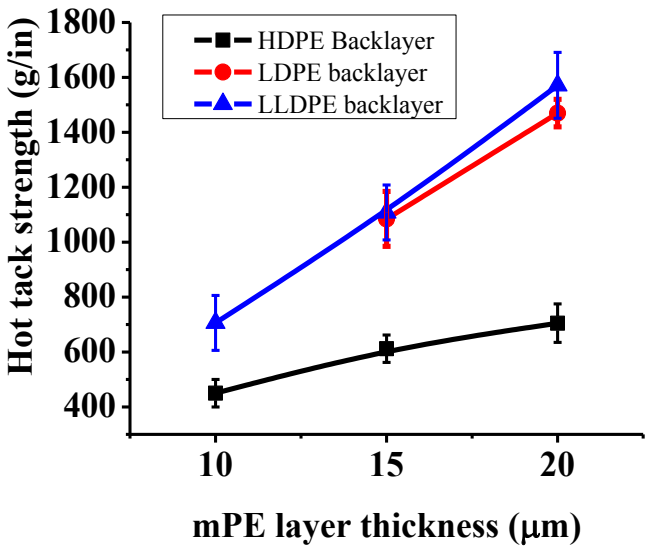

Figure 6.6 Hot tack strength of films with different back-layers as a function of mPE layer thickness. The measurements were done at 105°C, 0.5s dwell time and pressure of 0.27 N/mm^2.

All film samples showed peelable behavior during hot tack tests. The films with LDPE back-layer showed close performance to LLDPE back-layer films. Both LDPE and LLDPE back-layer films showed a continuous linear increase by inducing the thickness of mPE layer. On the other hand, the film with HDPE back-layer showed considerably lower hot tack strength compared to the other two films. In addition, the rate of increasing hot tack strength with mPE layer thickness in HDPE back-layer film was much lower than other two structures.

6.4.4 Effect of back-layer material and thickness on mechanical strength of the sealant film

As mentioned above, back-layer material can provide mechanical strength to support the soft mPE layer. Effects of back-layer material and mPE sealant thickness on storage modulus of the final multilayer film samples at different temperatures was examined and the results are shown in Figure 6.7.

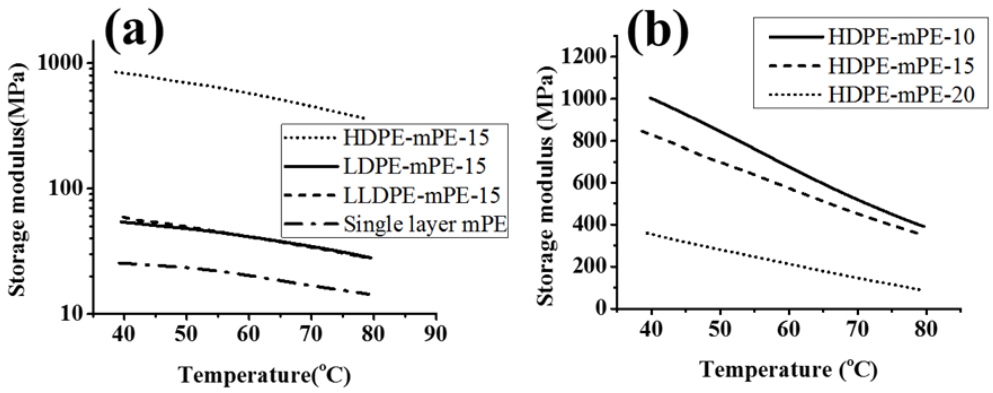

Figure 6.7 Storage modulus as a function of temperature for: (a) films with different back-layers and 15 μm mPE layer; (b) films with HDPE back-layer but at different mPE layer thicknesses.

In Figure 6.7 (a), single layer mPE film showed the lowest storage modulus which is in line with the soft and rubbery behavior expected from metallocene polyethylene. Both LDPE and LLDPE back-layer films showed higher mechanical strength compared to the single mPE film. Finally, the film with HDPE back-layer showed the highest modulus in all those samples. As can be seen in Figure 6.7 (b), increasing the thickness of mPE layer in films with HDPE back-layer considerably reduces the storage modulus of HDPE-mPE films especially above 15 μm. This emphasizes the importance of selecting the layer ratio on the final properties of multilayer sealant films.

In order to examine the type of peeling behavior, cross-section of peeled sample was observed by light microscopy and the result is shown in Figure 6.8. As can be seen, both mPE and HDPE layers had the same thicknesses as before sealing which indicates that the observed peeling occurred between mPE layers and not between mPE and HDPE back-layer

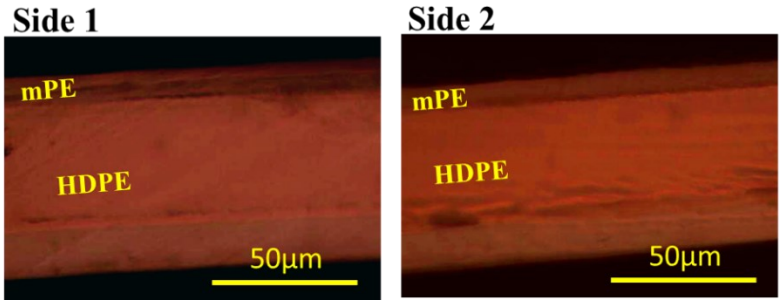

Figure 6.8 Light microscopy images of HDPE-mPE-10 film before and after sealing at 105°C, 0.5s dwell time and pressure of 0.27N/mm^2.

6.4.5 Effect of sealing temperature on hot tack strength

The results of hot tack measurements of the laminated back-layer films at 140°C are shown in Figure 6.9.

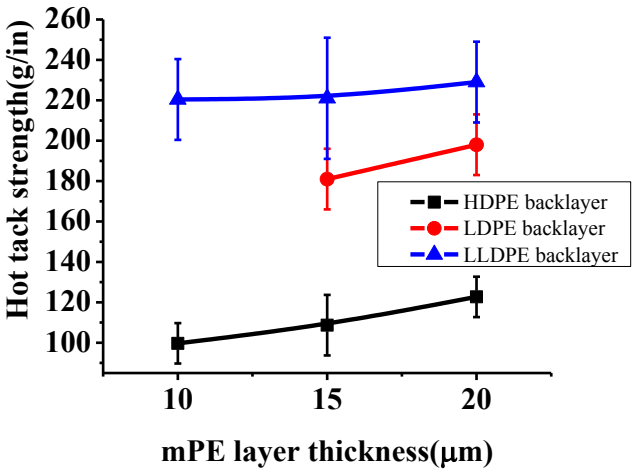

Figure 6.9 Hot tack strength at different mPE layer thicknesses in HDPE-mPE, LDPE-mPE and LLDPE-mPE films. All tests were done at 140°C, 0.5s dwell time and pressure of 0.27 N/mm^2

Increasing temperature reduced hot tack strength in all three back-layer films which is attributed to easier pullout of the diffused polymer chains at higher temperatures [35]. The same observed order of hot tack strength at 105°C was still observed in these samples in which films with LLDPE and LDPE back- layers showed the best performance and the films with HDPE back-layer had the lowest hot tack strength. This indicates that even at higher sealing temperature, type of the back-layer can affect the hot tack strength. Interestingly the observed increasing trend of hot tack strength by mPE layer thickness was considerably diminished at this temperature and increasing mPE layer thickness did not improve its hot tack considerably. Comparing the results of Figure 6.9 and Figure 6.6 indicates that increasing temperature reduced the effect of mPE layer thickness on hot tack strength.

6.4.6 Effect of delay time on hot tack evolution

Hot tack test provides valuable information regarding the performance of the sealant materials especially during vertical form fill sealing (VFFS) applications, but in most cases, there is a short

delay time between sealing and applying the stress to the seal area. During the delay time, the sealed area is cooled down due to the heat transfer to the surrounding environment. The effect of delay time on hot tack evolution of film samples with different back-layers and 15 μm mPE layer was investigated, and the results are presented in Figure 6.10 .

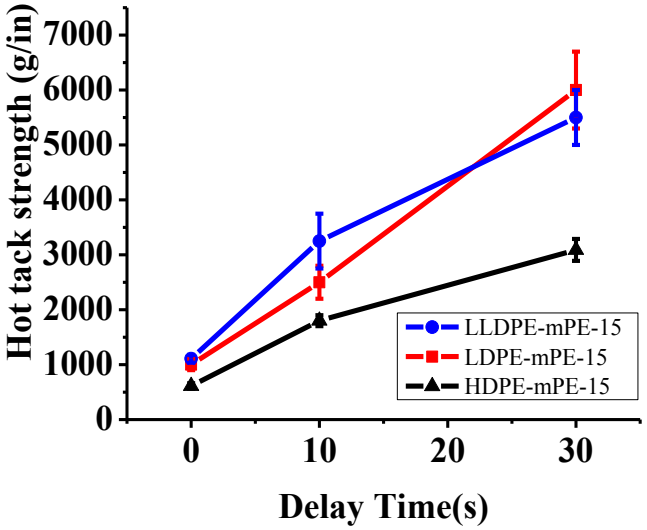

Figure 6.10 Hot tack evolution in films with different back-layers and 15μm mPE layer. Film samples were sealed at 105°C, 0.5s dwell time and pressure of 0.27N/mm^2.

All film samples showed improvement in the hot tack strength by increasing delay time which is attributed to the increasing molecular friction and much difficult pull out of polymer chains as the sealed area is cooled down [29, 33, 35, 40]. But it can be clearly seen that the hot tack evolution by delay time was faster in films with LDPE and LLDPE back-layers compared to those with HDPE back-layer. Considering the error bars in the measurement, it can be concluded that both LDPE and LLDPE back-layer films showed comparable results. At 10 s of delay time, LLDPE-mPE-15 had the highest hot tack strength among different back-layers followed by LDPE-mPE-15 and finally HDPE-mPE-15. It should be noted that all samples still showed peelable behavior at 10s delay time. By increasing delay time to 30 s, both LDPE-mPE-15 and LLDPE-mPE-15 showed lock-seal behavior with very high seal strengths while HDPE-mPE-15 still had peelable behavior.

In order to examine the effect of longer delay time on seal strength of HDPE-mPE-15, the seal strength for this sample was also measured 60s after sealing. Interestingly, this sample still showed

a peelable behavior with a seal strength of 3125 (g/in) which is comparable to the one obtained after 30 s of delay time. These results indicate that the nature of the back-layer did not only affect the hot tack evolution but also affected the seal behavior (peelable or lock-seal).

In order to examine the effect of mPE layer thickness on hot tack evolution with time, the hot tack evolution of HDPE-mPE-10 was also measured and the results are presented in Figure 6.11. It should be noted that HDPE back-layer film was used in this part of the work as they interestingly showed peelable behavior even after 60 s of delay time. Therefore, it is interesting to see how reducing mPE thickness can affect their hot tack evolution. The results of HDPE-mPE-15 are also presented again in this figure for the sake of comparison.

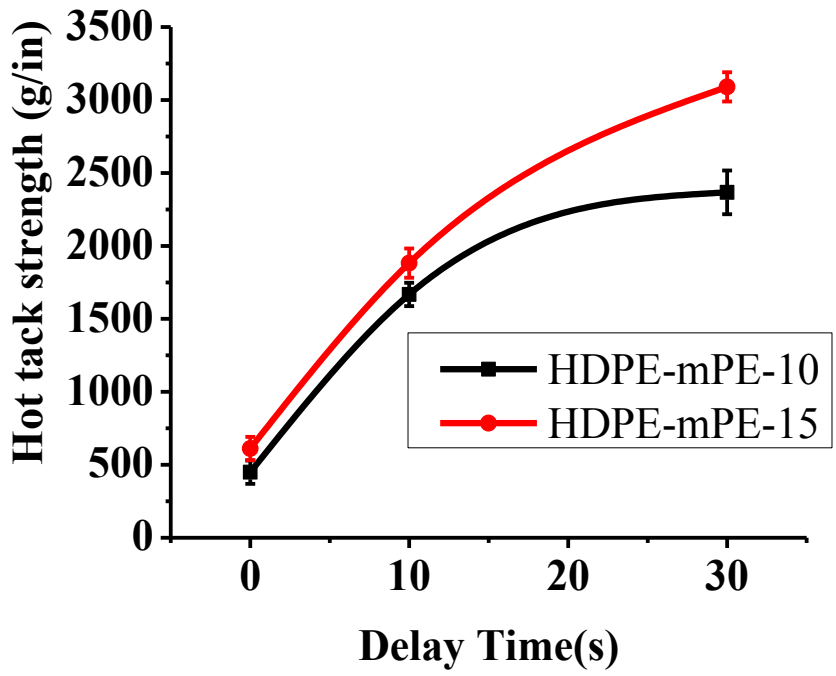

Figure 6.11 Hot tack strength versus delay time for films with HDPE back-layer at two different mPE layer thicknesses. heat sealing was done at 105°C, 0.5s dwell time and pressure of 0.27 N/mm^2.

Similar to the HDPE-mPE-15, increasing delay time increased the hot tack strength of HDPE-mPE-10. HDPE-mPE-15 showed slightly higher hot tack (at delay time=0 s) than HDPE-mPE-10. Increasing delay time led to increasing the gap between hot tack strength of the two films. Finally, the hot tack strength after 30s of delay time was still higher for HDPE-mPE-15. These results indicate that increasing mPE layer could improve hot tack evolution and seal strength.

6.4.7 Effect of dwell time

Dwell time is another important sealing parameter in heat sealing which can affect the seal performance considerably [33]. Effect of dwell time on hot tack evolution of HDPE-mPE-10 was examined by sealing these samples at 1s and 3s dwell times and measuring their hot tack strengths at different delay times. The obtained results are shown in Figure 6.12. All samples showed peelable behavior even after sealing at dwell time of 3s. It can be seen that increasing dwell time from 0.5s to 3 s did not have a considerable effect on hot tack strength evolution.

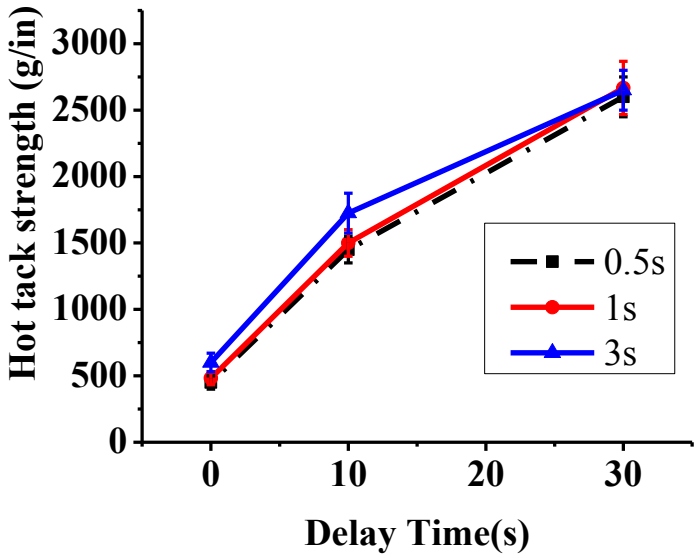

Figure 6.12 Hot tack evolution of HDPE-mPE-10 sealed at 105°C, and 0.27 N/mm^2 with 0.5, 1 and 3s dwell times.

6.4.8 Role of back-layer on hot tack evolution in multilayer sealant films

It has been well established in the literature that hot tack strength of a sealant (in the absence of contaminations in the seal area) is mainly controlled by molecular diffusion across the interfaces between seal sides [35, 41]. Faster molecular diffusion results in higher number of links created between seal sides and increases the diffusion depth of the molecules at the interface. Once the diffusion depth reaches a certain scale, the density of entanglements at the interface region between seal sides become similar to the one in the bulk which results in complete healing of the interface. Different diffusion length scales have been reported but the most common criteria is that the polymer molecules should diffuse at least a distance equal to their radius of gyration in the melt

[15, 36, 42, 43]. It has been shown in literature that the radius of gyration of polyethylene molecules in the melt with a molecular weight of 100 Kg/mol should be in the range of 14 nm [44, 45]. The molecular weight (MW) of the mPE used in this work was measured in a previous study and was found to be 96 (Kg/mol) [37]. Therefore, a diffusion length scale of 14 nm is likely to be enough for interface healing between mPE layers on the seal sides during heat sealing. It has also been shown that when two highly compatible polymers form an interface, a transition region between polymers exists instead of a sharp interface. This transition region is called interphase in which the molecular mobility of polymer chains is different than in the bulk [46]. As heat sealing in all cases was done at a temperature below or close to the melting temperatures of the back-layer (compared to mPE layer), therefore, it is likely to expect that a layer of metallocene polyethylene at the interface with the back-layer should experience a reduced molecular mobility compared to the molecules in the bulk of mPE layer. The length scale of the interphase region in highly compatible polymer blends has been shown to be in the range of 10 nm [47] to 1000 nm [48], depending on their compatibility. If the mPE layer thickness is thin enough that the reduced mobility of the interphase region can affect the molecular diffusion at the interface, then hot tack properties should be dramatically affected. The thickness of mPE layer in this study was always greater than 10 μm which is much larger than the length scale of the interphase region. Therefore, the observed reduced hot tack in the film samples with the back-layer cannot be due to the change in molecular mobility.

In our previous study [32], we found that increasing crystallinity of polyethylene materials in the seal layer can delay the heat transfer to the interface between seal sides. In order to examine the effect of back-layer on heat transfer, calculations on heat transfer in sealing of HDPE-mPE films with different thicknesses of mPE layer was done using COMSOL Multiphysics and the results are presented in Figure 6.13.

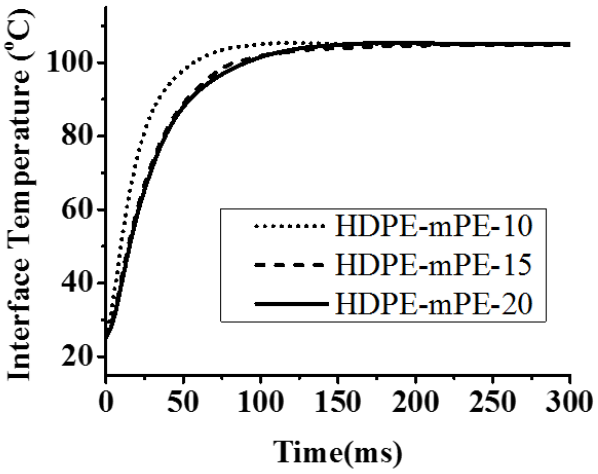

Figure 6.13 Simulation of the interface temperature evolution in HDPE-mPE films with different mPE layer thicknesses. Sealing temperature was set at 105°C.

The results show that after about 125 ms, the interface between seal sides almost reached the jaw temperature in all film samples. These results ensure that at dwell time of 0.5 s which is mostly used in this work, heat transfer should not be an issue. In addition, it was previously shown that increasing the dwell time up to 1s, did not influence the hot tack performance. Both of these results clearly indicate that the effect of back-layer on heat transfer cannot be the cause of the observed effects of back-layer on hot tack performance and evolution.

It was shown in a previous study that increasing amorphous content of sealant can improve hot tack and seal performance by improving molecular diffusion [2]. Although it was found that the crystallinity of the mPE layer was affected by the type of back-layer material, but DSC results in Table 6.2 clearly showed that the crystallinity of mPE in HDPE back-layer film was less than that in LLDPE and LDPE back-layer films. Therefore, if the variation of amorphous content in the sealant layer was the controlling factor in hot tack strength, then the hot tack of HDPE back-layer films should have been higher. However, the obtained experimental results showed that HDPE back-layer films had always lower hot tack strength compared to LDPE or LLDPE back-layer films.

In order to understand the origin of the back-layer material effect, it should be considered that when the stress is applied to the seal area, it is concentrated at the interface between seal sides. The peeling process during seal or hot tack tests can occur in the bulk of mPE layer or at the

interface between seal sides. In both cases, a crack should form and grow in the bulk or at the interface, respectively. The mechanism of crack growth in polymer materials has been discussed extensively in the literature [49-52]. In this process, two main energy dissipating mechanisms are involved [53]: (i) chain pull out and breakage and (ii) bulk viscoelastic energy dissipation. The first mechanism is limited to the crack tip area and the bulk viscoelastic energy dissipation has been shown to occur in a volume of the material in front of the crack tip which is known as the plastic zone. The plastic zone is a sphere with a radius that can be estimated using the following Equation [51]:

$$r_p = \frac{1}{2\pi}\left(\frac{K_C}{\sigma_y}\right)^2 \qquad \text{Eq. 6.2}$$

Where r_p, K_c and σ_y are the radius of the plastic deformation zone, the stress intensity factor and the yield strength of the material respectively. Stress intensity factor can be determined from the fracture toughness measurements based on ASTM E399-78. It has been shown that the reliable measurements require live measurements of crack tip radius and velocity using high resolution and high speed cameras [25]. Considering the experimental complexity of these measurements, stress intensity factors were taken from literature. The reported values for stress intensity factor for different types of polyethylene at room temperature are in the range of 0.72-1.382 MPa.m$^{1/2}$ for HDPE [14, 15, 54-56], 0.4 to 0.6 MPa.m$^{1/2}$for LDPE and LLDPE [57, 58]. Stress intensity factor for mPE was not found in literature, but considering its molecular structure, it is likely to expect that it should be similar or smaller than the values reported for LDPE or LLDPE. Therefore, a value of 0.4 MPa.m$^{1/2}$, which is the lower limit of the range reported for LDPE and LLDPE, was selected for this study. Using the yield strength of neat mPE (Table 6.1), the radius of the plastic zone in front of the crack tip can be estimated as 873 μm. The estimated plastic zone radius indicates that not only the mPE layer but the whole film structure should be involved in bulk viscoelastic energy dissipation in front of the crack tip. Energy dissipation is mainly controlled by viscous dissipation mechanisms which originate from vibrational and rotational movements of atoms as well as inter-molecular friction between polymer molecules [53]. The viscoelastic energy dissipation potential of polyethylene types used as back-layers can be examined by comparing their radii of plastic zone. Using the average of the reported stress intensity factors mentioned above for each type and the yield strength of the neat back-layer materials presented in Table 6.1,

the radii of plastic zones for HDPE, LDPE and LLDPE can be estimated as 240 μm , 330 μm and 525 μm, respectively. The estimated values indicate that HDPE has the lowest energy dissipation potential followed by LDPE and LLDPE. This indicates that upon applying stress to the sealed area in HDPE back-layer films, less bulk viscoelastic energy dissipation occurs and therefore crack growth and peeling can occur at lower stresses which results in lower hot tack strength. By changing back-layer to LDPE or LLDPE, the bulk viscoelastic energy dissipation in the plastic zone increases which results in higher energy and stress required for seal opening. Considering the experimental results and the estimated radii of plastic zone, it can be inferred that above a certain radius of the plastic zone, the required force for crack growth in the bulk or at the interface will be significant enough that no considerable difference could be observed between LDPE and LLDPE back-layer films.

The effect of mPE sealant layer thickness on hot tack evolution can also be explained using this approach. Increasing mPE sealant layer thickness does not affect the energy required for chain pull out and only increases the bulk viscoelastic energy dissipation and energy required for crack growth in the sealed area. It was shown that increasing sealing temperature reduced significantly the dependency of hot tack to mPE sealant layer thickness. This can be explained by considering that although increasing temperature can increase energy dissipation, it reduces at the same time the energy required for chain pullout at the tip of the crack. As a result, at high temperature, the effect of increasing energy dissipation by increasing mPE layer thickness is counterbalanced by reducing energy required for chain pull out at the crack tip. The obtained results indicate the observed effects of back-layer is limited to the bulk viscoelastic energy dissipation in the plastic zone in front of the crack tip in the sealed area.

6.5 Conclusion

Multilayer film samples composed of a metallocene polyethylene layer (mPE) and a back-layer of either HDPE, or LDPE, or LLDPE were produced using cast film co-extrusion. Effect of back-layer material on hot tack strength was examined at different mPE layer thicknesses. It was shown that all films with different back-layers showed peelable behavior in hot tack test. In addition, films with LDPE or LLDPE back-layers showed similar hot tack strength but films with HDPE back-

layer had always lowest hot tack strength. Hot tack strength increased in all films by increasing mPE layer thickness. However, this increase was at lower rate for HDPE back-layer compared to the films with LDPE or LLDPE back-layer. By increasing sealing temperature, it was found that hot tack strength decreased but still films with HDPE back-layer showed the least hot tack strength. However, the mPE sealant thickness dependency that was observed at lower temperature was not observed at high temperature. This indicates that increasing sealant thickness can be an effective approach in improving hot tack strength at low sealing temperatures but does not have a considerable effect at higher sealing temperatures. Effect of delay time on hot tack evolution of the film samples with 15 μm mPE sealant layer was examined and it was found that increasing delay time above 10 s led to a change in peeling behavior of LDPE and LLDPE back-layer films from a peelable to a lock seal. Increasing delay time was found to also increase the hot tack strength in HDPE back-layer film but at lower extent and didn't change the observed peelable behavior up to 60 s of delay time. Effect of dwell time on hot tack evolution of HDPE back-layer films was also studied and it was found that increasing dwell time from 0.5 to 3s, didn't change their hot tack evolution. Different mechanisms involved in growth of the crack during seal test were described in detail and it was shown that considering the bulk viscoelastic dissipation in front of the crack in the sealed area can explain the observed effects of back-layer and mPE layer thickness of hot tack evolution. These findings clearly indicate the significant importance of the choice of back-layer on controlling hot tack and seal properties of multilayer polyethylene sealant films.

6.6 Reference

1. Marsh, K. and B. Bugusu, *Food packaging—roles, materials, and environmental issues.* Journal of food science, 2007. **72**(3): p. R39-R55.
2. Najarzadeh, Z., A. Ajji, and J.-B. Bruchet, *Interfacial self-adhesion of polyethylene blends: the role of long chain branching and extensional rheology.* Rheologica Acta, 2015. **54**(5): p. 377-389.
3. Najarzadeh, Z., R.Y. Tabasi, and A. Ajji, *Sealability and Seal Characteristics of PE/EVA and PLA/PCL Blends.* International Polymer Processing, 2014. **29**(1): p. 95-102.
4. Lamnawar, K., F. Vion-Loisel, and A. Maazouz, *Rheological, morphological, and heat seal properties of linear low density polyethylene and cyclo olefine copolymer (LLDPE/COC) blends.* Journal of applied polymer science, 2010. **116**(4): p. 2015-2022.
5. Tabasi, R.Y., Z. Najarzadeh, and A. Ajji, *Development of high performance sealable films based on biodegradable/compostable blends.* Industrial Crops and Products, 2015. **72**: p. 206-213.

6. Scarfato, P., et al., *Three-layered coextruded cast films based on conventional and metallocene poly (ethylene/α-olefin) copolymers.* Journal of Plastic Film & Sheeting, 2014. **30**(3): p. 284-299.
7. Butler, T.I. and B.A. Morris, *PE-based multilayer film structures*, in *Multilayer flexible packaging*. 2016, Elsevier. p. 281-310.
8. Mihindukulasuriya, S.D. and L.-T. Lim, *Heat sealing of LLDPE films: Heat transfer modeling with liquid presence at film–film interface.* Journal of Food Engineering, 2013. **116**(2): p. 532-540.
9. Yuan, C.S., et al., *Heat sealability of laminated films with LLDPE and LDPE as the sealant materials in bar sealing application.* Journal of Applied Polymer Science, 2007. **104**(6): p. 3736-3745.
10. Sierra, J.D., M. del Pilar Noriega, and T.A. Osswald, *Effect of metallocene polyethylene on heat sealing properties of low density polyethylene blends.* Journal of Plastic Film & Sheeting, 2000. **16**(1): p. 33-42.
11. Wooster, J.J., et al., *Film layers made from ethylene polymer blends*. 2010, US Patents.
12. Poisson, C., et al., *Optimization of PE/Binder/PA extrusion blow-molded films. I. Heat sealing ability improvement using PE/EVA blends.* Journal of Applied Polymer Science, 2006. **99**(3): p. 974-985.
13. Poisson, C., et al., *Optimization of PE/binder/PA extrusion blow-molded films. II. Adhesion properties improvement using binder/EVA blends.* Journal of Applied Polymer Science, 2006. **101**(1): p. 118-127.
14. Philippe Mesnil, et al., *Seal Through Contamination Performance of Metallocene Plastomers*, in *TAPPI Polymers, Laminations & Coatings Conference*. 2000.
15. Halle, R.W. *Plastomer-mVLDPE Blends for High Performance Heat Sealing Applications*. in *TAPPI 2003 PLACE Conference Proceedings*. 2003.
16. Halley, R.W. and A.M. Malakoff, *A New High-Performance mVLDPE.* Journal of Plastic Film and Sheeting, 2005. **21**(1): p. 13-26.
17. Shih, H.-H., et al., *Hot tack of metallocene catalyzed polyethylene and low-density polyethylene blend.* Journal of Applied Polymer Science, 1999. **73**(9): p. 1769-1773.
18. Simanke, A.G., C. de Lemos, and M. Pires, *Linear low density polyethylene: Microstructure and sealing properties correlation.* Polymer Testing, 2013. **32**(2): p. 279-290.
19. Sadeghi, F. and A. Ajji, *Rheological, physical, and thermal characterization of single-site catalyst based polyethylenes for seal layer applications.* Polymer Engineering & Science, 2012. **52**(5): p. 1089-1098.
20. Liu, C., J. Wang, and J. He, *Rheological and thermal properties of m-LLDPE blends with m-HDPE and LDPE.* Polymer, 2002. **43**(13): p. 3811-3818.
21. Najarzadeh, Z., *Control and optimization of sealing layer in films*, in *chemical engineering*. 2014, École Polytechnique de Montréal. p. 165.
22. Viganò, S. *The use of metallocene polyethylene in co-extruded lamination film*. in *11 th European PLACE Conference. Athens, Greece*. 2007.
23. Viganò, S. *The Use of Metallocene Polyethylene in Co-Extruded Lamination Film*. in *TAPPI 2007 PLACE Conference Proceedings*. 2007.
24. Dil, E.J., N. Virgilio, and B.D. Favis, *The effect of the interfacial assembly of nano-silica in poly (lactic acid)/poly (butylene adipate-co-terephthalate) blends on morphology, rheology and mechanical properties.* European Polymer Journal, 2016. **85**: p. 635-646.

25. Wang, D., et al., *Compatibilization and morphology development of immiscible ternary polymer blends.* Polymer, 2011. **52**(1): p. 191-200.
26. Hemmati, M., H. Nazokdast, and H. Shariat Panahi, *Study on morphology of ternary polymer blends. II. Effect of composition.* Journal of Applied Polymer Science, 2001. **82**(5): p. 1138-1146.
27. Eslamian, M., R. Bagheri, and G. Pircheraghi, *Co-crystallization in ternary polyethylene blends: tie crystal formation and mechanical properties improvement.* Polymer International, 2016. **65**(12): p. 1405-1416.
28. Le Corroller, P. and B.D. Favis, *Droplet-in-Droplet Polymer Blend Microstructures: a Potential Route Toward the Recycling of Co-mingled Plastics.* Macromolecular Chemistry and Physics, 2012. **213**(19): p. 2062-2074.
29. Najarzadeh, Z. and A. Ajji, *A novel approach toward the effect of seal process parameters on final seal strength and microstructure of LLDPE.* Journal of Adhesion Science and Technology, 2014. **28**(16): p. 1592-1609.
30. Di Lorenzo, M.L. and C. Silvestre, *Non-isothermal crystallization of polymers.* Prog. Polym. Sci., 1999. **24**: p. 917-950.
31. Zhu , L., et al., *Physical Constants of Poly(ethylene)*, in *Polymer Handbook (4th Edition)*, J. Brandrup, et al., Editors., John Wiley & Sons. p. V-9.
32. Kanani Aghkand, Z., et al., *Simulation of Heat Transfer in Heat Sealing of Multilayer Polymeric Films: Effect of Process Parameters and Material Properties.* Industrial & Engineering Chemistry Research, 2018. **57**(43): p. 14571-14582.
33. Theller, H.W., *Heat sealability of flexible web materials in hot-bar sealing applications.* Journal of Plastic Film and sheeting, 1989. **5**: p. 66-93.
34. Meka, P. and F.C. Stehling, *Heat sealing of semicrystalline polymer films. I. Calculation and measurement of interfacial temperatures: Effect of process variables on seal properties.* Journal of Applied Polymer Science, 1994. **51**(1): p. 89-103.
35. Stehling, F.C. and P. Meka, *Heat sealing of semicrystalline polymer films. II. Effect of melting distribution on heat-sealing behavior of polyolefins.* Journal of Applied Polymer Science, 1994. **51**(1): p. 105-119.
36. Kim, Y.H. and R.P. Wool, *A theory of healing at a polymer-polymer interface.* Macromolecules, 1983. **16**(7): p. 1115-1120.
37. Najarzadeh, Z. and A. Ajji, *Role of molecular architecture in interfacial self-adhesion of polyethylene films.* Journal of Plastic Film & Sheeting, 2017. **33**(3): p. 235-261.
38. ROBERT, Y.L., A. SHANKS, and Z.H. STACHURSILIt, *kinetics of polymer crystallization.* Prog. Polym. Sci., 1995. **20**: p. 651-701.
39. Milner, S.T., *Polymer crystal–melt interfaces and nucleation in polyethylene.* Soft Matter, 2011. **7**(6): p. 2909-2917.
40. Wool, R.P., *Polymer entanglements.* Macromolecules, 1993. **26**(7): p. 1564-1569.
41. Wool, R.P., *Self-healing materials: a review.* Soft Matter, 2008. **4**(3): p. 400.
42. Wool, R.P., *Polymer Interfaces: Structure and Strength*. 1995: Hanser Publishers.
43. de Gennes, P.G., *CHAPTER 3 - Mechanical Properties of Polymer Interfaces A2 - Sanchez, Isaac C*, in *Physics of Polymer Surfaces and Interfaces*. 1992, Butterworth-Heinemann: Boston. p. 55-71.
44. Schelten, J., et al., *Small-angle neutron scattering studies of molten and crystalline polyethylene.* Polymer, 1976. **17**(9): p. 751-757.

45. Ashbaugh, H.S., et al., *Mesoscale model of polymer melt structure: Self-consistent mapping of molecular correlations to coarse-grained potentials.* The Journal of chemical physics, 2005. **122**(10): p. 104908.
46. Ajji, A. and L.A. Utracki, *Interphase and compatibilization of polymer blends.* Polymer Engineering & Science, 1996. **36**(12): p. 1574-1585.
47. Helfand, E. and Z.R. Wasserman, *Block copolymer theory. 4. Narrow interphase approximation.* Macromolecules, 1976. **9**(6): p. 879-888.
48. Ravati, S., et al., *Phase identification and interfacial transitions in ternary polymer blends by ToF-SIMS.* Polymer, 2014. **55**(23): p. 6110-6123.
49. Parsons, M., et al., *Effect of strain rate on stepwise fatigue and creep slow crack growth in high density polyethylene.* Journal of Materials Science, 2000. **35**(8): p. 1857-1866.
50. Bouchelarm, M.A., M. Mazari, and N. Benseddiq, *Stress Intensity Factor KI and T-Stress Determination in HDPE Material.* Journal of Failure Analysis and Prevention, 2017. **17**(5): p. 919-934.
51. Roylance, D., *Introduction to Fracture Mechanics*, C. Department of Materials Science and Engineering Massachusetts Institute of Technology, MA 02139, Editor. 2001, NBS Special Publication 647-1: Washington.
52. Wei, Y. and J. Hutchinson, *Interface strength, work of adhesion and plasticity in the peel test.* International Journal of Fracture, 1998. **93**(1-4): p. 315-333.
53. Sun, T.L., et al., *Bulk Energy Dissipation Mechanism for the Fracture of Tough and Self-Healing Hydrogels.* Macromolecules, 2017. **50**(7): p. 2923-2931.
54. EL-Bagory, T.M.A.A., H.E.M. Sallam, and M.Y.A. Younan, *Evaluation of Fracture Toughness Behavior of Polyethylene Pipe Materials.* Journal of Pressure Vessel Technology, 2015. **137**(6): p. 061402-(1-10).
55. Parsons, M., et al., *Effect of strain rate on stepwise fatigue and creep slow crack growth in high density polyethylene.* Journal of Materials Science, 2000. **35**(8): p. 1857-1866.
56. Huang, Y.-L. and N. Brown, *The effect of molecular weight on slow crack growth in linear polyethylene homopolymers.* Journal of materials science, 1988. **23**(10): p. 3648-3655.
57. Bretz, P.E., R.W. Hertzberg, and J.A. Mason, *A Correlation between Crack Growth Rate and Fracture Mode Transitions in Low-Density Polyethylene*. 1981, LEHIGH UNIV BETHLEHEM PA MATERIALS RESEARCH CENTER. p. 1-5.
58. Hashemi, S. and J. Williams, *A fracture toughness study on low density and linear low density polyethylenes.* Polymer, 1986. **27**(3): p. 384-392.

CHAPTER 7 GENERAL DISCUSSIONS

Here the experimental and modeling challenges in each part of the work will be discussed and the main outcomes and some guidelines to overcome common industrial issues will presented in the next chapter.

In this study, first attempts were made to examine effect of different parameters on interface temperature between two seal sides. In order to measure the interface temperature, initially a fine thermocouple with the wire thickness of 25 μm was purchased. However, the thermocouple was very thin and fragile and was damaged easily even when placed delicately on the film. When thick thermocouples with wire thickness of 125 μm were used, small bubbles were between the thermocouple and polymer which could reduce the precision of the measurements. Finally, when the thermocouple with 75 μm was used, reproducible readings without bubble trapping could be obtained. It was also necessary to tape the thermocouples legs to the film (out of the seal area) to prevent movement during sealing. To demonstrate effect of jaw/film contact and TCR boundary condition on heat sealing, conductive silver-based pastes were used to lightly cover the film surface or jaw surface with a thin layer of the paste and possibly eliminate or reduce the TCR effect. However, it was found that the conductivity of these pastes is not high enough and they rather induced a delay in the heat transfer instead of improving it.

In the second part of the project, effects of different sealing conditions and material viscosity on squeeze out flow was studied. Measuring SOF at low amounts was challenging and the error was considerable which made it difficult to analyze and make conclusions from the results. Initially we planned to also examine SOF at even lower temperatures where heat sealing of mLLDPE begins (~90^{o}C), however, as at these temperatures, the whole sealant has not melted, measuring rheological characteristics and analyzing the two-phase flow was too complicated and we found that it requires a dedicated study. In addition, it was planned to examine the effect of viscosity of sealant in thick sealant by preparing film with 130 μm of Exact 3139, but unfortunately the film was too sticky and stuck to the rolls of the calendar and we could not produce a film with stable sealant thickness. For simulation of SOF using COMSOL, it was very difficult to find related resources on implication of deforming geometry and moving mesh in squeeze flow problems in Cartesian coordination system.

In the third phase of the project, initially four layers structure of PA/tie/back-layer/mLLDPE was planned to be produced. However, when I tested the sample in hot tack test, the film showed considerable deformation which did not allow obtaining reliable results. Many attempts were made over the course of one year in my PhD to produce this film without showing deformation in hot tack. At the end, we found that this is the natural problem with PA. Although this result was interesting for our industrial partner, but it caused considerable delay in the project without a scientific contribution. Therefore, two-layer films of back-layer/mLLDPE, were produced by Co-extrusion and the samples then were sent to be laminated to a PET film in ProAmpac facility. In addition, producing a single layer of metallocene polyethylene (mPE) was very challenging as the film was very soft and sticky and after winding on the roll, it was very difficult to unwind the film without stretching it. We finally found that manual winding of the film could reduce considerably the tension and avoid film blocking issues. When the manually wound film was sent to ProAmpac for lamination, they also had many issues with the film and laminating the film took more than a month for them because they had to try multiple times to be able to run it without wrinkles and without sticking issues. Despite the difficulties that these delays made in the project, they clearly confirmed the drawbacks in processing and converting of single layer metallocene polyethyelene sealants. I also tried to produce single layer mLLDPE at 20 μm to compare the results with the films with back-layer and the same thickness of mLLDPE. After multiple trials, I found that the die gap needs to be much lower than the die gap we commonly used (250 μm instead of 700 μm). However, when the film was sent for lamination, after 2 months and many trials, when Proampac sent a small laminated sample, we found that due to the very small thickness of the film and the wrinkles due to its softness, when they applied corona treatment on the lamination side, the seal side was also treated. This defect, which is known as back treat in the industry, causes the seal properties to decrease significantly. Due to these issues, seal performance of single layer thinner mLLDPE film could not be compared with multilayer film.

CHAPTER 8 CONCLUSIONS AND RECOMMENDATIONS

8.1 Conclusions

In this dissertation, attempts have been made to provide new insight and understanding into heat sealing of multilayer plastic film with polyethylene sealants. Considering the significant importance of heat transfer in heat sealing and the lack of a comprehensive study on this subject in the literature, the first phase of the work was dedicated to understanding the heat transfer phenomenon in heat sealing process by simulation and experimental investigation. Three-layer films composed of a PA outer layer, PE-g-MA middle layer, and HDPE or metallocene LLDPE (mLLDPE) sealant layers were produced using cast film coextrusion. The interface temperature between films during heat sealing was measured with a fine thermocouple connected to a high-speed data accusation system. By comparing the measured interface temperature in different width and length locations within the seal area, it was shown that heat transfer in heat sealing can be considered as a unidirectional heat transfer in the film thickness direction. Effect of heated jaw temperature, sealant material, sealant thickness and sealing pressure were examined. Jaw temperature, sealant thickness, and sealant material were found to affect the interface temperature, but the sealing pressure did not have a considerable effect. Simulation of heat sealing was done using COMSOL Multiphysics software. Variation of materials properties including density, thermal conductivity, and specific heat capacity were measured experimentally at a wide range of temperature. In addition, surface roughness of film samples was measured using atomic force microscopy (AFM). The perfect interface assumption between layers was used as the films were prepared using co-extrusion process. Thermal contact resistance (TCR) was used as the boundary condition between the PA layer and heated jaws. As the heat sealing was done at temperatures much above the glass transition temperature of PA (T_g=60^{o}C), the plastic Cooper−Mikic−Yovanovich model (CMY) was used in this study which considers plastic deformation of surface asperities. Comparing the experimental results with simulation results showed that the simulation could predict well the interface temperature between seal sides in both HDPE and mLLDPE sealants with different sealant thicknesses and in a wide range of temperature. It was also shown that considering TCR boundary condition was essential in achieving a precise simulation. This indicates the importance of film surface and jaw surface quality and roughness.

Interestingly, it was found that using highly crystalline polymers such as HDPE induces a delay in heat transfer due to the considerable heat absorption during their melting process. The good agreement between the simulation results and experimental measurements indicated the potential of the simulation in reducing material selection cost in packaging design.

Despite its significant importance in industrial applications, squeeze out flow (SOF) is an aspect of heat sealing that has been poorly studied in the literature. In the second part of this work, attempts were made to determine the effects of different heat sealing condition and sealant material properties on SOF. The effects of sealing temperature, dwell time (sealing time), sealing pressure, sealant material type and sealant layer thickens on SOF in films with the structure of PA (outer layer)/PE-g-MA (tie)/mLLDPE (sealant) were examined. SOF was measured by determining volume of squeezed out sealant using SEM images taken from the sealed area. The difference between melt and solid density was used to determine the precise SOF amount. The obtained results showed that SOF depends considerably on sealing temperature and sealant thickness. It was also shown that reducing viscosity of sealant could improve SOF in thin sealants but only at high pressure and long dwell times. However, increasing sealing pressure was found not to be an effective tool in improving SOF. SOF was also modeled using three approaches: (i) one-dimensional model using power-law fluid behavior, (ii) one-dimensional model using Carreau-Yasuda fluid and finite difference method (FDM), (iii) two-dimensional model using Carreau-Yasuda fluid using COMSOL Multiphysics software. All models were based on an isothermal assumption and in the first two models, a quasi-steady state condition was assumed with a linear pressure profile within the sealant layer. The COMSOL simulation was based on the known squeezing velocity which was defined based on the experimental data for variation of sealant thickness during sealing. The obtained results showed that the power-law model always underestimated SOF. The COMSOL simulation results showed that the pressure profile within the sealant layer should be a non-linear pressure profile with pressure gradients smaller than the linear profile assumed in the power-law and the FDM mode. It was also found that considering the delay time induced in SOF due to heat transfer is needed for the FDM model to predict satisfactorily the experimental results. Both FDM and COMSOL simulation showed that the shear rates during SOF were in the transition zone between Newtonian plateau and Power-law region. This indicates the complexity of SOF in heat sealing and the significant potential of the FDM model in screening of sealant materials in packaging design.

Multilayer sealant films have been used widely in flexible packaging due to their flexibility in design, lower cost and ease of processing. However, the effect of back-layers on seal performance of these films have not been studied in the literature. In the third part of this dissertation, multilayer polyethylene films with a metallocene sealant layer (mLLDPE) and different back-layers of high-density polyethylene (HDPE), or low density polyethylene (LDPE), or linear low density polyethylene (LLDPE) were produced with different thicknesses of the metallocene layer. By comparing the hot tack performance of these films, it was found that using HDPE as the back-layer reduced considerably the seal strength of the film compared to the films with LDPE or LLDPE back-layers. Increasing the thickness of the mLLDPE was found to improve the hot tack but the effect was less pronounced in the films with HDPE back-layer. By measuring hot tack at different cooling times after sealing, it was found that cooling changed the seal behavior of films with LDPE or LLDPE back-layer from peelable to lock-seal. However, the film with HDPE back-layer always showed peelable behavior even at long cooling times. Increasing sealing time from 0.5 s to 3 s was found to have negligible effect on the observed peelable behavior in HDPE back-layer film. This result and the results of heat transfer simulation confirmed that the observed reducing effect of back-layer on seal performance cannot be attributed to the heat transfer during heat sealing. It was found that the observed effect of back-layer on seal properties can be well explained using bulk viscoelastic energy dissipation concept. By calculating of the radius of the plastic zone in front of the peeling zone, it was shown that not only sealant layer but also the back-layer contribute in the energy dissipation process during sealing tests. The obtained results highlighted the important effect of back-layer on seal properties which were not discovered in the literature before.

The obtained results in this dissertation, provide new insight on the effect of heat sealing condition and material properties on seal performance of plastic films in packaging industry. The numerical models and simulation can provide important tools for designing plastic films with much higher level of control on sealing performance at a much lower cost.

Some guidelines to common industrial challenges are addressed in the below table, which can be used to find the solutions in each case base on the present study

Table 8.1 Some guidelines for common industrial challenges

Problem/Challenge	Source	Guidelines
Setting process conditions due to these changes in the sealant film: **(a)Material** **(b)Thickness** **(b)Structure**	Changing the interface temperature between two side of seal area due to changes in heat transfer.	Use the heat transfer simulation to optimize time and temperature of the heat sealing process, with these inputs: a) Measure density and Cp variation with temperature for new material b) New thickness c) Add/remove layers due to new structure
Seal fails	1) Poor contact with Jaw 2) Low or high temperature 3) Low or high dwell time	1)Thermal contact resistance (TCR) between jaw and film is important, so to increase contact area: a) Use finer woven Teflon on the jaw surface b) Use serrated jaw 2,3) Optimize time and temperature with the heat transfer simulation
Leakage from seal area	Poor caulkability	➢ Process conditions: 1. Increase Jaw temperature 2. Increase Dwell time 3. Use FDM model to optimize the process conditions ➢ Material properties • Use material with lower viscosity
Need to lower the cost of the sealant film while maintaining the desired seal behaviour	Metallocene polyethylene's have very good seal performance and lock seal behaviour, but also have the high cost	Using multilayer sealant structure with: a) A thin layer of mPE in sealant side b) Conventional polyethylene as back-layer/s
Selecting and optimization of a sealant film material to reach: **a) lock seal behavior** **b) Peelable behavior**	Some material properties such as stiffness play a critical role in this area	Stiffness of the sealant film material can change pealing behavior: a) Use stiffer material as back-layer (ex: HDPE) b) Use softer material as back-layer (ex: LLDPE)

8.2 Original contributions

- The simulation interface temperature presented in the first part of this work is the first comprehensive simulation of heat sealing with very good agreement with experimental results in a wide range of sealing temperature, sealant material thickness and sealant material type. This simulation can provide a powerful designing tool for plastic packaging industry.
- A new method based on SEM image analysis was introduced for the first time to quantify SOF in heat sealing. This is the first and important step in being able to examine effects of different parameters on SOF.
- Effect of different sealing conditions, material properties and sealant thickness on SOF was examined systematically for the first time.
- A numerical model was introduced to predict SOF in heat sealing. The model predictions showed good agreement with experimental results. This indicates the potential of the model to be used in selection of sealant materials and sealing conditions.
- Back-layer material was found to considerably alter the seal performance of sealant films. The effect was explained by considering the back-layer effect on bulk viscoelastic energy dissipation during sealing test.

8.3 Recommendations

- In addition to coextrusion films, films prepared by lamination of PET films with sealant films are also very common in packaging industry. It will be interesting to examine the effect of different lamination methods on interface temperature during heat sealing
- Considering the observed important effect of interface with PA, it will be interesting to examine the effect of jaw pattern on interface temperature during heat sealing.
- Studying the interface temperature variation during cooling period (after sealing) in multilayer films is also very interesting as it provides information on cooling rates of different films with different structures and materials.
- Examining the ability of the FDM model by preparing different sealant films and comparing their performance in real packaging process of grain and powder products will be an interesting step in proving the potential of the model for industrial applications.

- Studying SOF in multilayer sealant films both experimentally and by simulation will be interesting as the next step for SOF part of the work. The effect of viscosity ratio between layers and layers thickness could be studied.
- Studying the effect of more layers in sealant film on seal performance will be interesting. What would be the effect of a third, fourth or even fifth layer on seal performance?
- Simulation of hot tack / seal strength build up during / after heat sealing process and compering the results with experimental data to be able to predict hot tack/seal strength of different sealant film materials and structures.

REFERENCES

1. Morris, B.A., *PREDICTING THE HEAT SEAL PERFORMANCE OF IONOMER FILMS.* Plastic Film and sheeting, 2002. **18**.
2. Najarzadeh, Z., *Control and optimization of sealing layer in films*, in *chemical engineering*. 2014, École Polytechnique de Montréal. p. 165.
3. D. Grewell and A. Benatar, *Welding of Plastics: Fundamentals and New Developments.* Intern. Polymer Processing 2007.
4. Bose, A., *Method for slitting and/or sealing plastic film material*. 1984, Google Patents.
5. Shanklin, F.G. and E.R. Lawson, *Seal wire heat control system*. 1994, Google Patents.
6. Waters, H.F., *Heat-sealing machine*. 1952, Google Patents.
7. Selke, S.E.M., J.D. Culter, and R.J. Hernandez, *Plastics Packaging: Properties, Processing, Applications, And Regulations*, ed. 2nd. 2004: Hanser Gardner Publications.
8. Theller, H.W., *Heat sealability of flexible web materials in hot-bar sealing applications.* Journal of Plastic Film and sheeting, 1989. **5**: p. 66-93.
9. Stehling, F.C. and P. Meka, *Heat sealing of semicrystalline polymer films. II. Effect of melting distribution on heat-sealing behavior of polyolefins.* Journal of Applied Polymer Science, 1994. **51**(1): p. 105-119.
10. Wool, R.P., *Polymer Interfaces: Structure and Strength*. 1995: Hanser Publishers.
11. Kim, Y.H. and R.P. Wool, *A theory of healing at a polymer-polymer interface.* Macromolecules, 1983. **16**(7): p. 1115-1120.
12. Wool, R.P., *Self-healing materials: a review.* Soft Matter, 2008. **4**(3): p. 400.
13. Wool, R.P. and K.M. O'Connor, *Time dependence of crack healing.* Journal of Polymer Science: Polymer Letters Edition, 1982. **20**(1): p. 7-16.
14. Wool, R.P. and K.M. O'Connor, *A theory crack healing in polymers.* Journal of Applied Physics, 1981. **52**(10): p. 5953-5963.
15. Brown, H., *The Adhesion Between Polymers*, A.R.M. Sci., Editor. 1991. p. 463-489.
16. Frederix, C., et al., *Kinetics of the non-isothermal fusion-welding of unlike ethylene copolymers over a wide crystallinity range.* Polymer, 2013. **54**(11): p. 2755-2763.
17. Zhang, M.Q. and M.Z. Rong, *Theoretical consideration and modeling of self-healing polymers.* Journal of Polymer Science Part B: Polymer Physics, 2012. **50**(4): p. 229-241.
18. Litvinov, V., et al., *Chain entanglements in polyethylene melts. Why is it studied again?* Macromolecules, 2013. **46**(2): p. 541-547.
19. Sperling, L.H., *Introduction to physical polymer science*. 2005: John Wiley & Sons.
20. Fox, T.G. and P.J. Flory, *Further Studies on the Melt Viscosity of Polyisobutylene.* The Journal of Physical Chemistry, 1951. **55**(2): p. 221-234.
21. de Gennes, P.G., *Reptation of a Polymer Chain in the Presence of Fixed Obstacles.* The Journal of Chemical Physics, 1971. **55**(2): p. 572-579.
22. Lin, Y.-H., *Polymer viscoelasticity: basics, molecular theories, experiments, and simulations*. 2011: World Scientific.
23. de Gennes, P.G., *CHAPTER 3 - Mechanical Properties of Polymer Interfaces A2 - Sanchez, Isaac C*, in *Physics of Polymer Surfaces and Interfaces*. 1992, Butterworth-Heinemann: Boston. p. 55-71.
24. Wool, R. and K. O'Connor, *Time dependence of crack healing.* Journal of polymer science: Polymer letters edition, 1982. **20**(1): p. 7-16.

25. Schuman, T., et al., *Interdiffusion of Linear and Branched Polyethylene in Microlayers Studied via Melting Behavior.* Macromolecules, 1998. **31**(14): p. 4551-4561.
26. Fleischer, G., *Temperature dependence of self diffusion of polystyrene and polyethylene in the melt an interpretation in terms of the free volume theory.* Polymer Bulletin, 1984. **11**(1): p. 75-80.
27. Bartels, C.R. and B. Crist, *Self-Diffusion Coefficient in Melts of Linear Polymers: Chain Length and Temperature Dependence for Hydrogenated Polybutadiene.* Macromolecules 1984. **17**: p. 2702-2708.
28. N. Z. Qureshi, et al., *Self-Adhesion of Polyethylene in the Melt. 1. Heterogeneous Copolymers.* Macromolecules 2001(34): p. 1358-1364.
29. Li, H. and S. Yan, *Surface-Induced Polymer Crystallization and the Resultant Structures and Morphologies.* Macromolecules, 2011. **44**(3): p. 417-428.
30. Shekhar, A., *A model for hot tack behaiveior in Ethylen Acid co-polymer films.* Tappi, 1994. **77**(1): p. 97-104.
31. *Standard Test Methods for Hot Seal Strength (Hot Tack) of Thermoplastic Polymers and Blends Comprising the Sealing Surfaces of Flexible Webs*. 2018.
32. Meka, P. and F.C. Stehling, *Heat sealing of semicrystalline polymer films. I. Calculation and measurement of interfacial temperatures: Effect of process variables on seal properties.* Journal of Applied Polymer Science, 1994. **51**(1): p. 89-103.
33. Diskin, M. *THE EFFECT OF POLYBUTYLENE ON SEAL STRENGTH OF EVA/POLYBUTYLENE SEAL BLENDS IN MEDICAL DEVICE PACKAGING*. in *ANTEK*. 2012.
34. Dodrill, D., *Advances in Peelable Sealant Technology.* Rollprint Packaging Products,Ink., 2005.
35. Yuan, C. and H. A, *Effect of bar sealing parameters on OPP/MCPP heat seal strength.* eXPRESS Polymer Letters, 2007. **1**(11): p. 773-779.
36. Giannico, S., et al., *Clinical Outcome of 193 Extracardiac Fontan Patients: The First 15 Years.* Journal of the American College of Cardiology, 2006. **47**(10): p. 2065-2073.
37. INTERNATIONAL, A., *12e1 Standard Test Methods for Hot Seal Strength (Hot Tack) of Thermoplastic Polymers and Blends Comprising the Sealing Surfaces of Flexible Webs*, in *F*. 1998.
38. Tetsuya, T., et al., *The effect of heat sealing temperature on the properties of OPP/CPP heat seal. I. Mechanical properties.* Journal of Applied Polymer Science, 2005. **97**(3): p. 753-760.
39. Aithani, D., et al., *Heat Sealing measurement by an innovative technique.* Packaging Technology and Science, 2006. **19**(5): p. 245-257.
40. Hashimoto, Y., et al., *Effect of heat-sealing temperature and holding time on mechanical properties of heat-sealed Poly(Lactic acid) films.* ANTEC, 2006.
41. Poisson, C., et al., *Optimization of PE/Binder/PA extrusion blow-molded films. I. Heat sealing ability improvement using PE/EVA blends.* Journal of Applied Polymer Science, 2006. **99**(3): p. 974-985.
42. Yuan, C.S., et al., *Heat sealability of laminated films with LLDPE and LDPE as the sealant materials in bar sealing application.* Journal of Applied Polymer Science, 2007. **104**(6): p. 3736-3745.
43. Planes, E., S. Marouani, and L. Flandin, *Optimizing the heat sealing parameters of multilayers polymeric films.* Journal of Materials Science, 2011. **46**(18): p. 5948-5958.

44. Mazzola, N., et al., *Correlation between thermal behavior of a sealant and heat sealing of polyolefin films.* Journal of Polymer Testing, 2012. **31**(7): p. 870-875.
45. Robertson, G.L., *Food Packaging ,Principles and Practice*. Third ed. 2012: CRC Press.
46. Najarzadeh, Z. and A. Ajji, *A novel approach toward the effect of seal process parameters on final seal strength and microstructure of LLDPE.* Journal of Adhesion Science and Technology, 2014. **28**(16): p. 1592-1609.
47. Pellingra, S., *Improving Line Efficiencies with Sealant Optimization*, AmpacPackaging, Editor. 2009.
48. Mueller, C., et al., *Heat sealing of LLDPE: relationships to melting and interdiffusion.* Journal of Applied Polymer Science, 1998. **70**(10): p. 2021-2030.
49. Philippe Mesnil, et al., *Seal Through Contamination Performance of Metallocene Plastomers*, in *TAPPI Polymers, Laminations & Coatings Conference*. 2000: Chicago.
50. Brodie, *hot tack procedures for flexible packaging structures.*
51. Vincent, B. *Hot tack of sealant resins*. in *TAPPI, Polymers,Laminations and coatings conference* 1986.
52. Kiang, W., *HOT tack and heat sealing properties of EVOH*, in *TAPPI PLACE,Lamination and coating* 1992.
53. Halle, R.W. and K.M. Cable, *A NEW mLLDPE FOR EXTRUSION COATING APPLICATIONS.* ExxonMobil Chemical Company, 1993.
54. Halle, R.W. *Plastomer-mVLDPE Blends for High Performance Heat Sealing Applications*. in *TAPPI 2003 PLACE Conference Proceedings*. 2003.
55. Shih, H.-H., et al., *Hot tack of metallocene catalyzed polyethylene and low-density polyethylene blend.* Journal of Applied Polymer Science, 1999. **73**(9): p. 1769-1773.
56. Moreira, A.C.F., P.C. Dartora, and F. Paulo dos Santos, *Polyethylenes in blown films: Effect of molecular structure on sealability and crystallization kinetics.* Polymer Engineering & Science, 2017. **57**(1): p. 52-59.
57. Jia-Ye, S. and Z. Lin-Xi, *The phase behaviour of single polyethylene chains with and without fixing one end.* Chinese Physics B, 2008. **17**(8): p. 3115-3122.
58. Teraoka, I., *Polymer solutions*. 2002: John Wiley & Sons, Inc.
59. Cotton, J.P., et al., *Conformation of Polymer Chain in the Bulk.* Macromolecules, 1974. **7**(6): p. 863-872.
60. Wang, X., X. Qiu, and C. Wu, *Comparison of the Coil-to-Globule and the Globule-to-Coil Transitions of a Single Poly(N-isopropylacrylamide) Homopolymer Chain in Water.* Macromolecules, 1998. **31**(9): p. 2972-2976.
61. Kim, S., et al., *Enhanced Interfacial Adhesion between an Amorphous Polymer (Polystyrene) and a Semicrystalline Polymer [a Polyamide (Nylon 6)].* ACS Applied Materials & Interfaces, 2011. **3**(7): p. 2622-2629.
62. Ebnesajjad, S., *Plastic films in food packaging: materials, technology and applications*. 2012: William Andrew.
63. Theller, H.W., *HEATSEALABILITY OF FLEXIBLE WEB MATERIALS IN HOT-BAR SEALING APPLICATIONS.* Plastic Film and sheeting, 1989. **5**: p. 66-93.
64. Sierra, J.D., M. del Pilar Noriega, and T.A. Osswald, *Effect of metallocene polyethylene on heat sealing properties of low density polyethylene blends.* Journal of Plastic Film & Sheeting, 2000. **16**(1): p. 33-42.
65. Kiang, W., *Hot Tack and Heat Sealing Properties of EVOH.* ANTEC 92--Shaping the Future., 1992. **1**: p. 1244-1249.

66. Morris, B.A., *The science and technology of flexible packaging: multilayer films from resin and process to end use*. 2016: William Andrew.
67. Morris, B.A., *Predicting the performance of ionomer films in heat-seal processes.* Paper, Film and Foil Converter, 2003. **77**(3): p. 207.
68. Bartels, C.R., B. Crist, and W.W. Graessley, *Self-diffusion coefficient in melts of linear polymers: chain length and temperature dependence for hydrogenated polybutadiene.* Macromolecules, 1984. **17**(12): p. 2702-2708.
69. Sperling, L.H., *INTRODUCTION TO PHYSICAL POLYMER SCIENCE*. 4th ed. 2006, New Jersey: John Wiley & Sons, Inc.
70. Najarzadeh, Z., A. Ajji, and J.-B. Bruchet, *Interfacial self-adhesion of polyethylene blends: the role of long chain branching and extensional rheology.* Rheologica Acta, 2015. **54**(5): p. 377-389.
71. Najarzadeh, Z. and A. Ajji, *Role of molecular architecture in interfacial self-adhesion of polyethylene films.* Journal of Plastic Film & Sheeting, 2017. **33**(3): p. 235-261.
72. Bartels, C.R., et al., *Self-diffusion in branched polymer melts.* Macromolecules, 1986. **19**(3): p. 785-793.
73. Qureshi, N.Z., et al., *Self-Adhesion of Polyethylene in the Melt. 2. Comparison of Heterogeneous and Homogeneous Copolymers.* Macromolecules, 2001. **34**(9): p. 3007-3017.
74. David T. Wu and G.H. Fredrickson, *Effect of Architecture in the Surface Segregation of Polymer Blends.* Macromolecules 1996, 29, 7919-7930, 1996. **29**: p. 7919-7930.
75. Schuman, T., et al., *Solid state structure and melting behavior of interdiffused polyethylenes in microlayers.* Polymer, 1999. **40**(26): p. 7373-7385.
76. ROBERT, Y.L., A. SHANKS, and Z.H. STACHURSILIt, *kinetics of polymer crystallization.* Prog. Polym. Sci., 1995. **20**: p. 651-701.
77. Di Lorenzo, M.L. and C. Silvestre, *Non-isothermal crystallization of polymers.* Prog. Polym. Sci., 1999. **24**: p. 917-950.
78. Zhu , L., et al., *Physical Constants of Poly(ethylene)*, in *Polymer Handbook (4th Edition)*, J. Brandrup, et al., Editors., John Wiley & Sons. p. V-9.
79. Miyata, K., et al., *The relationships between crystallization characteristics and heat sealing properties of high-density polyethylene films.* Journal of Plastic Film and Sheeting, 2014. **30**(1): p. 28-47.
80. Poisson, C., et al., *Optimization of PE/binder/PA extrusion blow-molded films. II. Adhesion properties improvement using binder/EVA blends.* Journal of Applied Polymer Science, 2006. **101**(1): p. 118-127.
81. Chen, Y., et al., *Melting and crystallization behavior of partially miscible high density polyethylene/ethylene vinyl acetate copolymer (HDPE/EVA) blends.* Thermochimica Acta, 2014. **586**: p. 1-8.
82. L. C. Nicastro, et al., *CHANGE IN CRYSTALLINITY DURING HEAT SEALING OF CAST POLYPROPYLENE FILM.* Plastic Film and sheeting, 1993. **9**.
83. Najarzadeh, Z., R.Y. Tabasi, and A. Ajji, *Sealability and Seal Characteristics of PE/EVA and PLA/PCL Blends.* International Polymer Processing, 2014. **29**(1): p. 95-102.
84. Lamnawar, K., F. Vion-Loisel, and A. Maazouz, *Rheological, morphological, and heat seal properties of linear low density polyethylene and cyclo olefine copolymer (LLDPE/COC) blends.* Journal of applied polymer science, 2010. **116**(4): p. 2015-2022.

85. Tabasi, R.Y., Z. Najarzadeh, and A. Ajji, *Development of high performance sealable films based on biodegradable/compostable blends.* Industrial Crops and Products, 2015. **72**: p. 206-213.
86. Scarfato, P., et al., *Three-layered coextruded cast films based on conventional and metallocene poly (ethylene/α-olefin) copolymers.* Journal of Plastic Film & Sheeting, 2014. **30**(3): p. 284-299.
87. Butler, T.I. and B.A. Morris, *PE-based multilayer film structures*, in *Multilayer flexible packaging*. 2016, Elsevier. p. 281-310.
88. Mihindukulasuriya, S.D. and L.-T. Lim, *Heat sealing of LLDPE films: Heat transfer modeling with liquid presence at film–film interface.* Journal of Food Engineering, 2013. **116**(2): p. 532-540.
89. Wooster, J.J., et al., *Film layers made from ethylene polymer blends*. 2010, US Patents.
90. Viganò, S. *The use of metallocene polyethylene in co-extruded lamination film*. in *11 th European PLACE Conference. Athens, Greece*. 2007.
91. Viganò, S. *The Use of Metallocene Polyethylene in Co-Extruded Lamination Film*. in *TAPPI PLACE*. 2007.
92. Faker, M., et al., *Rheology, morphology and mechanical properties of polyethylene/ethylene vinyl acetate copolymer (PE/EVA) blends.* European Polymer Journal, 2008. **44**(6): p. 1834-1842.
93. Li, C., et al., *Crystallization of partially miscible linear low-density polyethylene/poly (ethylene-co-vinylacetate) blends.* Materials Letters, 2004. **58**(27-28): p. 3613-3617.
94. Khonakdar, H., et al., *Rheology, morphology and estimation of interfacial tension of LDPE/EVA and HDPE/EVA blends.* Polymer Bulletin, 2005. **54**(1-2): p. 75-84.
95. Khonakdar, H., et al., *Dynamic mechanical properties and morphology of polyethylene/ethylene vinyl acetate copolymer blends.* Advances in Polymer Technology: Journal of the Polymer Processing Institute, 2004. **23**(4): p. 307-315.
96. Takidis, G., et al., *Compatibility of low-density polyethylene/poly (ethylene-co-vinyl acetate) binary blends prepared by melt mixing.* Journal of Applied Polymer Science, 2003. **90**(3): p. 841-852.
97. Shi, X., et al., *Multiple melting and partial miscibility of ethylene-vinyl acetate copolymer/low density polyethylene blends.* Journal of applied polymer science, 2009. **113**(5): p. 2863-2871.
98. McEvoy, R.L. and S. Krause, *Interfacial Interactions between Polyethylene and Polypropylene and Some Ethylene-Containing Copolymers.* Macromolecules, 1996. **29**(12): p. 4258-4266.
99. Zhao, L. and P. Choi, *A review of the miscibility of polyethylene blends.* Materials and manufacturing processes, 2006. **21**(2): p. 135-142.
100. Crist, B. and M.J. Hill, *Recent developments in phase separation of polyolefin melt blends.* Journal of Polymer Science Part B: Polymer Physics, 1997. **35**(14): p. 2329-2353.
101. Hameed, T. and I.A. Hussein, *Melt Miscibility and Mechanical Properties of Metallocene LLDPE blends with HDPE: Influence of M w of LLDPE.* Polymer journal, 2006. **38**(11): p. 1114-1126.
102. Bai, L., et al., *Rheological behavior and mechanical properties of high-density polyethylene blends with different molecular weights.* Journal of Applied Polymer Science, 2010. **118**(3): p. 1356-1363.

103. Wignall, G., et al., *Morphology of blends of linear and short-chain branched polyethylenes in the solid state by small-angle neutron and X-ray scattering, differential scanning calorimetry, and transmission electron microscopy.* Macromolecules, 2000. **33**(2): p. 551-561.
104. Alamo, R., et al., *Small angle neutron scattering investigations of melt miscibility and phase segregation in blends of linear and branched polyethylenes as a function of the branch content.* Macromolecules, 1997. **30**(3): p. 561-566.
105. Zhao, Y., S. Liu, and D. Yang, *Crystallization behavior of blends of high-density polyethylene with novel linear low-density polyethylene.* Macromolecular Chemistry and Physics, 1997. **198**(5): p. 1427-1436.
106. Yamaguchi, M. and S. Abe, *LLDPE/LDPE blends. I. Rheological, thermal, and mechanical properties.* Journal of Applied Polymer Science, 1999. **74**(13): p. 3153-3159.
107. Liu, C., J. Wang, and J. He, *Rheological and thermal properties of m-LLDPE blends with m-HDPE and LDPE.* Polymer, 2002. **43**(13): p. 3811-3818.
108. Hussein, I.A., *Influence of composition distribution and branch content on the miscibility of m-LLDPE and HDPE blends: Rheological investigation.* Macromolecules, 2003. **36**(6): p. 2024-2031.
109. Taylor, J. and J.J. Baik, *Benefits of coextruded LLDPE/LDPE film vs. blended LLDPE/LDPE film.* Journal of Plastic Film & Sheeting, 2000. **16**(3): p. 223-236.
110. Siegmann, A. and Y. Nir, *Structure-property relationships in blends of linear low-and conventional low-density polyethylene as blown films.* Polymer Engineering & Science, 1987. **27**(15): p. 1182-1186.
111. Beagan, C., G. McNally, and W. Murphy, *The blending and coextrusion of metallocene catalysed polyethylene in blown film applications.* Journal of Plastic Film & Sheeting, 1999. **15**(4): p. 329-340.
112. Viganò, S. *The Use of Metallocene Polyethylene in Co-Extruded Lamination Film*. in *TAPPI 2007 PLACE Conference Proceedings*. 2007.
113. Engmann, J., C. Servais, and A.S. Burbidge, *Squeeze flow theory and applications to rheometry: A review.* Journal of non-newtonian fluid mechanics, 2005. **132**(1-3): p. 1-27.
114. Dienes, G. and H. Klemm, *Theory and application of the parallel plate plastometer.* Journal of Applied Physics, 1946. **17**(6): p. 458-471.
115. Leider, P.J. and R.B. Bird, *Squeezing flow between parallel disks. I. Theoretical analysis.* Industrial & Engineering Chemistry Fundamentals, 1974. **13**(4): p. 336-341.
116. Ghnatios, C., F. Chinesta, and C. Binetruy, *3D Modeling of squeeze flows occurring in composite laminates.* International Journal of material forming, 2015. **8**(1): p. 73-83.
117. Gupta, P. and A. Gupta, *Squeezing flow between parallel plates.* Wear, 1977. **45**(2): p. 177-185.
118. Morris, B.A. and J.M. Scherer, *Modeling and experimental analysis of squeeze flow of sealant during hot bar sealing and methods of preventing squeeze-out.* Journal of Plastic Film and Sheeting, 2015. **32**(1): p. 34-55.
119. Shuler, S. and S. Advani, *Transverse squeeze flow of concentrated aligned fibers in viscous fluids.* Journal of Non-Newtonian Fluid Mechanics, 1996. **65**(1): p. 47-74.
120. Levy, A., G.P. Martel, and P. Hubert. *Modeling the Squeeze Flow of a Thermoplastic Composite Tape During Forming*. in *Proceedings of the 8th annual COMSOL conference*. 2012.

121. Picher-Martel, G.-P., A. Levy, and P. Hubert, *Compression moulding of carbon/PEEK randomly-oriented strands composites: A 2D finite element model to predict the squeeze flow behaviour.* Composites Part A: Applied Science and Manufacturing, 2016. **81**: p. 69-77.
122. Moffitt, R.D. *A MATHEMATICAL MODEL FOR THE HEAT SEALING OF LINEAR, SEMI-CRYSTALLINE POLYMERS*. in *ANTEC*. 2006.
123. Moffitt, R.D. *INDUSTRIAL APPLICATIONS OF HEAT SEALING MODELING*. in *ANTEC*. 2007.
124. De Gennes, P.-G., *Scaling concepts in polymer physics*. 1979: Cornell university press.
125. Reiichi Konishi , et al., *FRACTURE BEHAVIOR OFHEAT-SEALED POLY(LACTICACID) FILMS*, in *ANTEC*. 2006. p. 2231-2235.

APPENDIX

Supplementary Information for Article 2

S-1. Two-dimensional modeling of fluid flow without the knowledge of jaw approaching velocity and pressure gradient

Using equation of continuity and Navier-Stokes equations, the following governing equations can be derived for the 2D squeeze flow between two rectangular plates with a gap much smaller than other dimensions. u and V show the velocity components in x- and y- directions, respectively.

$$\frac{\partial P}{\partial x} = \frac{\partial}{\partial y}\left(\eta \frac{\partial u}{\partial y}\right) + \frac{\partial}{\partial x}\left(\eta \frac{\partial u}{\partial x}\right) \quad (1)$$

$$\frac{\partial}{\partial x}\left(\eta \frac{\partial V}{\partial x}\right) + \frac{\partial}{\partial y}\left(\eta \frac{\partial V}{\partial y}\right) = 0 \quad (2)$$

$$\frac{\partial V}{\partial y} + \frac{\partial u}{\partial x} = 0 \quad (3)$$

where η=f($\dot{\gamma}$) and

$$\dot{\gamma} = \sqrt{2\left(\frac{\partial V}{\partial y}\right)^2 + 2\left(\frac{\partial u}{\partial x}\right)^2 + \left(\frac{\partial u}{\partial y}\right)^2 + \left(\frac{\partial V}{\partial x}\right)^2} \quad (4)$$

Using the mass balance one can show that:

$$-\frac{dh}{dt} \times L \times W = 2W \int_0^{L/2} U\, dx \quad (5)$$

where L, W and U are the length, width(depth) and the velocity magnitude, respectively. It should be noted that $U = \sqrt{u^2 + V^2}$. The applied force the the multilayer film can be determined from:

$$F = 2W \int_0^{\frac{L}{2}} x \left(-\frac{\partial P}{\partial x}\right) dx \quad (6)$$

For the squeeze flow in heat sealing, the following boundary conditions can be considered:

x=0→ $\frac{\partial u}{\partial x} = \frac{\partial P}{\partial x} = \frac{\partial v}{\partial x} = 0$

x=±L/2→ P=0

y=0→ $\frac{\partial u}{\partial y} = 0$

y=h→ V=-dh/dt, u=0

y=-h→ V=0, u=0

In a case such as heat sealing, where only the applied force to the jaws is known and both $\frac{\partial P}{\partial x}$ and $\frac{dh}{dt}$ are unknown, finding an explicit solution for the above system of non-linear equations is not possible. This indicates the complexity of modelling SOF in heat sealing.

S-2- Flow Chart for numerical FDM model

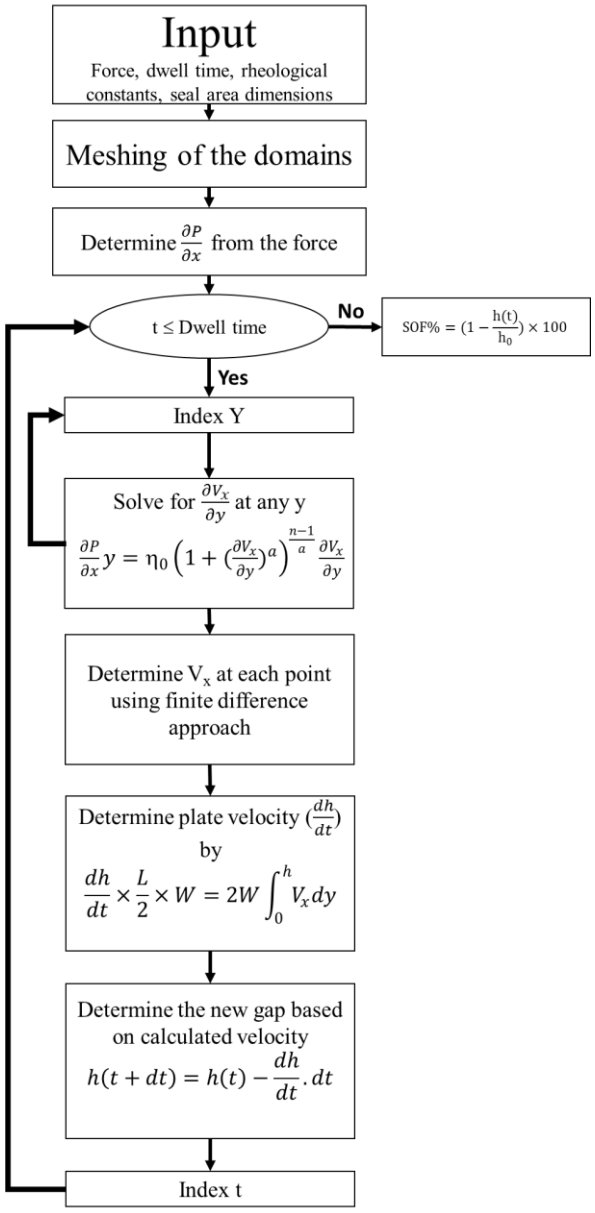

Figure S.1 Flow chart showing the steps in numerical modeling of the squeeze flow of the sealant layer

S.4 Rheological properties of PE-g-MA at 140 ºC

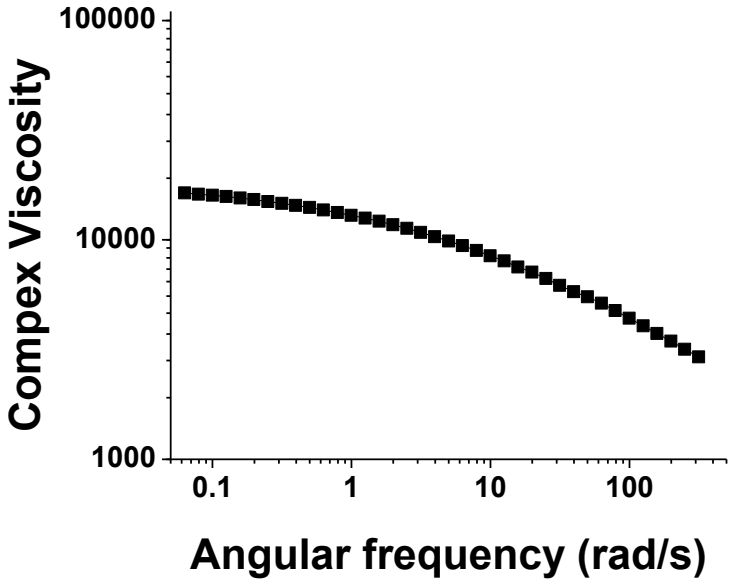

Figure S.2 Complex viscosity of PE-g-MA measured at 140ºC